Deciphering the Role of Long-chain Acyl-CoA Synthetase 6 in Brain Lipid Metabolism and Neuroprotection

By

Regina Fernández Fernández

April, 2021

Director of Dissertation: Jessica M. Ellis, Ph.D.

Major Department: Physiology

Abstract:

The omega-3 fatty acid, docosahexaenoic acid (DHA), is highly enriched in the central nervous system (CNS) and thought to protect against neurological dysfunction. Due to its neuroprotective nature, DHA is widely considered a medicinal preventative strategy and treatment. However, while dietary DHA supplementation increases DHA levels in peripheral tissues, it often fails to increase brain DHA levels. The indirect relationship between dietary-DHA and brain-DHA enrichment highlights the existence of unique mechanisms that allow DHA to be metabolized in the brain. The mechanisms regulating DHA enrichment in the brain remain unclear. The purpose of this dissertation was to answer fundamental questions about the mechanisms that regulate brain DHA metabolism by testing the hypothesis that a specific fatty acid metabolizing enzyme, long-chain acyl-CoA synthetase isoform 6 (ACSL6), is required for enrichment of DHA into the brain. As reviewed in my first-author literature review published in PLEFA in September 2020, ACSL6 is one of a large family of 26 acyl-CoA synthetase (ACS) enzymes that catalyze the initial step in cellular fatty acid metabolism and serve as potential master

regulators of brain phospholipid acyl-chain diversity. Of all the ACSs, ACSL6 is almost exclusively expressed in the CNS and has been shown to have substrate preference for DHA. To test our hypothesis, we genetically targeted ACSL6 to create a novel conditional ACSL6-deficient mouse (*Acsl6*$^{-/-}$). We discovered that whole-body *Acsl6* deletion results in a significant 35-72% reduction in DHA-containing phospholipids in the CNS. Our initial findings for this animal model were published as my first first-author research article in PNAS in October of 2018, and our findings were of such great interest that the article was mentioned on the cover of the issue and was accompanied by a complementary commentary highlighting the importance of our discovery. We then went on to combine *in situ* fluorescence hybridization, several genetically targeted mouse models, lipidomics, and MALDI lipid imaging to demonstrated that ACSL6 in neurons regulates the enrichment of DHA in the brain. We also have shown that ACSL6 expressed in astrocytes does alter membrane acyl-chain content, but does not impact DHA, which we mechanistically explain is due to cell-type specific expression of ACSL6 variants that contain altered fatty acid binding domains. After many behavioral assessments, we found that ACSL6 knockout mice were hyporesponsive to auditory and foot-shock sensory stimulation, exhibited hyperlocomotion, and showed altered short-term working spatial memory. *Acsl6*$^{-/-}$ mice displayed exacerbated astrogliosis in an age-dependent manner and accompanied with increased inflammation and gliosis. This neuroinflammation occurred independent of changes in pro- and anti-inflammatory lipid mediators suggesting there is an alternative mechanism triggering the neuroinflammation. RNA-seq data revealed downregulation of synaptic proteins' gene expression in *Acsl6*$^{-/-}$ mice as early as 2 months of age. Thus, we hypothesized that ACSL6-mediated DHA deficiency results

in gradual synaptic function deregulation that contributes to increased neuroinflammation during aging. These age-dependent findings are currently under revisions for publication. Together, these data identified ACSL6 in neurons as an important regulator of DHA metabolism that plays a neuroprotective role during aging and on memory and motor function. This dissertation work has led to the discovery of an important and fundamental mechanism by which the parenchyma of the central nervous system controls fatty acid metabolism, particularly for the neuroprotective omega-3 fatty acid DHA.

Deciphering the Role of Long-chain Acyl-CoA Synthetase 6 in Brain Lipid Metabolism and Neuroprotection

A Dissertation

Presented to the Faculty of the Department of Physiology

East Carolina University

In Partial Fulfillment of the Requirements for the Degree

Doctor of Philosophy in Biomedical Science

Concentration in Physiology

By

Regina Fernández Fernández

April, 2021

Deciphering the Role of Long-chain Acyl-CoA Synthetase 6

in Brain Lipid Metabolism and Neuroprotection

By

Regina Fernández Fernández

Approved by:

Director of Dissertation: _____
Jessica M. Ellis, PhD

Committee Member: _____
Stefan Clemens, PhD

Committee Member: _____
Espen E. Spangenburg, PhD

Committee Member: _____
Michael J. Wolfgang, PhD

Chair of the Department of Physiology: _____
Robert M. Lust, PhD

Dean of the Graduate School: _____
Paul J. Gemperline, PhD

In memory of my uncle Raúl Fernandez Urquidi

“Thank you for your part in my journey”

ACKNOWLEDGEMENTS

The work in this dissertation would not have been possible without the help, guidance, and support of many people. First and foremost, I would like to thank my advisor Dr. Jessica Ellis for the opportunity of working on such an exciting project, for always encouraging me to be better, and for training me to become a successful scientist.

I would like to thank my committee members from Purdue University, Dr. Kimberly Kinzig, Dr. Kimberly Buhman, and Dr. John Burgess, for the support and feedback provided throughout my first three years in graduate school. I thank Dr. Burgess for the teaching opportunity and for sharing his passion for nutrition education. I would also like to acknowledge my dissertation committee members at ECU, Dr. Espen Spangenburg, Dr. Stefan Clemens, and Dr. Michael Wolfgang (John Hopkins University) for their guidance during my transition to ECU and the remaining of my doctoral studies.

I am grateful to current and former lab members of the Ellis Lab, including Sora Kim and Yingwei Zhao, who significantly contributed to the work described in this dissertation. Further gratitude goes to Dr. Andrea Pereyra who not only shared her scientific expertise but also provided me with moral support, her friendship, and good Argentinian wine during my doctoral studies.

Special thanks to the ECDOI gang. I truly enjoyed working in such a collaborative and supportive environment. Thanks for adding the word “mitochondriac” to my lexicon.

I am deeply thankful to my family for their love and support. Despite the 3216 kilometers that separate us, you have always been there for me. I am thankful to Abue Lupita (grandmother) and my aunt Cecilia who inspired me to become a scientist. Finally, I thank Ilya Boykov and all my friends that have been part of this journey for their support.

TABLE OF CONTENTS

LIST OF TABLES

LIST OF FIGURES

LIST OF ABBREVIATIONS

AA	Arachidonic acid
ACS	Acyl-CoA synthetase
ALA	Alpha-linolenic acid
ATP	Adenosine triphosphate
BM	Barnes maze
CA3	Cornu Ammonis 3
CDP	Cytidine diphosphate pathway
CoA	Coenzyme A
COX	Cyclooxygenases
CYP	Cytochrome P450
DAG	Diacylglycerol
DEGs	Differentially expressed genes
DG	Dentate gyrus
DHA	Docosahexaenoic acid
EETs	Epoxyeicosatrienoic acids
EH	Epoxy hydrolase
EPA	Eicosapentanoic acid
ER	Endoplasmic reticulum
FATP	Fatty acid transport protein
GFAP	Glial fibrillary acidic protein
GO	Gene onthology
GPAT	Glycerol-3-phosphate acyltransferase
HDoHE	Hydroxydocosahexaenoic acid
IBA-1	Ionized calcium binding adaptor molecule 1
LA	Linoleic acid
LOX	Lipoxygenases
LPA	Lysophosphatidic acid

LPAAT	LPA-acyltransferase
LPxAT	Lysophosphatidylx acyltransferase
LPS	Lipopolysaccharide
MAG	Monoacylglycerol
MALDI	Matrix-assisted laser desorption/ionization
MBOAT	Membrane bound-O-acyltransferases
Meg3	Maternally expressed 3
Mfsd2a	Major facilitator superfamily domain containing 2A
NA	Non-enzymatic oxidation
OA	Oleate
OF	Open field
PA	Palmitate
PC	Phosphatidylcholine
PE	Phosphatidylethanolamine
PG	Phosphatidylglycerol
PI	Phosphatidylinositol
PLAs	Phospholipases
PS	Phosphatidylserine
PUFA	Polyunsaturated fatty acid
RBC	Red blood cells
ROS	Reactive oxygen species
smFISH	Single molecule *in situ* hybridization
SREBP	Sterol regulatory element-binding protein
TAG	Triacylglycerol
TLC	Thin layer chromatography
Vgat	Vesicular inhibitory amino acid transporter
Vglut1	Vesicular glutamate transporter

CHAPTER I

INTRODUCTION

Over the last decade, neurological diseases have become a leading cause of disability and death worldwide, partially due to the fast growth of the aging population (>65 years old) (2, 3). Emerging evidence suggests that neurological disease risk is inversely correlated to consumption of the neuroprotective omega-3 docosahexaenoic acid (DHA) (4-9). DHA is the most abundant polyunsaturated fatty acid in the brain thought to be protective due to its ability to modulate membrane fluidity, serve as an antioxidant, and its anti-inflammatory properties (10). However, the mechanisms regulating DHA enrichment and metabolic handling in the brain remain unknown.

We predict that cellular fatty acid metabolic fate is controlled in part by a family of enzymes called acyl-CoA synthetases (ACS) that convert fatty acids into their activated Coenzyme A (CoA) esters. Once these acyl(fatty acid)-CoAs are formed, the fatty acids are then trapped within the cell and activated for metabolism into downstream pathways, such as phospholipid synthesis. From the 25 and 26 ACSs expressed in rodents and humans, respectively, we are particularly interested in long-chain ACS isoform 6 (ACSL6) because ACSL6 is almost exclusively expressed in the central nervous system suggesting that it may play a crucial role in brain fatty acid metabolism. Moreover, ACSL6 overexpression in cell culture enhances DHA metabolism and promotes membrane formation. Thus, we ***hypothesize*** that ACSL6 is required for DHA incorporation into phospholipids to maintain neural health. To determine the role of ACSL6 *in vivo* we generated a novel conditional ACSL6 deficient mouse (*Acsl6*$^{-/-}$). *Acsl6*$^{-/-}$ mice show a striking 35-72% reduction in DHA-containing phospholipids across tissues that highly

express ACSL6 (brain, retina, spine, and testes). Importantly, the loss of ACSL6 resulted in impaired motor and memory function and age-related neuroinflammation, indicators of neural dysfunction. Our ***objective*** is to delineate how ACSL6 regulates DHA metabolism in the brain. Our ***long-term goal*** is to elucidate the molecular mechanisms that regulate fatty acid metabolism and link ACSL6-mediated DHA metabolism to neuroprotection to inform preventive and therapeutic strategies for neurological disorders.

The work in this dissertation will improve the scientific knowledge by resolving the mechanisms through which cellular fatty acid metabolism is regulated within the brain, with a particular emphasis on the neuroprotective omega-3 fatty acid DHA. Understanding the role of ACSL6 is critical to further elucidate the effect of DHA deficiency on neurological diseases.

Specific aims:

- **Aim 1: Determine the role of ACSL6 in brain cellular fatty acid metabolism and neurological health.** Because ACSL6 is almost exclusively expressed in the brain and prefers DHA as its substrate we ***hypothesize*** that ACSL6 is required for enriching the brain with DHA. ***Approach:*** We broadly assessed lipid content and the metabolic, physiological, motor, inflammatory, and antioxidant outcomes regulated by ACSL6.

- **Aim 2: Determine the role of ACSL6 in the age-related neurological decline.** Emerging evidence suggests that dysregulated fatty acid metabolism and DHA deficiency is causal in the development of age-related neurological diseases. Thus, we ***hypothesize*** that ACSL6 activity is necessary for protecting the brain against age-related neural dysfunction. ***Approach:*** We used our novel *Acsl6*$^{-/-}$ mice to examine lipid, molecular, and histological changes in brain parenchyma and perform behavioral assessments at different ages across the mouse lifespan.

CHAPTER II

REVIEW OF LITERATURE

Each individual cell-type is defined by its distinct morphology, phenotype, molecular and lipidomic profile. The importance of maintaining cell-specific lipidomic profiles is exemplified by the numerous diseases, disorders, and dysfunctional outcomes that occur as a direct result of altered lipidome. Therefore, the mechanisms regulating cellular lipidome diversity play a role in maintaining essential biological functions. The brain is an organ particularly rich in phospholipids, the main constituents of cellular membranes. The phospholipid acyl-chain profile of membranes in the brain is rather diverse due in part to the high degree of cellular heterogeneity. These membranes and the acyl-chain composition of their phospholipids are highly regulated, but the mechanisms that confer this tight regulation are incompletely understood. A family of enzymes called acyl-CoA synthetases (ACSs) stands at a pinnacle step allowing influence over cellular acyl-chain selection and subsequent metabolic flux. ACSs perform the initial reaction for cellular fatty acid metabolism by ligating a Coenzyme A to a fatty acid which both traps a fatty acid within a cell and activates it for metabolism (Figure 2.1). The ACS family of enzymes is large and diverse consisting of 25-26 family members that are nonredundant, each with unique distribution across and within cell types, and differential fatty acid substrate preferences. Thus, ACSs confer a critical intracellular fatty acid selecting step in a cell-type dependent manner providing acyl-CoA moieties that serve as essential precursors for phospholipid synthesis and remodeling, and therefore serve as

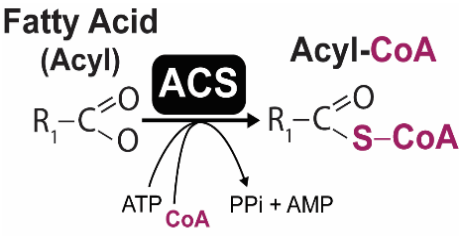

Figure 2.1. **ACS reaction**

a key regulator of cellular membrane acyl-chain compositional diversity. The present chapter includes material from my first-author literature review published in PLEFA because it nicely describes how the contribution of individual ACSs towards brain lipid metabolism has only just begun to be elucidated and discusses the possibilities for how ACSs may differentially regulate brain lipidomic diversity (1).

Introduction

Fatty acids are critical substrates for numerous metabolic processes, have high potential for energy production, and serve as the foundation for cellular membrane hydrophobic regions. Across the body, the distribution and metabolic fate of fatty acids are highly differential. Metabolically, fatty acid fate can be placed into three major categories: oxidation for energy, storage as triacylglycerol, and use for phospholipid synthesis and remodeling. While the oxidation and storage of fatty acids are the main metabolic fates for certain cell types or in response to feeding/fasting conditions, the use of fatty acids for incorporation into phospholipids, either new or during remodeling, is a major metabolic fate of all cells across the body and under all metabolic conditions because phospholipids are critical structural components of all membranes.

The brain is very lipid-rich, due to its high phospholipid content, and is considered the second most fatty organ next to adipose tissue. The importance of lipid metabolism in maintaining healthy brain function is exemplified by the numerous models of neurological diseases that stem from primary defects in lipid metabolism. For instance, Niemann Pick, Tay-Sachs, Mabry syndrome, and numerous mental retardations, narcolepsies, and paraplegias are caused by primary inherited defects in lipid metabolism (11). Many neurological diseases and disorders that do not necessarily result from an

inherited defect in a lipid-metabolizing gene are characterized by clear defects and abnormalities in lipid metabolism and lipid content. Yet the role of these lipid-related defects in the etiology and progression of disease remains unclear (11). Previously, we showed that a lipid-metabolizing enzyme, acyl-CoA thioesterase 7, is critical for preventing neuronal lipotoxicity, ALS-like symptoms, and seizure susceptibility in mice (12, 13). These outcomes were later confirmed to occur in the first report of a human with an inherited defect in acyl-CoA thioesterase 7 (14). Thus, it is possible that cases of neurological diseases and disorders with unknown etiologies are yet to be linked to lipid metabolism as the primary defect.

Historically, the brain is not thought to oxidize fatty acids for energy. This concept is challenged with data supporting beta-oxidation of the omega-3 fatty acid eicosapentaenoic acid (EPA) in the brain (15) and the ability of astrocytes to oxidize fatty acids (16-18). The overall contribution and criticality of fatty acids as an energy source in the brain remained unclear until a recent report demonstrated that mitochondrial fatty acid oxidation is seemingly dispensable for the brain (19). Namely, the brain-specific loss of carnitine palmitoyltransferase 2, a nonredundant enzyme required for mitochondrial oxidation of long-chain fatty acids, does not result in a major overt phenotype in mice (19). The opposing metabolic fate of fatty acid oxidation is fatty acid storage in triacylglycerol. Neurons are not known to store lipids as triacylglycerol; however evidence demonstrates that neurons contain triacylglycerol lipase, suggesting that these cells have the ability to metabolically degrade stored lipids (20). Yet consensus remains that very little fat is stored as triacylglycerol in the brain. Above all, the major metabolic fate for fatty acids in the brain is for incorporation into phospholipids.

Lipids constitute 50% of the brain's dry weight, predominantly in the form of phospholipids (21). Phospholipids are the major component of cell membranes encasing all cells, organelles, and vesicles (Figure 2.2). Membranes and their fatty acid composition are in constant flux through the actions of membrane remodeling, vesicle endocytosis and exocytosis, autophagy, and the formation, expansion, and retraction of cells and organelles (11). These cellular processes occur at particularly high rates in the brain. At synapses, synaptic vesicles undergo exocytotic fusion with the presynaptic plasma membrane, followed by endocytosis-mediated retrieval to regenerate synaptic vesicles. This vesicle recycling process requires membrane reorganization at each step to provide an adequate lipid environment for sustaining synaptic responses (22-24). Dendritic spines are constantly changing in number and shape and undergo enlargement or shrinkage upon stimuli that affect total plasma membrane area (25-27). Other cellular processes that involve lipid remodeling include the axoplasmic transport of vesicles containing proteins and lipids, myelination, and axon regeneration (28-30). Furthermore, all these processes are influenced by learning, memory formation, age, and pathogenic conditions (31). Thus, phospholipids are dynamic molecules essential for physiological brain function.

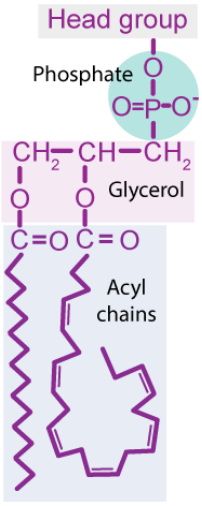

Figure 2.2 Phospholipid structure

Influence of phospholipid acyl-chain diversity on membrane properties and cellular function

Cellular membranes are highly heterogeneous assemblies comprised of proteins and lipids, predominated by phospholipids. Membrane diversity arises from the structural components of phospholipids, which consist of a headgroup and a hydrophobic tail

containing two-fatty acids. Membrane composition influences various membrane properties including membrane curvature, bending, packing defects, and recruitment and stability of lipid-binding proteins and membrane-spanning proteins. While the headgroup can affect these properties (11), so too can the acyl-chain. The length of the phospholipid acyl-chain directly regulates membrane thickness and is important for proper transmembrane protein fit and function, whereby the hydrophobic region of the phospholipid membrane needs to match the length of the hydrophobic segments of the protein. A hydrophobic mismatch can be relieved by membrane lipid remodeling or can result in lateral displacement of the protein and/or alterations in protein folding, which can ultimately affect protein function (32). In addition to acyl-chain length, its unsaturation also affects membrane properties such as membrane bending. A high percentage of straight-chained saturated fatty acids will render the membrane tight and rigid, whereas the incorporation of kinked unsaturated fatty acids will confer flexibility and introduce packing defects and deformation (33, 34). Thus, an increase in unsaturated fatty acid content will facilitate processes, such as membrane vesicle cycling that require membrane deformation. In the brain, membrane vesicle cycling at neural synapses is crucial for neurotransmission and highly influenced by the lipid composition of the synapse (35). Besides influencing the architecture of the membrane, some proteins interact selectively with specific lipids to mediate synaptic vesicle fusion, which highlights the importance of lipids in mediating protein function required for cellular processes (22, 36). Given that the phospholipid acyl-chain modulates membrane biophysical properties, it is predicted that small changes in acyl-chain composition have the potential to impact numerous essential biological functions.

In addition to the many functions of membrane acyl-chains, membrane fatty acids serve as precursors for the synthesis of signaling molecules. For instance, the omega-6 polyunsaturated fatty acid (PUFA), arachidonic acid (AA, C20:4n6) can be cleaved from membrane phospholipids by phospholipase activity and be subsequently enzymatically processed into pro-inflammatory bioactive lipid-derivatives such as thromboxanes, leukotrienes, and prostaglandins(37) and into anti-inflammatory mediators such as EETs and lipoxins (38, 39). The omega-3 PUFA docosahexaenoic acid (DHA, C22:6n3) can be similarly cleaved and enzymatically metabolized into a different class of anti-inflammatory and neuroprotective bioactive lipid-derivatives called pro-resolving mediators such as neuroprotectins (40, 41). The pro-resolving mediators generated from the enzymatic oxidation of DHA elicit biological actions including modulation of apoptosis, neurotransmission, and play key roles in the resolution of inflammation (42, 43). An additional metabolic fate of fatty acids is their ligation to amines, amino acids, or neurotransmitters forming lipoamines with biological activity(44). One such lipoamine is N-docosahexaenoyl-ethanolamide (synaptamide) which promotes synaptogenesis and is anti-inflammatory (45, 46). Given the wide variety of neuroprotective functions that PUFAs play in the brain, it is speculated that modulating the levels of these PUFAs in membrane phospholipids directly impacts brain function, response to injury, and disease susceptibility.

Tissue-specific phospholipid acyl-chain diversity

The acyl-chain composition of phospholipids is highly distinct across tissues. To demonstrate this variance, heatmaps were generated from primary data using broad and unbiased phospholipid profiling across several tissues (Figure 2.3). Phospholipid profiling

was performed with Purdue University's Bindley Metabolite Profiling Facility across mouse tissues, as previously described (47, 48). The data are presented as a percentage of total ion counts and include lipid species that are ≥2% in abundance in at least one of the tissues. These data not only demonstrate the diversity of phospholipid composition across tissues but also demonstrate clustering for specific lipid species in either the central nervous system (CNS) or in the periphery. For instance, the CNS had high abundance of phosphatidylcholine (PC) with 0- to 1- unsaturated bonds, whereas peripheral tissues were robustly enriched in PCs with 2-unsaturated bonds (Figure 2.3A). Among PCs with 3 or more unsaturated bonds, peripheral tissues had high abundance but roughly equal distribution of 3-, 4-, 5-, and 6-unsaturated PCs. However, there was an exceptional enrichment of specific species in isolated tissues, such as enrichment of C34:4 in the heart, C38:5 in the testes, and C38:6 in the soleus muscle. The CNS was particularly enriched with 4- and 6-unsaturated PCs, but not unsaturated PCs of 3- (none of which were more than 2% in total phosphatidylcholine) or 5- (which may reflect the low abundance of EPA in the brain) unsaturations. Among brain regions, the hippocampus is particularly enriched with PC36:4 and the cerebellum with PC38:6 and PC40:6 likely reflecting enrichments with the omega-6 AA (C20:4n6) and the omega-3 DHA (C22:6n3) in these regions, respectively. The plasma displayed a highly distinct phospholipid profile when compared to tissues. These results are of interest because plasma lipids are often used as surrogate indicators for whole-body lipid/fatty acid status. The incongruencies between plasma and tissue fatty acid composition challenge the validity of such generalizations. Indeed, the disconnect between plasma and tissue abundance of a particular PUFA, DHA, is well documented by numerous studies that nicely demonstrate

the effectiveness of DHA supplementation to increase DHA in plasma and peripheral tissues, but not in the brain (49-54). This effect is independent of the dietary molecular format of DHA and is demonstrated for supplementation of DHA in the form of a phospholipid, ether ester, free acid, triacylglycerol, and lysophospholipid (49, 53, 54). Therefore, the notion that plasma fatty acid profiles accurately represents that of the CNS remains unvalidated (50).

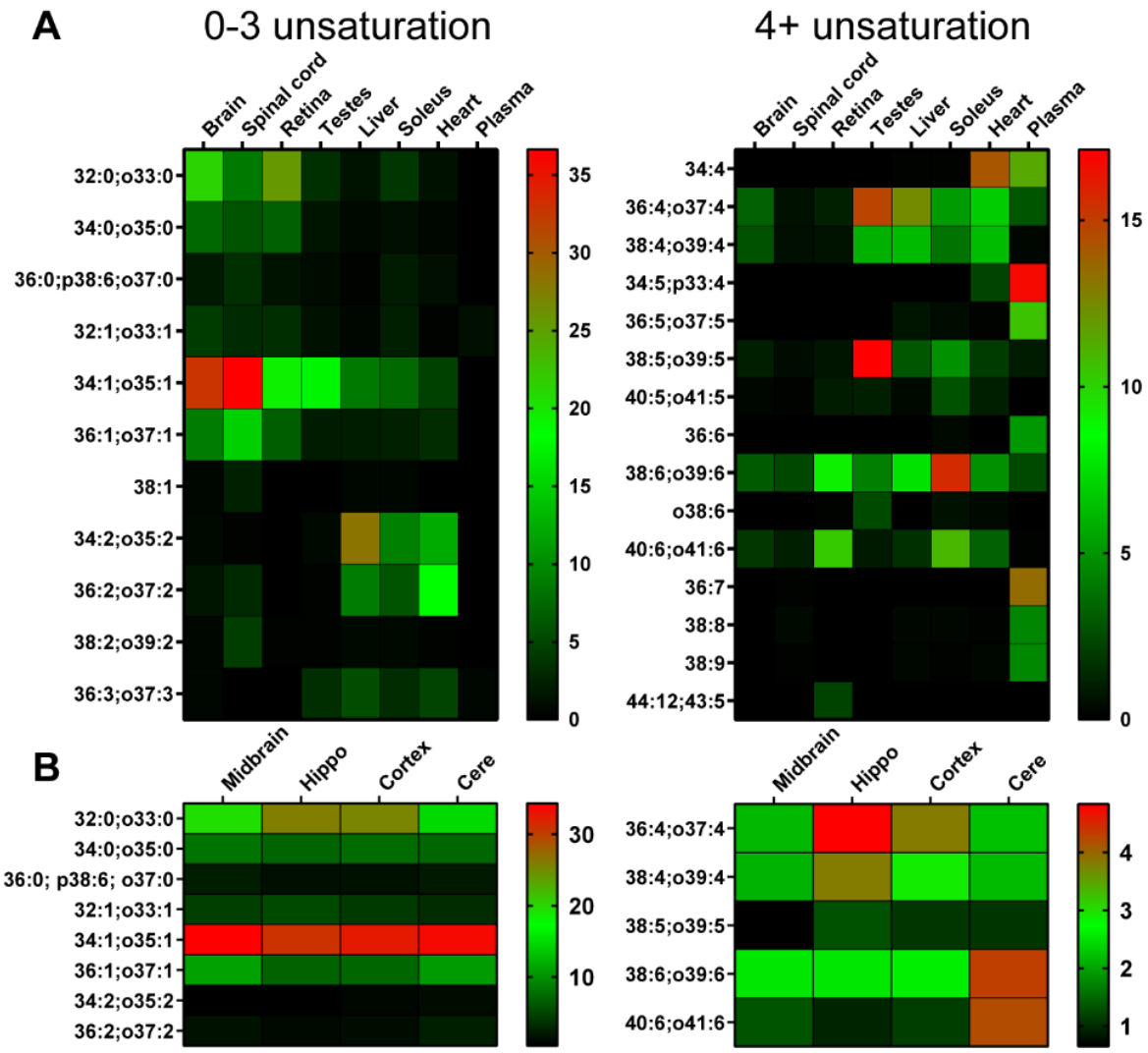

Figure 2.3. Phosphatidylcholine acyl-chain diversity across tissues
Heatmap of PC by acyl-chain length and degree of saturation across A) mouse tissues and B) brain regions, n=6. Data represent percent of total ion count. Hippo, hippocampus; cere, cerebellum (1).

Across brain regions, the overall phospholipid profile was similar (Figure 2.3B). Like the periphery, brain phospholipids contain large amounts of saturated fatty acids, such as palmitate and stearate. However, the high content of phospholipids in the brain results in a unique enrichment with the polyunsaturated fatty acids: AA and DHA, which are 3-4 fold higher in the central nervous system compared to the periphery (55). The uniqueness of the PUFAs, AA and DHA, is largely defined by the unsaturated bonds located at the omega-6 and omega-3 position, respectively. Mammals cannot desaturate fatty acids at the omega-3 or -6 position thus, fatty acids with these bonds must be consumed from exogenous dietary sources and are therefore essential dietary nutrients. Omega-6 fatty acids are found in land plants and grains and are thus high in plant-based foods and oils, and grains, grain-products, and grain-fed animal products. The omega-3 fatty acid, DHA, is particularly abundant in sea plants, thus predominantly consumed indirectly via marine animal (i.e. fish) consumption. The precursor to DHA is alpha-linolenic acid (ALA), which can be found in certain nuts and vegetables; however, very little ALA is metabolically converted to DHA within land animals, making direct DHA consumption via marine products the ideal dietary source to increase bodily DHA.

The importance of omega-3 and omega-6 fatty acids is exemplified by the effects of insufficient dietary intake of these fatty acids, which leads to impaired cognition and increased risk for neurological disorders (56-60). Omega-3 and omega-6 fatty acid accretion in the brain is particularly high during the brain growth spurt, a period that includes the last trimester of gestation and up to the first two years of life when deficient consumption of omega-3 fatty acids is associated with impaired cognition (61-64). Cognitive deficits associated with low omega-3 fatty acid intake can be observed beyond

development, during aging (65-68). Numerous age-related neurological diseases and disorders are inversely associated with omega-3 fatty acids (4, 67-72). While several observational, animal, and randomized control trial studies show positive outcomes, null outcomes between omega-3 fatty acid consumption and brain health are also widely reported (72-76). The reason that omega-3 fatty acid consumption fails to mediate beneficial effects in some intervention studies remains debated (65, 77). One plausible explanation relates to unexplained variable rates of absorption and membrane integration of dietary and/or supplemental forms of omega-fatty acids into the brain (49-54). Here, we will focus on examining a class of enzymes, acyl-CoA synthetases, that likely contribute to the metabolic enrichment of fatty acids into brain phospholipids.

Acyl-CoA Synthetases as regulators of cellular phospholipid acyl-chain diversity in brain

Phospholipids acquire their acyl-chain composition through two major pathways: *de novo* synthesis and remodeling of phospholipids. The *de novo* synthesis of phospholipids occurs predominantly through the Kennedy pathway and cytidine diphosphate (CDP) pathways. The initial step in these pathways is the activation of a fatty acid by Acyl-CoA Synthetase (ACS) followed by the ligation of the acyl-CoA to the sn-1 position of glycerol-3-phosphate by glycerol-3-phosphate acyltransferase (GPAT) to form a lysophosphatidic acid (LPA). A second acyl-CoA, generated by ACS, is then ligated onto the LPA by an LPA-acyltransferase (LPAAT/AGPAT) to form a phosphatidic acid. Thus, the acyl composition of the phosphatidic acid, the common precursor of all newly synthesized phospholipids, is influenced by the concerted action of ACS, GPAT, and LPAAT/AGPAT. Phosphatidic acid is metabolized to diacylglycerol (DAG) by the action

of phosphatidic acid phosphatase (PAPase/lipin) for synthesis of phosphatidylethanolamine, -choline, and -serine. The synthesis of phosphatidylglycerol and cardiolipin in the mitochondria, or phosphatidylinositol at the ER is mediated by the conversion of phosphatidic acid to CDP-DAG by CDP-diacylglycerol synthetase. Each step of this pathway that stands to influence the acyl-chain specificity by substrate preferences for either fatty acids (ACSs) or acyl-CoAs (acyltransferases) is comprised of enzyme families that consist of up to 5 members, except for the ACS family, which consists of 26 family members in humans and 25 in rodents (78-81). Thus, the selectivity of the acyl-chain in *de novo* phospholipid synthesis may largely depend on the ACS family.

The second pathway that regulates the acyl-chain composition of phospholipids is by remodeling via the Land's cycle, which is a highly active process in the brain (82-84). The Land's cycle involves the hydrolysis of fatty acids from phospholipids within membranes by phospholipases (PLAs). The resulting lysophospholipid is re-acylated using a new acyl-CoA, generated by ACS. Re-acylation is performed by lysophosphatidylx acyltransferase (LPxAT), 'x' referring to the head group of the lysophospholipid substrate. The contribution of LPxATs to acyl-chain diversity is widely investigated (11, 85-87). LPxATs are members of the LPAAT/AGPAT and the membrane bound-O-acyltransferases (MBOAT) families of enzymes that incorporate acyl-CoAs into the sn-2 position of phospholipids, the primary site of PUFA esterification. Studies on knockout mice demonstrate that LPxATs can regulate PUFA levels in membrane lipids in a substrate- and tissue-specific manner (Reviewed extensively in (81, 88)). For example, LPAAT3 deficient mice exhibit reductions in DHA-containing phospholipids in the retina

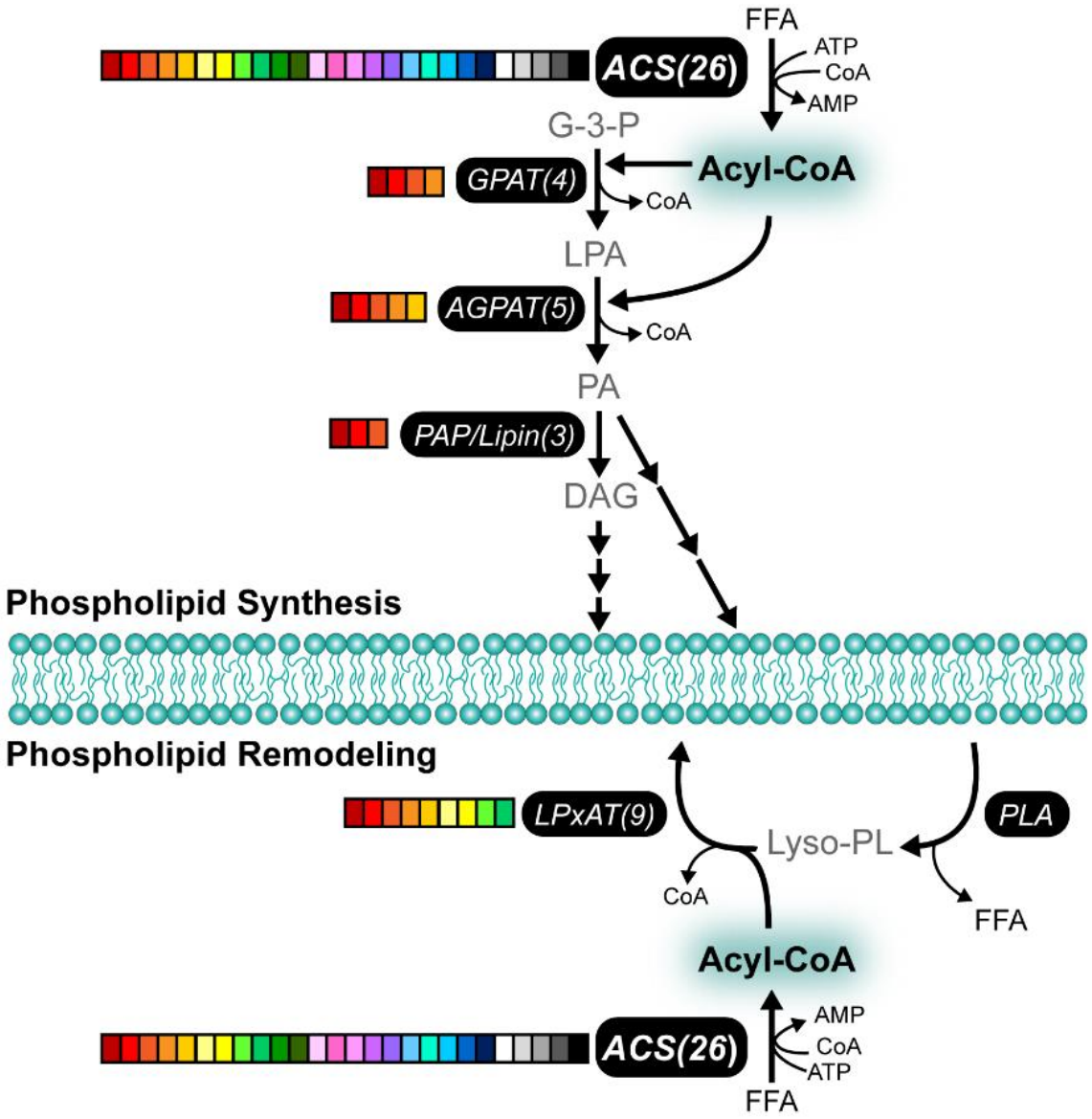

Figure 2.4 Greatest genetic diversity for ACSs within phospholipid metabolism Schematic representation of the major enzymes involved in de novo phospholipid synthesis (top) and phospholipid remodeling (bottom). Colored boxes represent the number of genes in the enzyme family (1).

and testes while LPIAT1/MBOAT7 deficient mice show a defect in the remodeling of AA within phosphatidylinositol (89-92). While LPxAT activity affects acyl-chain diversity, we highlight that the substrate for LPxATs are acyl-CoAs, the product of ACS enzyme activity. Hence, the addition of a new acyl-chain during the Land's cycle is driven by the

combined preferences of LPxATs and the availability of ACS-generated acyl-CoA substrates. It is important to consider that cellular acyl-CoAs concentrations are rather low and will result in toxicity upon accumulation, therefore acyl-CoAs are rapidly metabolized suggesting that substrate selection may predominately fall to ACS enzyme action rather than acyltransferases. This concept was exemplified by our recent work demonstrating that loss of one particular ACS, Acsl6, greatly diminishes membrane DHA in the brain (48). In summary, both the Kennedy and Land's cycle rely on ACS action, performed by a large and diverse family of enzymes, which likely shapes fatty acid selectivity for phospholipid acyl-chain diversity by providing the limiting substrate, acyl-CoA.

To better understand the possible role the large family of ACS enzymes in regulating acyl-chain diversity, the totality of ACS enzymatic action should be considered. For instance, ACS not only performs the initiation reaction required for cellular fatty acid metabolism, it is also an energy-dependent and therefore committing step for fatty acid cellular retention. Thus, the formation of an acyl-CoA accomplishes two outcomes: First, it traps the fatty acid within the cell, and second, it activates the fatty acid for downstream metabolism (93, 94). The notion that each ACS uniquely contributes to regulating cellular lipidome diversity is predicated upon several observations. First, the existence of 26 ACSs in humans and 25 in rodents, all encoded by distinct genes and whose phylogenetic expansion increases with higher ordered organisms, suggests non-redundancy and selectivity at a functional level (78, 95, 96). Second, each ACS enzyme exhibits diverse and unique tissue- and subcellular-specific dispersion throughout the body (97-99). Third, each ACS enzyme has distinct enzyme kinetics, substrate preferences, and regulatory

mechanisms (78). Fourth, members of the ACS family cannot compensate for one another (100-104). Fifth, mounting evidence demonstrates that each ACS enzyme directly regulates the channeling of fatty acids towards specific metabolic fates (100-104). Sixth, ACS action sits at the committed and pinnacle site in cellular lipid metabolism where acyl-chain selectivity ultimately occurs. Acyl-CoA partitioning by ACS enzymes is a long-established theory to explain the regulatory mechanisms that control cellular fatty acid metabolic flux (80, 93, 94, 105). This theory is founded on the many nuances of the ACS family (78, 80, 97, 98, 106, 107). Data supporting this theory was generated from *in vitro* models of ACS overexpression or knockdown where distinct ACSs exert distinct effects on fatty acid metabolic flux and cannot compensate for one another (103, 108-110). This theory was largely confirmed by *in vivo* data demonstrating that several different ACS enzymes direct fatty acids towards specific downstream metabolic pathways (48, 98, 101, 111). The ability of ACS enzymes to channel fatty acids towards metabolic fates is predicted to depend, in part, on the subcellular location and the binding partners of a particular ACS, properties which can vary between cell-types and physiological conditions, even for the same ACS enzyme. For example, one such ACS, ACSL1, is predominantly localized to the mitochondria and is shown to preferentially guide fatty acids to mitochondrial beta-oxidation in the heart, muscle, and brown adipose (100, 112). However, ACSL1 also regulates cardiolipin acyl-chain composition, suggesting a role for ACSL1 in mitochondrial beta-oxidation and phospholipid metabolism simultaneously (113). The regulation between these dual roles for this enzyme is partly explained by transient protein-interactions of ACSL1 that are mediated by metabolic states. Specifically, ACSL1 binds to lipid droplet proteins only in the nutrient-deprived state when

fatty acids are needed for energy production through beta-oxidation (114, 115). These data suggest that temporary ACS-protein interactomes facilitate fatty acid metabolic flux through demand-driven mechanisms. Here, we will describe the potential roles that ACSs may play in regulating brain lipidome diversity.

Acyl-CoA Synthetase nomenclature

The ACS family of enzymes is large and thus the nomenclature is an important consideration. The nomenclature of the ACS family is primarily based upon the preferred fatty acid chain-length and is broken into subfamilies termed short (ACSS), medium (ACSM), long (ACSL), and very-long-chain (FATP/ACSVL) ACSs, with several other subfamilies including the family-member (ACSF) and bubblegum (ACSBG) ACSs (Table 2.1) (78, 116). Of note, the ACSVL subfamily is often referred to as the fatty acid transport protein (FATP) subfamily. While each of the six members of the FATP/ACSVL family has acyl-CoA synthetase activity, the use of FATP rather than the ACSVL designation results in the interpretation that FATPs are transporter proteins transporting fatty acids across the plasma membrane (117). Debate remains regarding the ability of FATPs to transport fatty acids, independent of ACS activity (116). However, it is speculated that the ability of FATPs, as well as all other ACS enzymes, to increase cellular fatty acid uptake is mediated by the activation of fatty acids after passing through the plasma membrane, thereby trapping fatty acids as a direct result of their CoA-ligation via ACS activity, a concept termed ‘vectorial acylation’ (118). Importantly, endogenous FATP/ACSVLs are not localized to the plasma membrane negating their role as fatty acid transporters for cellular fatty acid uptake (117). Despite attempts to rename the FATP subfamily of enzymes to ACSVLs (119, 120), the widespread use of FATP nomenclature continues,

often resulting in erroneous experimental designs and data interpretations. The ACS nomenclature is further complicated by differences between species (i.e. humans, mice, rats, etc. reviewed elsewhere (78, 117, 120); thus caution is advised when using nomenclature as a basis for assigning ACS protein function and for interspecies interpretations.

Acyl-CoA Synthetases in the brain

Of the 26 ACS enzymes, not all are robustly expressed in the brain. Based on the human protein atlas [www.proteinatlas.org] (121) the following ACSs are detectable in the brain: all 3 short-chain ACSs, 2 of the 7 medium-chain ACSMs (ACSM3 and -5), 1 of the 2 bubblegum ACSs (ACSBG1), all 3 family member ACSFs, all 5 of the long-chain ACSLs, and all 6 of the very-long-chain ACSVLs/SLC27As (Table 2.1). Of all the ACSs only two are specifically enriched in the brain when compared to peripheral tissues: ACSBG1 and ACSL6 (121). ACSM6 is found in humans and expressed in the brain, but this family member is not present in rodents, suggesting that it may create a further advantage for cognitively enhanced organisms. Except for ACSM6, human, mouse, and rat tissues have similar expression patterns of the ACSs (97). The detection of the majority of ACSs in the brain suggests a high degree of fatty acid metabolic control in this organ. The expression of ACSs highly enriched in the brain compared to peripheral tissues suggests specific and potentially unique roles for these ACSs in modulating fatty acid metabolism within the central nervous system.

ACS	Human Protein Aliases	Tissue enriched	Detected in Brain
ACSS1	ACAS2L, AceCS2L, dJ568C11.3, MGC33843	Placenta	Y
ACSS2	ACAS2, AceCS, ACS, ACSA, dJ1161H23.1	Skeletal muscle	Y
ACSS3	FLJ21963	-	Y
AACS	ACSF1, FLJ12389, SUR-5	-	Y
ACSF2	ACSMW, FLJ20920	Kidney	Y
ACSF3	-	-	Y
ACSM1	BUCS1, MACS1	Breast	-
ACSM2A	A-923A4.1, ACSM2, MGC150530	Kidney, Liver	-
ACSM2B	ACSM2, HXMA, HYST1046	Kidney, Liver	-
ACSM3	SA, SAH	Liver, ovary, pancreas	Y
ACSM4	-	Lymphoid tissue, testis	-
ACSM5	FLJ20581	Liver	Y
ACSM6	bA310E22.3, C10orf129	Lymphoid tissue, pancreas, stomach	-
ACSL1	ACS1, FACL1, FACL2, LACS, LACS1, LACS2	Adipose, liver	Y
ACSL3	ACS3, FACL3, PRO2194	Parathyroid gland	Y
ACSL4	ACS4, FACL4, LACS4, MRX63, MRX68	-	Y
ACSL5	ACS2, ACS5, FACL5	Intestine	Y
ACSL6	ACS2, FACL6, KIAA0837, LACS2, LACS5	Brain, testis, seminal vesical, ductus deferens	Y
ACSBG1	BG1, BGM, FLJ30320, hBG1, hsBG, KIAA0631, MGC14352	Adrenal, brain, skin	Y
ACSBG2	BGR, DKFZp434K1635, PRTD-NY3	Testis	-
ACSVL1	SLC27A2 FACVL1, FATP2, hFACVL1, HsT17226, VLACS, VLCS	Liver	Y
ACSVL2	SLC27A6, FACVL2, FATP6, VLCS-H1	Adrenal gland	Y
ACSVL3	SLC27A3, FATP3, MGC4365	-	Y
ACSVL4	SLC27A4, FATP4	Intestine	Y
ACSVL5	SLC27A1FATP, FATP1, FLJ00336, MGC71751	-	Y
ACSVL6	ACSB, SLC27A5, FACVL3, FATP5, FLJ22987, VLACSR, VLCS-H2, VLCSH2	Liver	Y

Table 2.1. Human ACS proteins in the brain
‘-‘ denotes lack of alias, enrichment, or detection in brain (1).

Acyl-CoA synthetases in the brain by cell type

The brain consists of several distinct broad cell type classifications. Neurons are a major class of cells in the central nervous system whose function is to transmit information across the brain and to the periphery (122). A second major class of cells in the brain is glial cells, which can be subdivided into distinct cell types such as astrocytes, oligodendrocytes, and microglia (122). Thus, each cell type performs specific, metabolically distinct functions. To estimate if different ACSs may differentially regulate the lipidome in each brain cell type, cell-type-specific ACS expression needs to be defined. To this end, information on differential expression of ACSs across cell types of the brain can be gleaned from large-scale omics studies on isolated cell-types. The ideal timepoint to successfully isolate and obtain a high yield of distinct, purified cell types from the brain is early postnatal development (123-125). However, age is an important factor when assessing cell-type expression of genes in the brain because neurons, astrocytes, and microglial undergo significant maturation processes during fetal and post-natal development that significantly change expression profiles. In agreement, not all of the ACS genes are expressed in early postnatal development, for instance, Acsl6 which is one of the two ACSs most enriched in the brain, is expressed at very low levels in early postnatal period and increases greatly across post-natal development (48, 126). Thus, any gene that changes between early postnatal and adult is not well captured in these databases. Advances in technology have overcome these obstacles with the advent of single-cell transcriptomics to define distinct cell type transcripts from adult human brain (127, 128). The total counts per million from adult human brain data is graphically represented (Figure 2.5). Here, we observe that some ACSs are highly enriched in a

single cell type. For example, Acsbg1 is nearly exclusively expressed in astrocytes, Acsm5 is exclusive to microglia, and Acss1 is most abundant in astrocytes. Acsl6 is split between two cell types, astrocytes and neurons. Yet most of the ACSs are expressed at variable degrees across all cell types. The neuronal cells are further dissected in the database and are broadly separated into either GABAergic or glutamatergic neurons. Interestingly none of the ACSs showed dominance in either GABAergic or glutamatergic neurons, but rather segregate into more narrow cell populations that are differential for each ACS. The milieu of ACSs expressed in distinct cell types and variation of their relative abundance likely contributes to the highly differential regulation of acyl-chain composition across the various cell types of the central nervous system, as demonstrated by brain lipid imaging (129-131). The use of mass spectrometry-based approaches to resolve single-cell lipidomic fingerprints and high-resolution imaging in the brain has begun to further define cell-type specific lipid composition (132, 133). Linking the

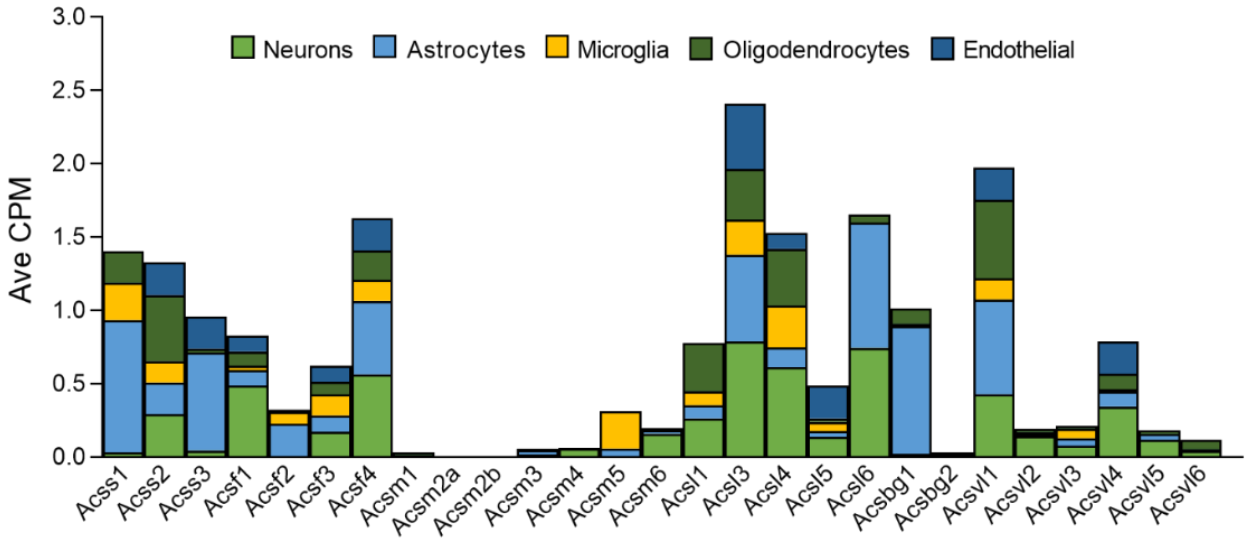

Figure 2.5. Brain ACS enzyme abundance and cell-type distribution
RNA, counts per million (CPM), averaged for the different cell types using human brain RNAseq data from the Allen Brain Atlas Transcriptomics Explorer application for each ACS (1).

enzymatic lipid metabolizing machinery to the regulation of the cell-specific lipidome requires further investigation.

When considering the diversity of membrane acyl-chains across cell types and regions of the brain, it is important to distinguish the regulation of acyl-chain uptake from retention. Retention of a given fatty acid within a cell or organ system is mainly driven by the ACS reaction which traps and commits fatty acids for cellular metabolism. However, two factors contribute to acyl-chain composition: first, ACS-mediated selectivity for committing fatty acids to cellular metabolism; and second, the pool of available fatty acid substrates that a given cell is exposed to. The available fatty acid pool is particularly enigmatic when considering the brain because of the long-standing mystery regarding the mode and key players regulating fatty acid transport across the blood-brain barrier, particularly the transport of PUFAs such as DHA. In 2014, Mfsd2a was reported to act as a transporter of lysophospholipids (lysoPLs), preferring DHA-containing lysoPLs (134). Mfsd2a is highly expressed in the endothelium of the blood-brain barrier and the loss of Mfsd2a in mice reduced brain DHA content by half (134). These data suggest that transport of lysoPL through Mfsd2a is a major contributor to brain DHA. However, Mfsd2a is also required for cargo exchange across the blood-brain barrier, thus its deficiency results in neuronal loss, thereby reducing brain DHA as a direct result of lower neuronal abundance (135, 136). Moreover, kinetic studies demonstrate that free DHA, rather than lysoPL-DHA, is the major contributor to brain DHA content (137). Taken together, these data cast doubt on the role of Mfsd2a as a major regulator of brain DHA. The transport of free DHA across the blood-brain barrier can occur independent of proteins, as free fatty acids can freely cross membranes. However, retention of free fatty acids such as DHA

requires their activation within the parenchyma of the brain, thereby requiring the action of ACS (138). Beyond acquisition of new fatty acids within the parenchyma, retention of pre-existing membrane acyl-chains also requires ACS action during the highly active process of brain phospholipid remodeling (82-84). Thus, the combined need for ACSs in phospholipid remodeling, phospholipid de novo synthesis, and brain fatty acid retention, implies that ACSs have the major role in regulating brain acyl-chain specificity in membranes. The requirement of ACS activity in the regulation of brain fatty acid uptake and retention was nicely depicted in the highly complimentary commentary that accompanied my PNAS research article (Figure 2.6)(48, 138).

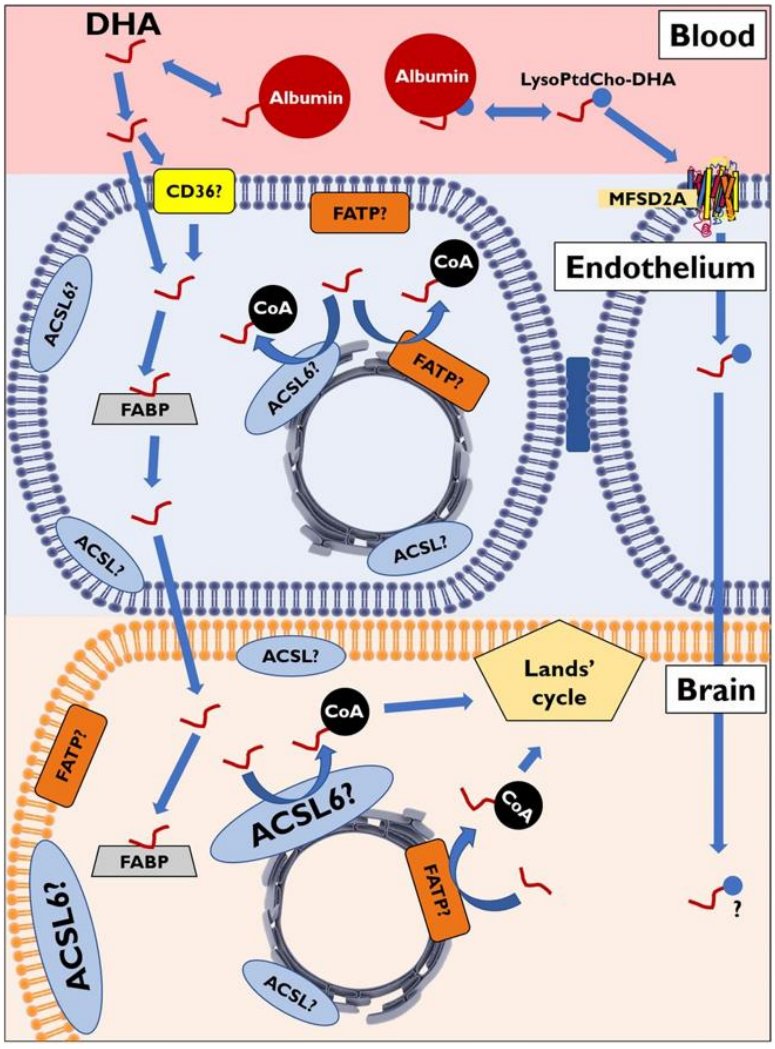

Figure 2.6. Regulation of brain DHA uptake and retention
The transport of DHA across the brain microvascular endothelial cells is proposed to be by passive diffusion and via transport proteins (i.e. Mfsd2a). FATP/ACSVL, FABP, and ACS are predicted to facilitate brain DHA uptake and retention (138).

Evidence of ACSs in regulating brain lipidome diversity

Because brain ACS isoforms have different substrate preferences, subcellular locations, and are expressed differently across cells of the brain, brain ACSs likely have distinct functions in regulating the brain lipidome. Here, we provide a brief summary of relevant findings related to high brain expressing ACSs that regulate the metabolism of long-chain fatty acids, as these are the predominant fatty acids that populate the phospholipidome.

Acsl1: Acsl1 is expressed across the body but highly in adipose, liver, and muscle tissues (97). Acsl1 predominantly channels fatty acids into mitochondrial oxidative metabolism for energy production (100, 112, 139). Acsl1 prefers saturated fatty acids as substrate but also has activity for PUFAs such as AA and linoleic acid (LA, C18:2n6) (140). While conditionally deficient Acsl1 mice are reported (100, 112, 113, 139, 141-144), the effects of Acsl1 deficiency on brain metabolism, lipidome, and phenotypic outcomes remain unknown.

Acsl3: Acsl3 is expressed in adipose, liver, and adult brain, but most abundantly expressed in the brain during fetal development (97, 145). ACSL3 has high substrate preference for alpha-linolenic acid (ALA, C18:3n3), LA, and AA, but very little activity for DHA (146). *In vitro* studies and association-based research suggests that Acsl3 has many roles in regulating lipid and cell function, including regulation of transcription, ferroptosis, inflammation, and in channeling fatty acids towards beta-oxidation and phospholipid synthesis (103, 147-149). The role that Acsl3 plays in brain remains unknown.

Acsl4: Acsl4 is expressed in the brain, but also widely expressed throughout the body. Acsl4 is distributed across brain cell types and found in the mitochondria, ER, and

peroxisomes (150, 151). Acsl4 has a high preference for EPA and AA, and also uses eicosanoids and related metabolites (146) as substrate (80, 140, 152, 153). AA is highly abundant in the brain and is substrate for pro- and anti-inflammatory metabolites, and while conditionally deficient Acsl4 mice are reported, the effects of brain Acsl4 deficiency in mice remain unreported (38, 154). In humans, ACSL4 is implicated in bipolar disorders because valproate, a common drug used to treat bipolar disorders, is a substrate for ACSL4 and appears to disrupt Acsl4-mediated metabolism (155-157). ACSL4 is also suspected to be important for neural development, a process when neural membrane and phospholipid synthesis increases the incorporation of AA in the brain (64, 158). *In vitro* evidence demonstrates that Acsl4 protein expression increases in response to nerve growth factor and that the loss of Acsl4 impairs neuronal differentiation and dendritic spine formation (158, 159). In agreement, ACSL4 is associated with neural development disorders, such as nonspecific X-linked mental retardation (160-163). These data suggest an important role for Acsl4 in brain development and eicosanoid metabolism, however, further investigation is warranted.

Acsl6: Acsl6 is particularly enriched in the brain, has a high preference for DHA as its substrate, and its manipulation *in vitro* is directly correlated with neurite extensions (97, 108, 140, 146, 164). In 2018, we reported the first Acsl6 deficient mouse model and demonstrated that Acsl6 regulates the incorporation of DHA into neural membranes, resulting in ~50% depletion of brain DHA in *Acsl6* deficient mice (this dissertation) (48, 138). While we showed that Acsl6 is required for brain DHA enrichment, the substrate preferences for Acsl6 are a complicated matter due to the identification of at least 5 variants of Acsl6, each with variable enzyme kinetics (146, 165-167).

ACSL6 encodes two AUG-start-codon containing exons that can be alternatively spliced to generate products that differ by 25 amino acid residues in the N-terminus, a region that controls ACSL6 subcellular targeting (94). ACSL6 also encodes two mutually exclusive gate domain (i.e. fatty acids binding domain) encoding exons that contain either tyrosine or a phenylalanine residues that are critical for determining substrate preferences and are referred to as the Y-exon and F-exon, respectively (168). Since the gate controls the access to the catalytic site, changes in single amino acids alter substrate selectivity (168). Specifically, the Y-exon prefers linoleic acid and ALA whereas the F-exon strongly prefers DHA and ALA over palmitate (146). All variants are detectable in the brain by mRNA, however the protein abundance and cell-type expression remain unknown (94, 111, 165, 166, 168). Thus, the role of each variant in regulating the brain lipidome is unclear. Data presented in this dissertation show that neuronal ACSL6 but not astrocyte ACSL6 expresses the DHA-preferring domain and thus, is a major contributor of DHA enrichment in the brain.

In humans, mutations in ACSL6 are linked to schizophrenia and addictive behaviors such as tobacco smoking (169-174). Interestingly, people with schizophrenia tend to be heavy smokers. These data strongly suggest a critical role for Acsl6 in enriching the brain with DHA for neuroprotection. Research to determine the nuances of Acsl6-mediated metabolic control, its relation to brain function and disease, and mechanisms therein is ongoing.

Acsbg1: Acsbg1 is highly enriched in the brain and nearly exclusively in astrocytes. Acsbg1 has broad substrate preference for long-chain saturated and unsaturated fatty acids (175, 176). The knockdown of Acsbg1 *in vitro* reduces ACS activity and fatty acid

oxidation (176). Thus, while these data suggest a role for Acsbg1 in long-chain fatty acid oxidation in astrocytes, its role *in vivo* in brain metabolism and function remain unknown.

Acsvl1/Fatp2: Fatp2 is a very-long-chain fatty acid preferring ACS detectable in the brain (97). The overexpression of Fatp2 *in vitro* increases uptake of omega-3 fatty acids, ALA and DHA (177). Fatp2 is the center of controversy regarding the role of FATP proteins in mediating fatty acid uptake in a manner independent or dependent of its ACS activity. This is because two variants of Fatp2 exist, Fatp2a and Fatp2b, the latter of which is void of ACS activity due to the absence of an ATP binding site (178). Because Fatp2b expression *in vitro* increases fatty acid uptake, it is speculated that ACS activity is not necessary for FA uptake by FATPs (178). However, ACSs are predicted to dimerize, thus the ACS activity of Fatp2b's dimer partner may facilitate FA uptake in Fatp2b overexpressing cells (179). The brain expresses Fatp2a, not Fatp2b, yet the global deletion of Fatp2 does not result in observed brain-related phenotypes, reductions in total brain ACS activity, or changes in brain very-long-chain fatty acid content (180). Thus, the role that Fatp2 plays in brain metabolism appears to be negligible.

Acsvl4/Fatp4: Fatp4 is highly expressed in the brain, intestine, oxidative skeletal muscle, skin, sperm, and retina (97, 98). Fatp4 has preference for very-long-chain fatty acids which are abundantly found in the skin, sperm, and retina, where Fatp4 is enriched (119, 181, 182). Global FATP4 deficient mice present with degeneration of rod photoreceptors and neonatally lethal restrictive dermopathy characterized by wrinkle-free skin and severe defects in the skin barrier that cause death within hours of birth (182-186). As expected, the loss of FATP4 reduces ≥26-carbon fatty acids in phosphoglycerolipids in the epidermis by more than 50%. FATP4 may also activate hydroxy fatty acids, intermediates

of the acyl-ceramide pathway, which may further contribute to skin barrier dysfunction in FATP4 null mice (187). Within the brain, FATP4 is found in microvessel endothelial cells, but also diffusely across the brain (126, 188). FATP4 null mice show reductions in very-long-chain fatty acids in the brain, yet neurological phenotypes are not reported.

Acsvl5/Fatp1: Fatp1 is expressed in the brain, retina, muscles, adipose, kidney, lung, skin and endothelium, and has high ACS activity for the very-long chain fatty acid lignocerate (C24:0) relative to palmitic acid (C18:0) (97, 189). The global loss of FATP1 in mice results in protection from high-fat diet-induced insulin resistance and is required for thermogenic regulation by brown adipose tissue (190-192). FATP1 is expressed in the retina and null mice present with reduced response to light by electroretinogram and enhanced age-related morphological deterioration of the retina (193). Brain lipid composition and the neurological phenotype of the FATP1 null mice remain unknown.

In summary, the phospholipid composition of membranes is highly regulated with considerable contribution from ACS enzymes. ACSs are a family of enzymes that confer the first and committed step in cellular metabolism of fatty acids and whom we predict are critical regulators of phospholipid diversity. The work in this dissertation demonstrates a critical role for one such ACS, Acsl6, in regulating brain membrane enrichment with the neuroprotective omega-3 fatty acid DHA (48, 138). Continued investigations of ACSs in the central nervous system will improve our understanding of normal brain physiology as well as the link between lipid metabolism and pathophysiology of neurological disorders. The substrate preferences, effects on fatty acid metabolic flux, and subcellular localizations of the ACSs and their variants in the central nervous system remain largely unresolved. Determining how fatty acid metabolism is regulated within each cell type, and

by which ACS will greatly increase our understanding of how lipid metabolism within and between different cell types leads to proper brain function and disease prevention to inform personalized nutrition and therapeutic strategies.

CHAPTER III

ROLE OF ACSL6 IN BRAIN CELLULAR FATTY ACID METABOLISM

To date, all studies directly investigating ACSL6 properties in relation to the brain have been performed *in vitro*. To investigate the role of ACSL6 in a physiologically relevant model we generated a novel conditional *Acsl6* deficient mouse (*Acsl6*$^{-/-}$). Here, we demonstrate that the loss of ACSL6 reduces phospholipid DHA levels in the brain suggesting that ACSL6 activity is essential for brain DHA enrichment. Moreover, our findings show that *Acsl6* deletion in mice disrupts motor function and induces microglia activation and astrogliosis. These data identify ACSL6 as an important regulator of DHA metabolism in the brain that confers protection against neural dysfunction.

Acyl-CoA synthetase 6 enriches the neuroprotective omega-3 fatty acid DHA in the brain

Regina F. Fernandez[a], Sora Q. Kim[b], Yingwei Zhao[b], Rachel M. Foguth[c], Marcus M. Weera[4], Jessica L. Counihan[e], Daniel K. Nomura[e], Julia A. Chester[d], Jason R. Cannon[c], Jessica M. Ellis[a,1]

[a] Department of Physiology, East Carolina University, Greenville, NC, 25878

[b] Department of Nutrition Science, Purdue University, West Lafayette, IN, 47907

[c] School of Health Sciences, Purdue University, West Lafayette, IN, 47907

[d] Department of Psychological Sciences, Purdue University, West Lafayette, IN, 47907

[e] Department of Nutritional Sciences and Toxicology, University of California Berkeley, Berkeley, CA, 94720

[1] To whom correspondence should be addressed. Email: ellisje18@ecu.edu

Abstract

Docosahexaenoic acid (DHA) is an omega-3 fatty acid that is highly abundant in the brain and confers protection against numerous neurological diseases, yet the fundamental mechanisms regulating the enrichment of DHA in the brain remain unknown. Here, we have discovered that a member of the long-chain acyl-CoA synthetase family, Acsl6, is required for the enrichment of DHA in the brain by generating an Acsl6-deficient mouse ($Acsl6^{-/-}$). Acsl6 is highly enriched in the brain and lipid profiling of $Acsl6^{-/-}$ tissues reveals consistent reductions in DHA-containing lipids in tissues highly abundant with Acsl6. $Acsl6^{-/-}$ mice demonstrate motor impairments, altered glutamate metabolism, and increased astrogliosis and microglia activation. In response to a neuroinflammatory lipopolysaccharide injection, $Acsl6^{-/-}$ brains show similar increases in molecular and pathological indices of astrogliosis compared with controls. These data demonstrate that Acsl6 is a key mediator of neuroprotective DHA enrichment in the brain.

Significance

Neurodegenerative diseases are a leading cause of morbidity and mortality among older adults, the fastest growing segment of the US population. Neurodegenerative disease risk is reduced by high dietary intake of the omega-3 fatty acid, docosahexaenoic acid (DHA), a highly abundant lipid in the brain. Yet the fundamental mechanisms regulating brain DHA enrichment remain unknown. Here, we have made a key discovery that Acyl-CoA Synthetase 6 (Acsl6) is required to specifically enrich DHA in the brain. Of importance, mice lacking Acsl6 have impaired motor function and increased astrogliosis, demonstrating the critical need for Acsl6-mediated lipid metabolism in neurological health.

This work provides critical insight into longstanding mysteries surrounding brain DHA metabolism and has broad-reaching health implications.

Keywords: fatty acid metabolism, neurometabolism, docosahexaenoic acid, acyl-CoA synthetase, brain lipids

Introduction

The omega-3 docosahexaenoic acid (DHA) and omega-6 arachidonic acid (AA) are the most abundant polyunsaturated fatty acids in the brain as the healthy brain contains ~15% DHA, three to four times higher than the amount of DHA in any other tissue, and ~13% AA (55, 194-196). Importantly, low dietary intake of DHA, afflicting a majority of the US population (197), increases the risk of neurodegenerative diseases and related molecular events in rodents and humans (4-6). The neuroprotective properties of DHA are attributed to its ability to act as an antioxidant, increase membrane fluidity, and serve as the precursor for specialized proresolving mediators that attenuate inflammation and oxidative stress (40, 42, 198, 199). Thus, low brain DHA results in neurodegenerative symptomology, suggesting a role for brain DHA metabolism in the onset and progression of neurodegeneration. However, little is known about the fundamental regulatory mechanisms controlling brain fatty acid metabolism and incorporation into phospholipids.

Cellular fatty acid metabolism is initiated by the activation of free fatty acids to form acyl-CoA to trap fatty acids within cells and provide the substrate for nearly all fatty acid metabolic processes, including membrane phospholipid biosynthesis. The generation of acyl-CoAs is mediated by the Acyl-CoA synthetase (ACS) family of enzymes with diverse substrate preferences, regulatory mechanisms, binding partners, expression patterns across tissues, and subcellular localization (78, 97, 98, 120). We and others have shown that these distinct properties allow the ACS family of enzymes to channel specific fatty acids toward directed metabolic fates (100, 101, 112). Of these ACS enzymes, ACSL6 is nearly exclusively expressed in the brain according to mRNA abundance, suggesting that

it may play an important and unique role in regulating brain lipid metabolism (97, 167, 200). However, the role of Acsl6 in regulating brain lipid metabolism in vivo has remained unknown. We have generated an Acsl6-deficient mouse ($Acsl6^{-/-}$) and show that Acsl6-deficient mice exhibit reduced abundance of brain DHA, suggesting that Acsl6 is required for the incorporation and enrichment of the omega-3 fatty acid DHA in the brain. In agreement with the neuroprotective effects of DHA, $Acsl6^{-/-}$ mice exhibit motor dysfunction and increased astrogliosis. These data demonstrate that Acsl6 is critical for DHA metabolism in the central nervous system and that Acsl6-mediated lipid metabolism is critical for normal brain function and neuroprotection.

Results

Acsl6 Is Highly Enriched in the Central Nervous System

To confirm that Acsl6 protein, like its mRNA, is enriched in the central nervous system, an antibody was generated and used to demonstrate enrichment of ACSL6 protein in mouse brain, with minor expression detected in the spine, eye, and testis (Fig. 1A). Expression of Acsl6 was barely detected in all other tissues assayed (Fig. 1A). Acsl6 protein was abundant across brain regions but compared with hypothalamus, hippocampus, and cortex, Acsl6 was most abundant in the midbrain, medulla/pons, and cerebellum (Fig. 1B). Along the course of development, Acsl6 mRNA and protein was detectable at low levels in embryonic and early postnatal brain but increased at ∼7 d of age and linearly up to day 28, remaining abundant up to 1 y of age, data that represents a combination of male and female mice (Fig. 1C and D). Thus, brain Acsl6 protein is induced 25-fold from fetus to adult brain, later in development than several DHA-metabolizing enzymes (FABP5 and Mfsd2a) (126, 201, 202). These data suggest that mouse Acsl6 is a developmental-induced central nervous system and testes-specific protein.

Generation of Acsl6 Knockout Mice

To determine the role and importance of Acsl6-mediated fatty acid metabolism and function, we generated an Acsl6 conditionally deficient mouse strain ($Acsl6^{flox/flox}$) and bred these mice to CMV-Cre expressing mice to generate a total body germ-line deletion of Acsl6 ($Acsl6^{-/-}$) (SI Appendix, Fig. S1A). $Acsl6^{-/-}$ mice were viable and born at expected Mendelian ratios (SI Appendix, Fig. S1B). The loss of Acsl6 protein in $Acsl6^{-/-}$

was confirmed by Western blotting (Fig. 2 A and B). The mRNA of other Acsl isoforms were not induced to compensate for the loss of Acsl6 (Fig. 2C). Initial rates of ACS activity were measured in total membrane fractions using radiolabeled fatty acid substrates, encompassing potential activity from all 25 ACS enzymes and assay conditions optimized using oleate (OA) as the substrate (SI Appendix, Table S1). The loss of Acsl6 reduced total ACS activity for palmitate (PA) (C16:0) by 44%, OA (C18:1n9) by 41%, AA (20:4n6) by 36%, and DHA (22:6n3) by 37% in the midbrain (Fig. 2D), and similarly in the cortex (SI Appendix, Fig. S1C). Thus, the total ACS activity was reduced ~40% in Acsl6$^{-/-}$ brain. The loss of Acsl6 did not alter body length, weight, or food intake compared with littermate controls (SI Appendix, Fig. S1 D–F), nor did it alter brain weight, length, and width (SI Appendix, Fig. S1G and H) or cerebellar ultrastructure (SI Appendix, Fig. S1I) at 2 mo of age. Together, these data show that the loss of Acsl6 does not impact viability and that Acsl6 contributes to ~40% of total ACS activity in the brain.

To gain insight into how Acsl6 affects neurometabolism more broadly, an unbiased metabolomics analysis was performed on control and Acsl6$^{-/-}$ hippocampus from 2-mo-old mice following an overnight fast. Acsl6$^{-/-}$ mice exhibit alterations in hippocampal tryptophan, glutathione, methionine, and cysteine that have potential implications for disruptions in antioxidant and neurotransmitter homeostasis (Fig. 2E). Several metabolites related to glucose and energy metabolism were altered in the Acsl6$^{-/-}$ hippocampus including, lactate, glucose-6-phosphate, phosphoenolpyruvate, fumarate, and pantothenate (CoA synthesis) (Fig. 2F). Acsl6$^{-/-}$ hippocampal nucleotides, cytosine and uracil, and the nucleotide synthesis intermediate, CDP, were altered (Fig. 2G), which may reflect altered nucleic acid synthase or transcriptional activity.

Acsl6 Deficiency Decreases Brain Omega-3 Docosahexaenoate-Containing and Increases Omega-6 Arachidonate-Containing Lipids

To determine how the loss of Acsl6 affects brain lipid composition, global unbiased lipidomic profiling of the cerebellum from 2-mo-old control and Acsl6$^{-/-}$ female mice was performed. The fatty acid profile of Acsl6$^{-/-}$ cerebellum, compared with controls, was marked by 22–71% reductions in phospholipids, lysophospholipids, monoacylglycerol, and diacylglycerol containing DHA and 25–61% increases in nearly every lipid species containing AA (Fig. 3). The pattern of reduced DHA and increased AA in Acsl6$^{-/-}$ cerebellum was also reflected in the free fatty acid and in the ether-linked and plasmalogen lipids (SI Appendix, Table S2). This level of reduced DHA, and increased AA, is similar to that seen after two generations of breeding rodents on an omega-3 deficient diet, suggesting that Acsl6 is a major contributor to brain DHA enrichment (203). Phospholipids containing the monounsaturated fatty acid OA remained generally unchanged between genotypes. To determine if overnight fasting altered lipid composition in this genetic model, lipidomics was performed on cerebellum of control and Acsl6$^{-/-}$ mice challenged with overnight fasting to reveal similar genotypic alterations compared with the fed state (SI Appendix, Table S2). Together, these data show that loss of Acsl6 reduced brain DHA content with a concomitant increase in the omega-6 fatty acid AA, suggesting that Acsl6 is critical for the incorporation of DHA into brain lipids.

To confirm Acsl6-mediated DHA deficiency across brain regions and spine, lipidomics was performed in midbrain, hippocampus, cortex, and spine of 2-mo-old female control and Acsl6$^{-/-}$ mice. All Acsl6$^{-/-}$ brain regions and spine had consistent 24–40% reductions in predicted DHA-containing and 26–54% increases in AA-containing

phospholipids (Fig. 4A–D), similar to the cerebellum (Fig. 3). To determine if Acsl6 deficiency altered peripheral lipid homeostasis, lipidomics was performed on liver (Fig. 4E) and soleus muscle (Fig. 4F) in control and Acsl6$^{-/-}$ mice to reveal no genotype effect on lipid content in these tissues. These data suggest that tissues expressing Acsl6 require it for DHA enrichment and that loss of Acsl6 does not impact whole-body lipid homeostasis.

To determine if Acsl6 deficiency-mediated impact on brain lipid metabolism was similar across sexes and with aging, lipidomics was performed on 6-mo-old male cerebellum (Fig. 4G) to demonstrate similar fatty acid profile compared with 2-mo-old female mice (Fig. 3). To determine the cell type-specific contribution of Acsl6-mediated lipid metabolic control, an astrocyte specific Acsl6 knockout mouse (Acsl6$^{G-/-}$) was generated resulting in a 57% reduction in Acsl6 protein in cerebellum (Fig. 4I). Acsl6$^{G-/-}$ cerebellum lipidomic analysis revealed similar reductions in DHA compared with Acsl6$^{-/-}$ mice; however, AA was decreased, rather than increased, in Acsl6$^{G-/-}$ (Fig. 4G and H). These data suggest that approximately half of brain Acsl6 is expressed in astrocytes and that Acsl6 is critical for DHA enrichment independent of cell type.

Loss of Acsl6 Disrupts Motor Function

Because dietary DHA deficiency perturbs motor function in rodents (70) and Acsl6 loss results in brain and spine DHA deficiency, we assessed motor and neurosensory function in Acsl6$^{-/-}$ mice. Acsl6$^{-/-}$ performed poorly during a wire hang test compared with controls (Fig. 5A). Poor performance during a wire hang test could be due to reduced strength; however, the control and Acsl6$^{-/-}$ mice performed similarly in the neuromuscular grip strength assessment, suggesting no disruption in upper body strength (SI Appendix,

Fig. S2A). Rotarod tests were performed to assess motor coordination and showed a trend toward reduced performance by Acsl6$^{-/-}$ mice at 12 mo of age (Fig. 5B). Open field data showed no alterations in time spent in center versus periphery and no differences in locomotor activity, suggesting that Acsl6$^{-/-}$ mice do not have altered anxiety in the open field test (SI Appendix, Fig. S2B). Sensorimotor assessment by adhesive removal test showed similar time spent attempting to remove the sticker between Acsl6$^{-/-}$ and control, but the Acsl6$^{-/-}$ made more failed attempts to remove the adhesive compared with controls (Fig. 5C). The startle response of Acsl6$^{-/-}$ mice trended toward a reduction in response to an electrical impulse to the footpad and was significantly reduced in response to acoustic stimuli (Fig. 5D and E). However, fear potentiated startle and prepulse inhibition were not different between genotypes (SI Appendix, Fig. S2C and D). Together these data show impaired neurosensory and motor function in Acsl6$^{-/-}$ mice.

Acsl6$^{-/-}$ Mice Exhibit Potentiated Astrogliosis and Microglia Activity

DHA has been shown to attenuate neuroinflammation in response to lipopolysaccharide (LPS) exposure in some, but not all, reports (204-208). To determine if Acsl6-mediated DHA deficiency altered neuroinflammation in the brain and in response to LPS, control and Acsl6$^{-/-}$ male mice were given a single i.p. injection of LPS. No genotype effect was observed for immobility or hippocampal mRNA abundance of the inflammatory genes with or without LPS at 2 and 6 mo of age (Fig. 6A–C and SI Appendix, Fig. S2E). However, the mRNA abundance of the microglia markers, CD68 and CD11b, was increased in Acsl6$^{-/-}$ hippocampus, compared with saline-injected controls (Fig. 6D), and immunohistochemical staining of microglia by Iba1 in the substantia nigra showed morphology consistent with microglia activation, as demonstrated by the retracted

processes and increased cell body size, in Acsl6$^{-/-}$ mice (Fig. 6E) (209). Motor controlling dopaminergic neurons originate in the substantia nigra and extend to the striatum. Quantification of Acsl6$^{-/-}$ striatal terminal density of tyrosine hydroxylase-positive dopaminergic neurons increased, compared with controls (SI Appendix, Fig. S2F). Together these data suggest increased microglia activation and/or activity in Acsl6$^{-/-}$ mice.

LPS-induced inflammatory response includes altered glutamate homeostasis, oxidative stress, and astrocyte activation (210-212). The mRNA abundance of genes related to glutamate metabolism, oxidative stress, and astrocyte activation in hippocampus were increased in Acsl6$^{-/-}$ compared with controls (Fig. 7A–C). In agreement, immunohistochemistry in the cerebellum of Acsl6$^{-/-}$ mice compared with controls showed increased GFAP signal (Fig. 7D). Specifically, in cerebellar gray matter, GFAP immunoreactivity in the protoplasmic astrocytes surrounding Purkinje cells was increased in Acsl6$^{-/-}$, compared with controls, with and without LPS (Fig. 7D). In cerebellar white matter where fibrous astrocytes reside, GFAP immunoreactivity was increased 7% and 9% in Acsl6$^{-/-}$ mice compared with controls with or without LPS, respectively, suggesting increased reactivity of the Acsl6-deficient astrocytes (Fig. 7D and E). Furthermore, the area occupied by GFAP+ cells in white matter was increased 45% in Acsl6$^{-/-}$ mice, compared with controls, suggesting increased number of astrocytes (Fig. 7F). Together, these data show that loss of Acsl6-elevated glutamate and oxidative stress-related gene markers, and increased astrogliosis, an effect that remains elevated after a proinflammatory LPS challenge.

Discussion

While DHA is the most abundant polyunsaturated fatty acid in the brain, models to study DHA in the brain are limited. The most predominant model is to modify dietary omega-3 fatty acid intake for multiple generations, a model confounded by whole-body and transgenerational effects. A model of DHA deficiency was reported in mice lacking major facilitator superfamily domain containing 2A (Mfsd2a). These mice have a ~50% reduction of DHA in brain due to impaired uptake of DHA-containing lysophospholipids through the blood–brain barrier (134). While this work provides evidence for a mechanism of DHA uptake into the brain, the contribution of lysophospholipids to brain DHA pool is minimal (137). Here, we report the loss of Acsl6, resulting in brain DHA deficiency. The requirement of Acsl6 to ligate DHA to the glycerol backbone argues a mechanism for Acsl6-mediated DHA enrichment that is independent of Mfsd2a. To date, the metabolic handling of blood-derived lipids once inside brain parenchyma has remained unclear. Here, we provide critical insight into Acsl6 as a major mediator of brain parenchyma DHA metabolism.

The existence of Acsl6 splice variants in the brain and their reported alternative substrate preferences, as well as Acsl6 cell type-specific expression, have complicated the implications of Acsl6 in lipid biology. Here, we were surprised to find nearly equivalent reductions in ACS activity for saturated, monounsaturated, omega-3 and omega-6 fatty acids in the Acsl6$^{-/-}$ brains relative to controls. We used the monounsaturated fatty acid oleate to optimize the enzyme assay conditions, thus optimization of the assay conditions using each substrate individually may be warranted to more accurately depict substrate-dependent enzyme activity. However, our lipidomic profiling reveal consistent and

significant reductions in DHA-containing lipids, strongly suggesting that, in vivo, Acsl6 is critical for DHA incorporation into brain lipids. Acsl6 deficiency induced reduction in brain DHA is likely due to compounding mechanisms that control substrate (i.e., DHA) accessibility via shuttling-, transport-, or phospholipid remodeling-related processes in a cell type-dependent manner, an area of research that requires further investigation.

DHA has received recent attention for its antiinflammatory properties (40, 42, 198, 213-215). However, not all reports are consistent with reduced neuroinflammation by DHA (46, 204-208, 216, 217). Because dietary DHA manipulation involves whole-body metabolism of DHA, the neuroprotective effects could be elicited by responses outside the central nervous system. Recently, the i.c.v. injection of LPS to mice with increased DHA content, due to dietary fish oil supplementation or fat-1 transgene expression, revealed little to no protective role for DHA in the neuroinflammatory response to LPS (207). In agreement with these results, our data show that the neuroinflammatory response to LPS was not augmented in male Acsl6-mediated DHA deficiency. However, at baseline, the loss of Acsl6 did increase microglia activation and astrogliosis. These data suggest that brain neuroinflammatory responses are increased by Acsl6 deficiency, potentially due to the loss of DHA and increase in AA; however, LPS-mediated inflammation is not dependent on Acsl6-mediated lipid metabolism.

Several human genome mapping studies have linked the ACSL6 loci to schizophrenia (170-172, 218). Here, we demonstrate motor symptoms, alterations to glutamate and dopaminergic homeostasis, all of which are consistent with characteristics of schizophrenia observed in patient and animal models (4, 62, 219). Several of these characteristics are also indicative of parkinsonism, such as alterations in the motor

function, dopaminergic, glutamate, and microglia homeostasis consistent with symptoms and pathology of Parkinson's disease patients and animal models (208, 220, 221). Thus, future investigation into the effects of Acsl6 on age-related neurodegenerative and psychiatric diseases are warranted.

In summary, we show that the loss of Acsl6 reduces DHA content in tissues in which it is highly expressed. The loss of Acsl6 disrupted brain metabolism, impaired motor function, and induced microglia activity and astrogliosis, indicative of neurological stress.

Experimental Procedures

Acsl6 knockout mice were created using a vector designed by the NIH-sponsored knockout mouse program to target Acsl6 exon 2 and injected into C57BL/6 embryonic stem cells to generate Acsl6 conditional mice ($Acsl6^{flox/flox}$) by Ingenious Targeting, Inc. $Acsl6^{flox/flox}$ mice were bred to CMV-Cre (Jackson Laboratories stock no. 006054) or GFAP-Cre (Jackson Laboratories stock no. 024098) transgenic mice to produce germ-line global ($Acsl6^{-/-}$) or GFAP-driven astrocyte-specific ($Acsl6^{G-/-}$) knockout mice. Mice were maintained on chow diet with soy oil as lipid source (Teklad Global 18% Protein Rodent Diet; Envigo) and 12-h light-dark cycles. All experiments were approved by Purdue Animal Care and Use Committee. For the LPS challenge, 6-mo-old male mice were injected intraperitoneally with sterile saline or Escherichia coli lipopolysaccharide (0.33 mg/kg; 396,000 EU/kg; serotype 0127:B8; Sigma) and tissues harvested 8 h after injection (222, 223).

Acknowledgments

We thank Natalie Mudd for assistance with mouse behavior assessment, Kolapo Ajuwon for use of the oxymax apparatus, and Shihuan Kuang for use of the grip strength apparatus.

Supplementary Information

This article contains supporting information.

Figure 3.1. Acsl6 is highly enriched in the central nervous system

Quantification of Western blot for Acsl6 normalized to HSP60 in mouse tissues (A), brain regions (B), and mRNA (C) and protein (D) in brain across development, n=3. BAT, brown adipose tissue; Cere, cerebellum; Epi, epididymal white adipose tissue; Gastro, gastrocnemius; Hipp, hippocampus; Hyp, hypothalamus; Med/Pons, medulla oblongata and pons; Mid, midbrain. Data represent averages ± SEM.

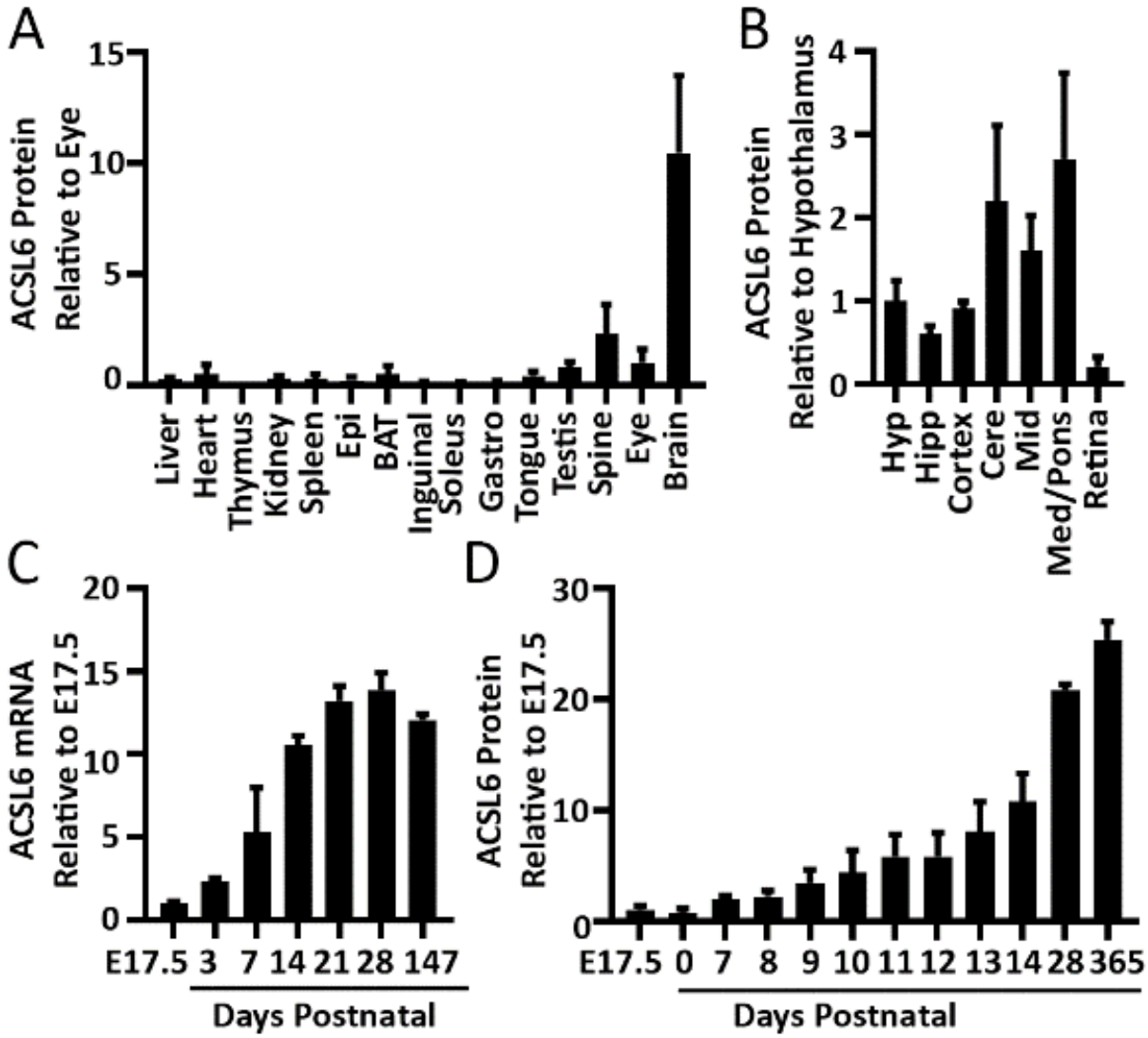

Figure 3.2. Generation of Acsl6 knockout mice

Quantification (A) and Western blot (B) image of Acsl6 protein from control and Acsl6$^{-/-}$, n=3. (C) mRNA abundance of Acsl isoforms 1, 3, 4, and 5 from control and Acsl6$^{-/-}$ hypothalamus, n=5. (D) Initial rate of ACS activity for [14C]16:0, [14C]18:1n9, [14C]20:4n-6, and [14C]22:6n-3 from control and Acsl6$^{-/-}$ midbrain, n=5–6. Amino acid (E), glucose and TCA (F), and nucleotide (G) metabolites in 2-mo-old female Acsl6$^{-/-}$ hippocampus relative to control, n=8. Data represent averages ± SEM; *P ≤ 0.05 by Student's t test.

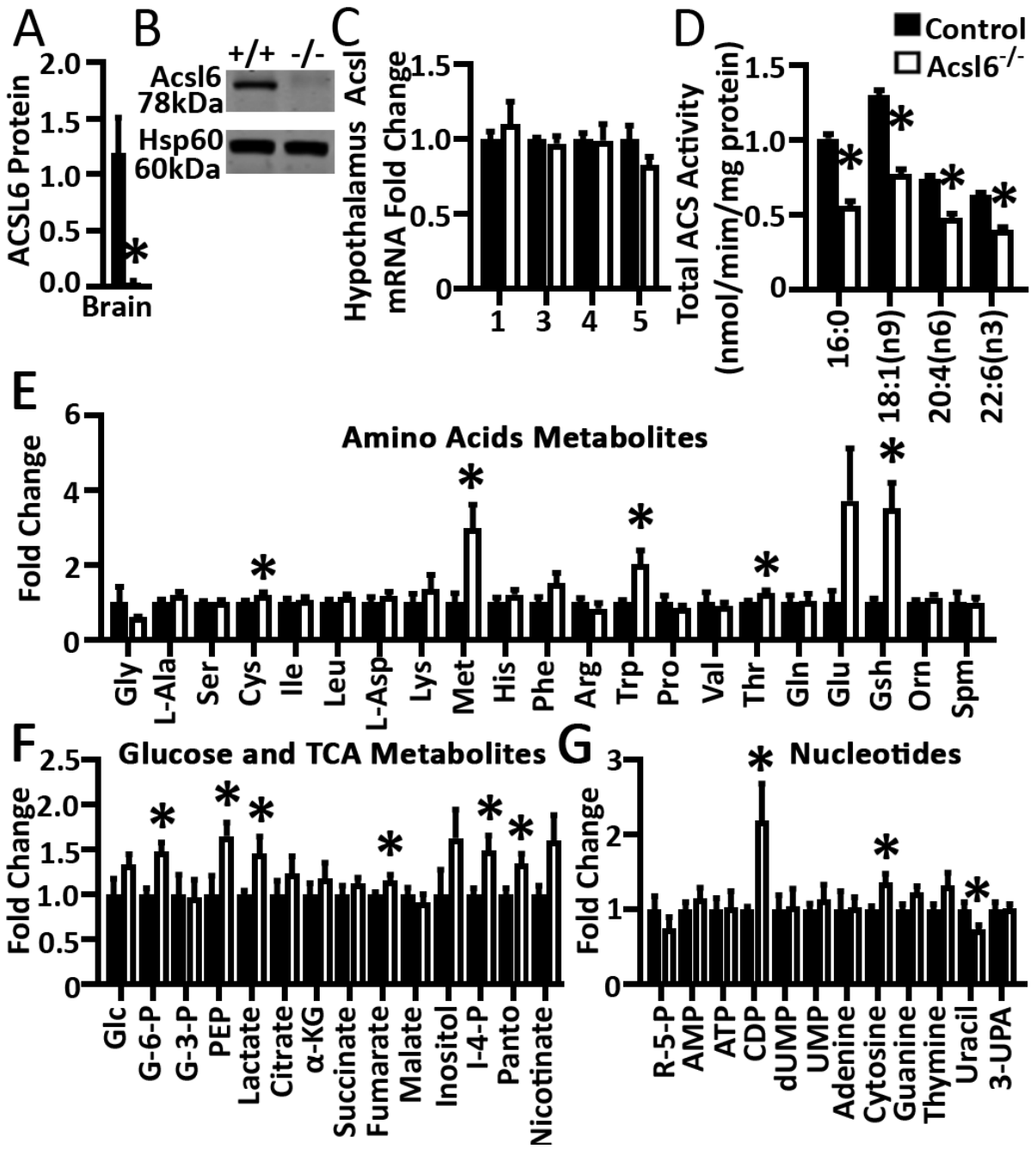

Figure 3.3. Acsl6 deficiency decreases brain omega-3 docosahexaenoate-containing and increases omega-6 arachidonate-containing lipids

Lipid profile of phospholipids (A), lysophospholipids (B), MAG, DAG, and TAG (C) in 2-mo-old female cerebellum expressed as % change in the Acsl6$^{-/-}$ brains relative to the control samples, n=5–6. Data represent averages ± SEM; *P ≤ 0.05 by Student's t test.

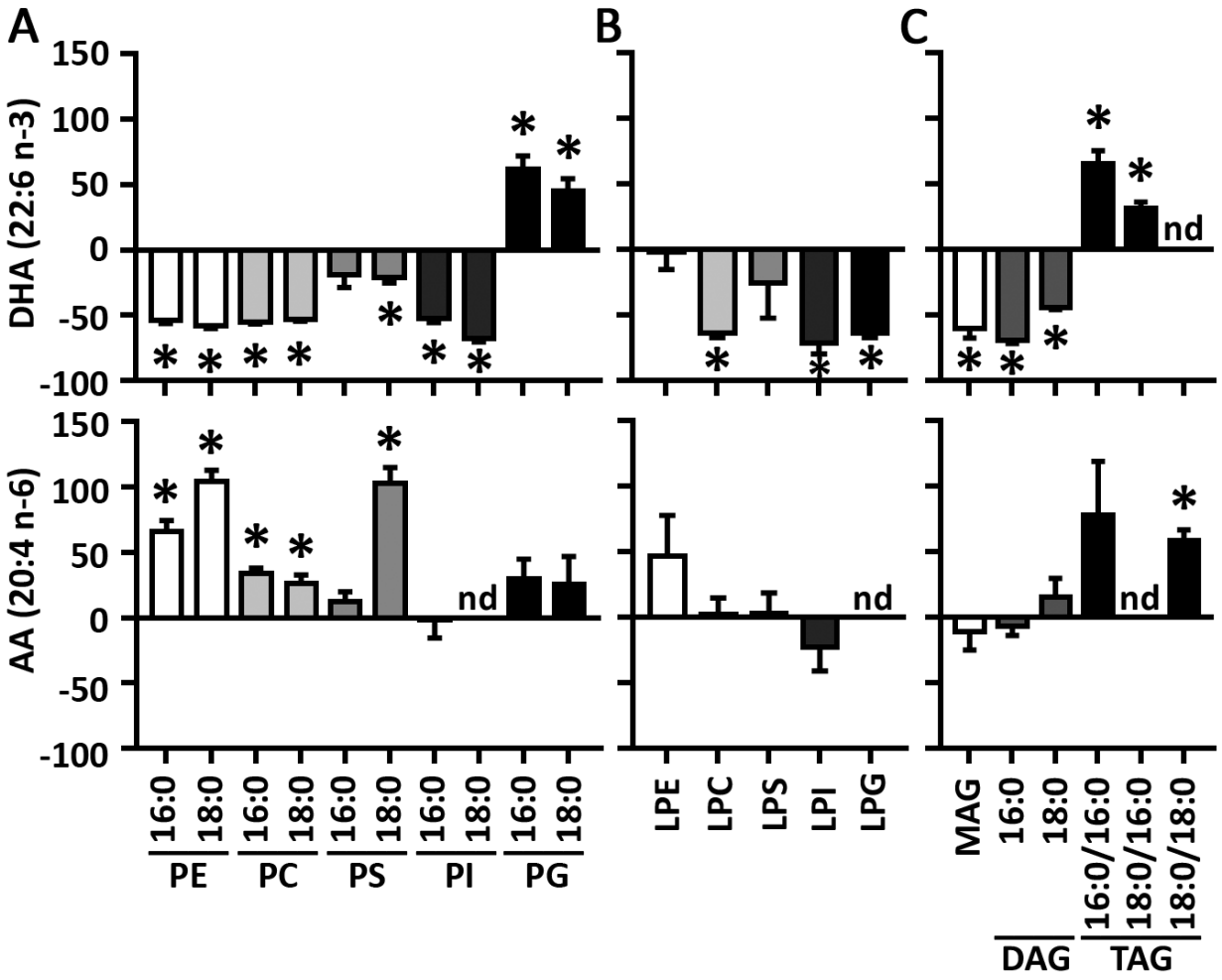

Figure 3.4. Acsl6 deficiency decreases omega-3 docosahexaenoate across the central nervous system

Phosphatidylethanolamine profile in 2-mo-old female midbrain (A), hippocampus (B), cortex (C), spine (D), liver (E), soleus (F), 6-mo-old male cerebellum (G), and 4- to 7-mo-old male Acsl6$^{G/-}$ cerebellum (H) expressed as % ion intensity distribution in Acsl6$^{-/-}$ or Acsl6$^{G-/-}$ relative to control, x axis represents carbon:unsaturated bonds, predicted fatty acid composition, or m/z, n=5–6. (I) Western blot quantification of Acsl6 from control and Acsl6$^{G-/-}$ cerebellum normalized to β-tubulin, n=5. Data represent averages ± SEM; *P ≤ 0.05 by Student's t test.

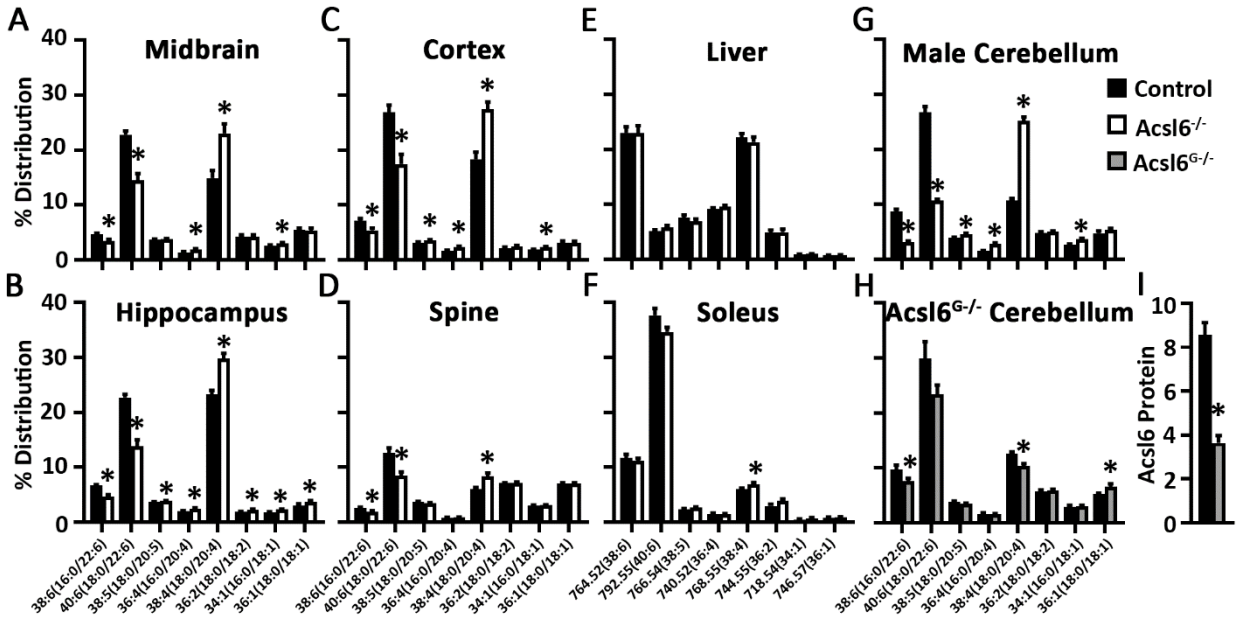

Figure 3.5. Loss of Acsl6 disrupts motor control

(A) Control and Acsl6$^{-/-}$ 6-mo-old mice average latency to fall in the wire hang test normalized to body weight, n=14–15. (B) Rotarod performance for 12-mo-old male control and Acsl6$^{-/-}$ mice during three consecutive days, n=15–16. (C) Adhesive removal test removal time (Left) and number of failed attempts (Right) by 12-mo-old control and Acsl6$^{-/-}$ mice. (D) Average startle response during the fear conditioning session (FC) to a foot shock and during the fear testing session (FT) to a 100-dB tone (noise=N) and to noise + light stimulus in 6-mo-old control and Acsl6$^{-/-}$ mice, n = 28–30. (E) Average startle response to acoustic stimuli in 6-mo-old control and Acsl6$^{-/-}$ mice. Data represent averages ± SEM; *P ≤ 0.05 by Student's t test.

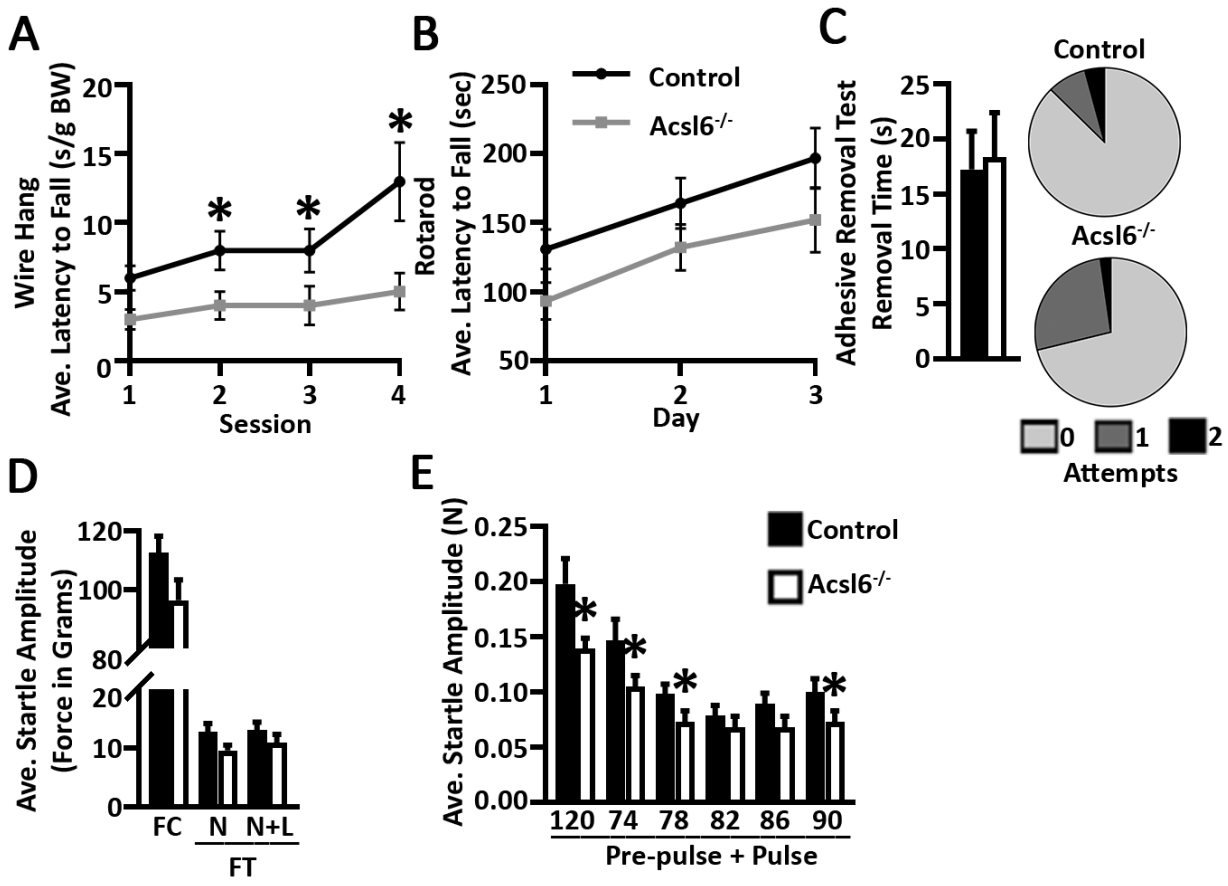

Figure 3.6. Acsl6 deficiency increases microglia activity

Percent immobility (A) and hippocampal mRNA abundance of inflammatory (B and C) and microglial genes (D) in control and Acsl6$^{-/-}$ saline (Sal) or LPS treated 6-mo-old male mice, n=7–8. (E) Representative images of Iba1 and tyrosine hydroxylase (TH) stained substantia nigra of control and Acsl6$^{-/-}$ mice injected with saline or LPS, n=5. (Scale bars: 50 μm.) Data represent averages ± SEM; * by genotype, δ by treatment, P ≤ 0.05 by Student's t test.

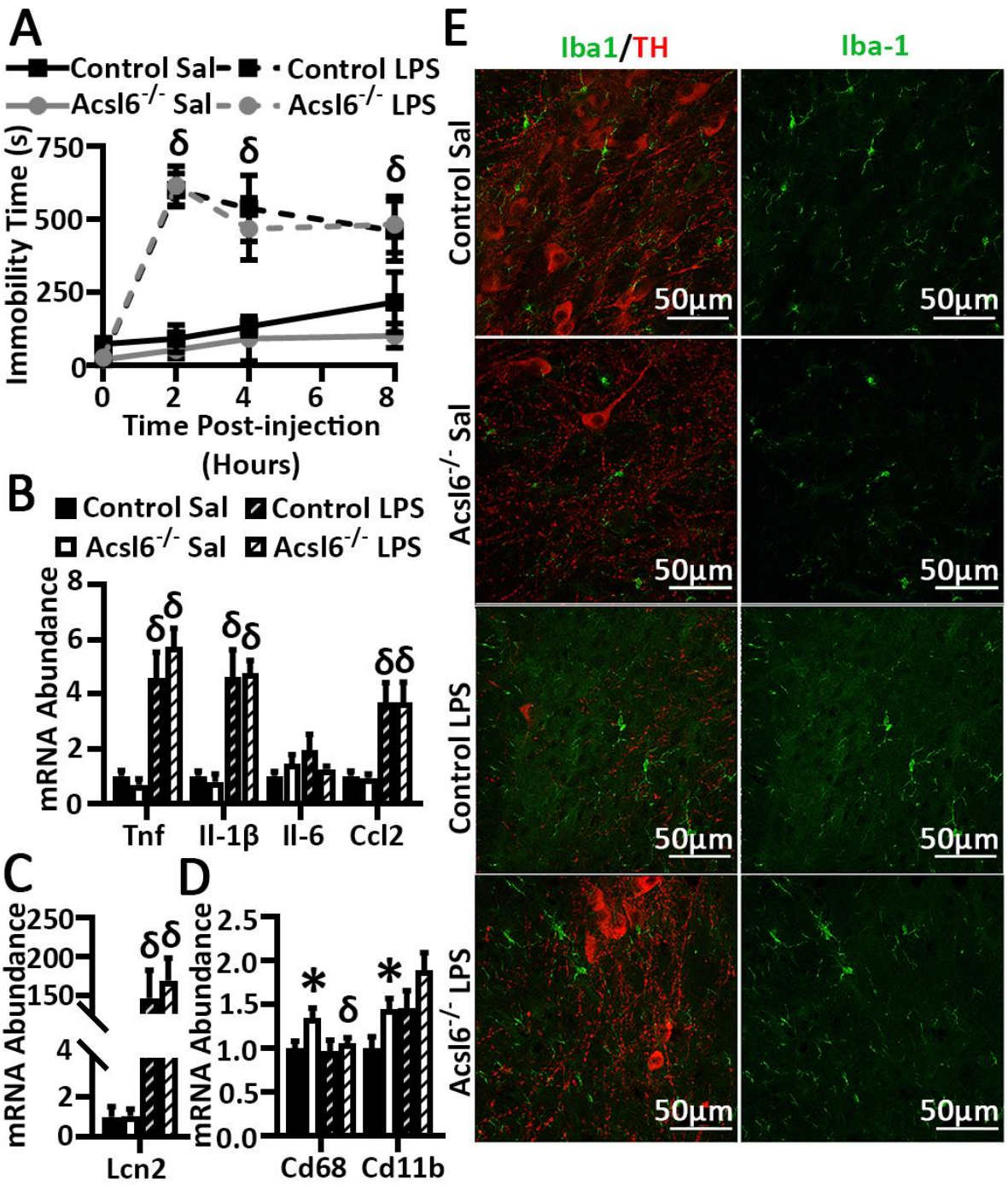

Figure 3.7. Increased astrogliosis in Acsl6$^{-/-}$ mice

mRNA abundance of oxidative stress (A), glutamate metabolism (B), and astrocyte markers (C) in hippocampus of control and Acsl6$^{-/-}$ saline (Sal) or LPS treated 6-mo-old male mice, n=7–8. Representative (D) and quantification (E and F) of GFAP (green) and NeuN (red) stained in the cerebella of control and Acsl6$^{-/-}$ mice injected with saline or LPS, n=5. (Scale bars: 50 μm.) Data represent mean ± SEM; * by genotype, δ by treatment, P ≤ 0.05 by Student's t test.

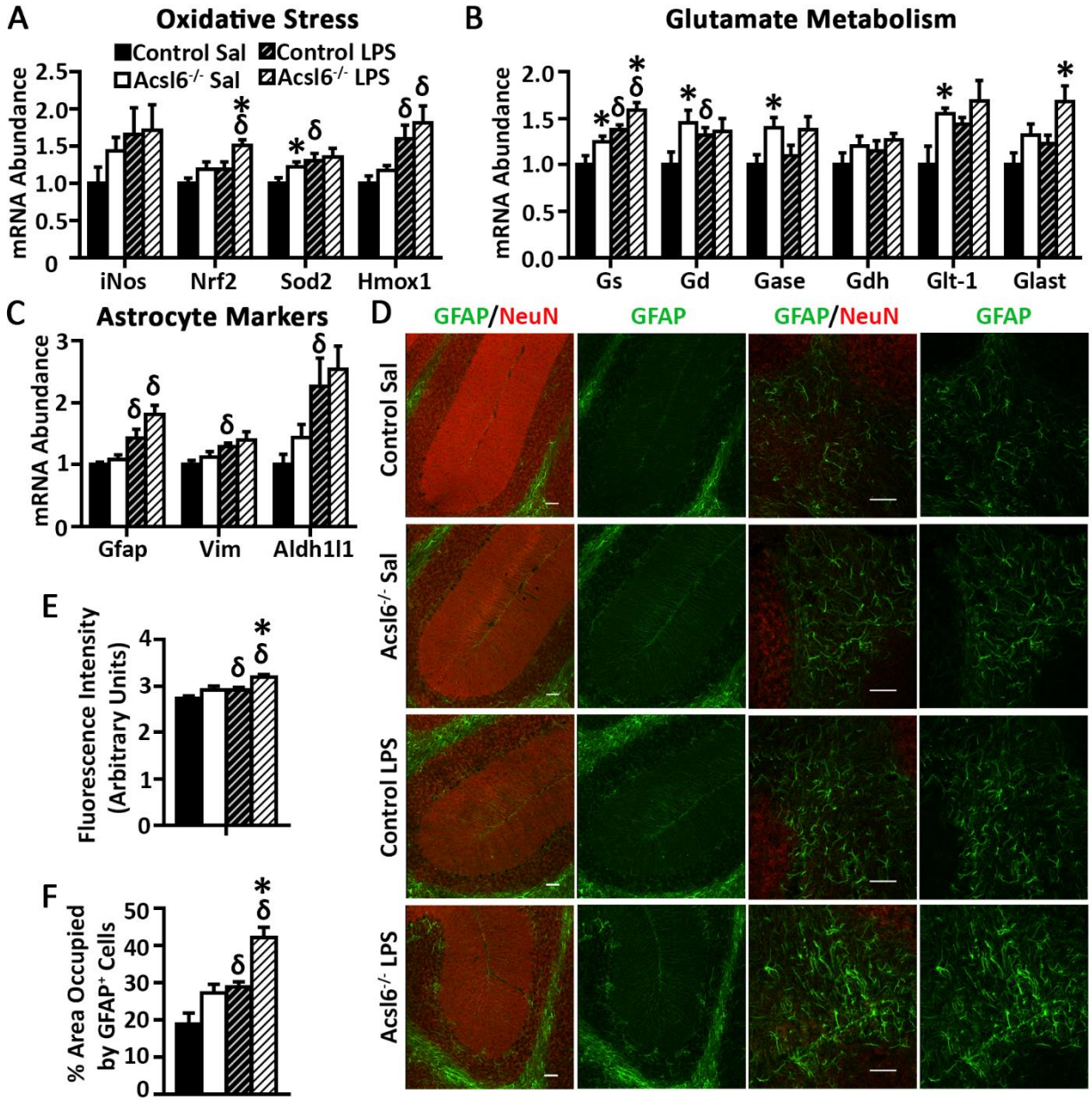

Supplementary Figure 1 (3.8)

(A) Schematic of Acsl6 targeting construct and representative PCR genotyping results of control, Acsl6$^{-/-}$, and heterozygous mice. (B) Mendelian ratios for Acsl6 heterozygous mating. (C) Initial rate of ACS activity for [14C]16:0, [14C]18:1n9, [14C]20:4n-6, and [14C]22:6n-3 from control and Acsl6$^{-/-}$ cortex, n=5-6. (D) Body length from 2-mo-old control and Acsl6$^{-/-}$, n=13- 14, (E) Body weight over time of female control and Acsl6$^{-/-}$, n=13-14. (F) Daily food intake of 5-6-mo-old control and Acsl6$^{-/-}$, n=13-14. (G) Brain weight, (H) length, and width from 2-mo-old control and Acsl6$^{-/-}$, n=13-14. (I) TEM images representing granular neurons (left), myelinated axons (middle), and axonal mitochondria (right). Data represent averages ± SEM; *, p≤0.05 by Student's t-test.

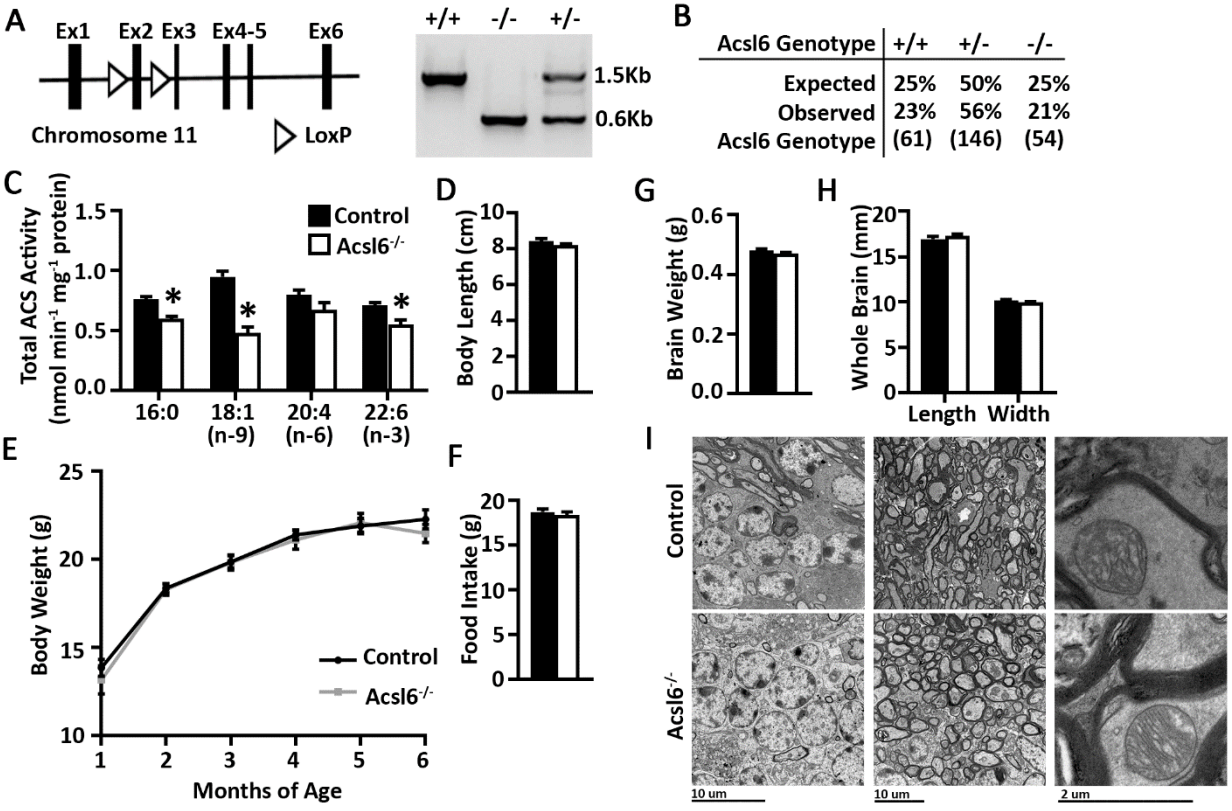

Supplemental Figure 2. (3.9)

(A) Forelimb grip strength in Newtons (N) for 4-5-mo-old control and Acsl6$^{-/-}$ mice, n=10. (B) Number of breaks (left) and percent time spent in the center (right) in the open field over a 20-minute period for 6-mo-old control and Acsl6$^{-/-}$ mice. (C) Fear potentiated startle and (D) percent pre-pulse inhibition in in 6-mo-old control and Acsl6$^{-/-}$ mice, n=28-30. (E) mRNA abundance of inflammatory genes in control and Acsl6$^{-/-}$ LPS treated 2-mo-old male mice, n=3. (F) Striatal terminal density of control and Acsl6$^{-/-}$ 6-mo-old mice injected with saline or LPS, n=5. Data represent averages ± SEM* by genotype, δ by treatment, p≤0.05 by Student's t-test.

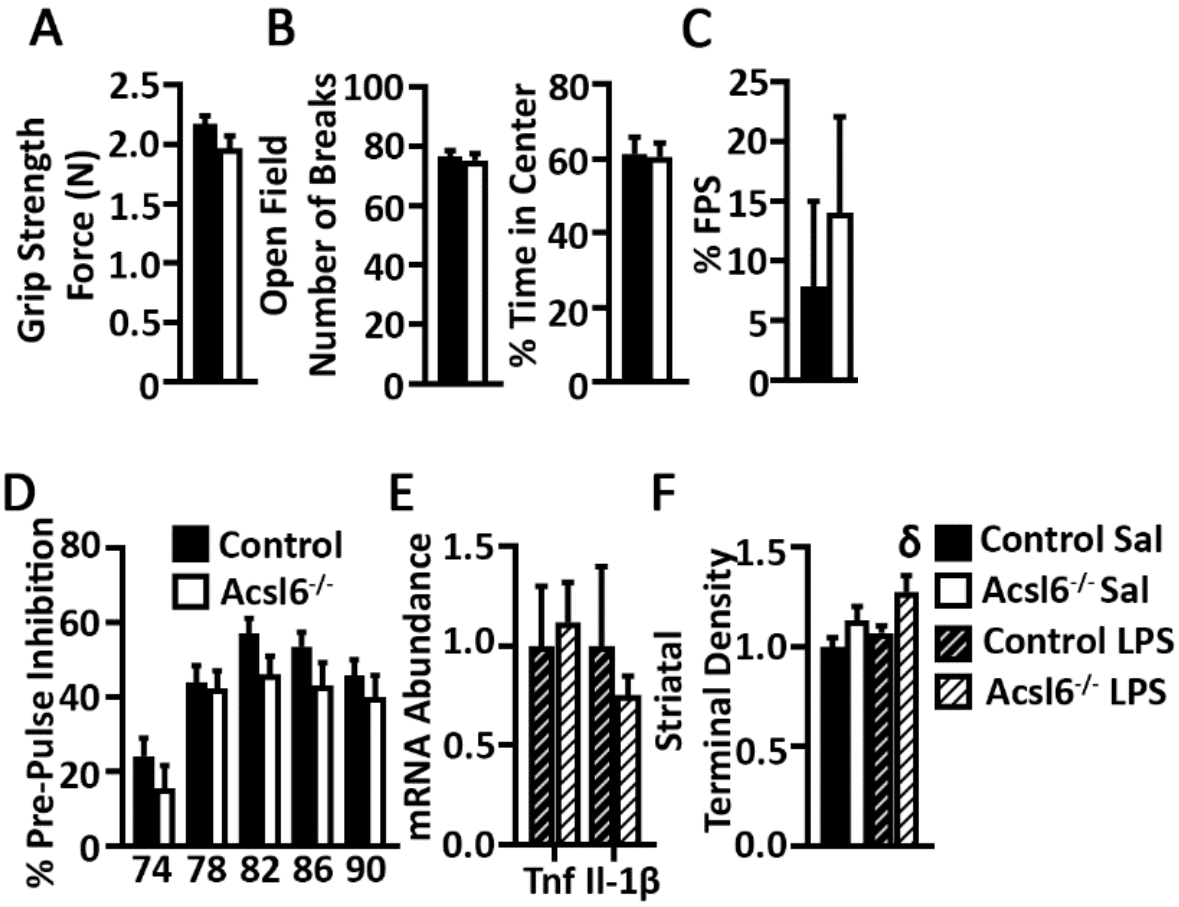

Supplemental Table 1 (3.1). ACS Assay optimization

Total counts of radiation from ACS assay optimization on brain using oleate as substrate at a concentration of 50uM.

		Triton-X		
		0.5	**1**	**5**
ATP	**1**	2012		
	5	1939	1937	2153
	20		-183	
	50			-140
Time	**5**	2244		
	10	3070		
Protein	**10**	18189		
	20	34938		
	40	58715		
	60	79180		

Supplemental Table 2 (3.2). Lipidomic profile

Lipidomic profile of 2-month old female cerebellum with or without overnight fasting, expressed as fold change in the Acsl6$^{-/-}$ brains relative to the control samples, n=5-6. Data represent averages ± SEM; significance represents Student's t-test between genotype.

Supplemental Table 2.				
Lipid Species	Control Fed	Acsl6-/- Fed	Control Fast	Acsl6-/- Fast
C16:0 FFA	1±0.06	0.96±0.05	0.96±0.07	0.93±0.05
C18:1 FFA	1±0.04	1.22±0.12	1.07±0.03	1.19±0.11
C18:0 FFA	1±0.05	1.00±0.03	1.10±0.09	1.04±0.05
C20:4 FFA	1±0.03	1.15±0.06[a]	1.12±0.08	1.10±0.08
C20:0 FFA	1±0.46	1.06±0.26	1.15±0.25	0.89±0.14
C22:6 FFA	1±0.16	0.56±0.08[a]	1.00±0.16	0.58±0.10[a]
C22:0 FFA	1±0.14	1.06±0.13	1.02±0.10	1.01±0.15
C24:0 FFA	1±0.10	0.93±0.14	0.91±0.18	0.78±0.10
C20:5 FFA	1±0.10	0.94±0.10	0.95±0.07	1.03±0.25
C22:6 FFA	1±0.14	0.45±0.03[a]	1.13±0.08	0.59±0.13[a]
C16:0 LPA	1±0.25	0.79±0.18	1.28±0.21	0.97±0.17
C18:1e LPAe	1±0.13	0.96±0.17	1.26±0.16	1.18±0.17
C18:0e LPAe	1±0.22	0.99±0.23	0.98±0.27	0.51±0.15
C18:1 LPA	1±0.18	0.76±0.18	1.21±0.23	1.02±0.23
C18:0 LPA	1±0.22	0.70±0.14	1.15±0.15	0.84±0.12
C20:4 LPA	1±0.07	1.18±0.25	1.38±0.16	1.13±0.09
C22:6 LPA	1±0.09	1.05±0.11	1.22±0.09	1.00±0.14
C16:0 LPI	1±0.26	0.79±0.21	1.34±0.29	1.07±0.28
C18:1 LPI	1±0.17	1.08±0.22	1.34±0.20	1.30±0.33
C18:0 LPI	1±0.16	0.83±0.18	1.46±0.23	1.13±0.22
C20:4 LPI	1±0.20	0.77±0.18	1.45±0.25	1.04±0.25
C18:2 LPI	1±0.15	1.31±0.31	1.38±0.20	1.18±0.31
C20:5 LPI	1±0.16	1.39±0.40	2.03±0.51	0.86±0.22
C22:6 LPI	1±0.12	0.28±0.08[a]	1.33±0.23	0.21±0.04[a]
C20:4 LPC	1±0.12	1.02±0.13	0.83±0.07	1.02±0.06
C18:1e LPCe (lysoPAF)	1±0.14	0.99±0.12	1.12±0.10	1.21±0.07
C20:0 LPC	1±0.15	0.82±0.12	1.01±0.10	1.03±0.09
C16:0e LPCe	1±0.10	0.90±0.06	1.06±0.06	1.06±0.04
C16:0e LPCe (lysoPAF)	1±0.11	0.92±0.06	0.94±0.06	1.07±0.03[b]

C16:0 LPC	1±0.16	0.77±0.12	0.95±0.11	0.99±0.09
C18:1e LPCe	1±0.18	0.83±0.10	1.04±0.14	0.94±0.09
C18:0e LPCe (lysoPAF)	1±0.09	0.99±0.14	1.18±0.10	1.36±0.12
C18:0e LPCe	1±0.16	0.67±0.11	0.94±0.10	0.97±0.09
C18:1 LPC	1±0.14	0.86±0.11	0.89±0.07	1.00±0.07
C18:0 LPC	1±0.16	0.77±0.12	1.00±0.10	1.00±0.09
C18:2 LPC	1±0.16	1.53±0.65	1.60±0.38	1.24±0.32
C20:5 LPC	1±0.08	0.87±0.08	0.79±0.07	0.80±0.06
C22:6 LPC	1±0.05	0.36±0.03[a]	1.15±0.21	0.50±0.10[a]
C18:2 LPG	1±0.03	1.33±0.11[a]	1.34±0.13[b]	1.54±0.14
C20:5 LPG	1±0.06	0.94±0.11	1.15±0.25	0.99±0.10
C22:6 LPG	1±0.05	0.36±0.03[a]	1.14±0.21	0.50±0.10[a]
C18:0e LPSe	1±0.10	1.01±0.20	1.08±0.20	1.15±0.11
C16:0 LPS	1±0.20	0.83±0.18	1.98±0.15	0.96±0.14
C18:1 LPS	1±0.19	0.75±0.17	1.06±0.19	0.94±0.19
C18:0 LPS	1±0.27	0.70±0.22	1.06±0.20	0.95±0.29
C18:2 LPS	1±0.05	0.49±0.05[a]	1.08±0.15	0.63±0.07[a]
C20:4 LPS	1±0.08	1.03±0.16	1.11±0.14	1.28±0.14
C20:5 LPS	1±0.10	1.17±0.10	1.01±0.26	1.22±0.11
C22:6 LPS	1±0.14	0.75±0.27	1.31±0.36	0.55±0.14
C22:6 LPS	1±0.15	0.75±0.27	1.31±0.37	0.56±0.15
C16:0e LPEe	1±0.15	0.83±0.15	1.04±0.12	1.11±0.12
C16:0 LPE	1±0.20	0.78±0.15	1.70±0.11	1.03±0.13
C18:1e LPEe	1±0.15	0.91±0.17	1.13±0.12	1.19±0.13
C18:0e LPEe	1±0.16	0.92±0.19	1.19±0.14	1.33±0.16
C18:0 LPE	1±0.17	0.87±0.17	1.15±0.11	1.28±0.19
C18:2 LPE	1±0.09	0.85±0.09	0.94±0.08	0.93±0.07
C20:4 LPE	1±0.15	1.47±0.31	1.13±0.15	1.77±0.36
C22:6 LPE	1±0.05	0.98±0.13	0.99±0.11	0.98±0.08
C18:1 LPE	1±0.13	1.05±0.15	1.03±0.11	1.24±0.14
C16:0e/18:1 PAe	1±0.08	1.12±0.20	1.21±0.11	1.13±0.10
C16:0/C18:1 PA	1±0.09	1.02±0.15	1.17±0.12	1.06±0.09
C16:0e/20:4 PAe	1±0.13	0.95±0.16	1.10±0.09	0.85±0.07[a]
C18:0e/C18:1 PAe	1±0.09	1.09±0.19	1.19±0.11	1.13±0.12
C16:0/C20:4 PA	1±0.05	0.87±0.13	1.03±0.10	0.91±0.07
C18:0/C18:1 PA	1±0.11	1.04±0.16	1.14±0.11	1.08±0.10
C18:0e/C20:4 PAe	1±0.10	0.98±0.16	1.07±0.09	0.97±0.11
C18:0/C20:4 PA	1±0.10	0.91±0.13	1.08±0.11	0.99±0.09

C16:0/C18:2 PA	1±0.07	1.35±0.14	1.18±0.05	1.25±0.13
C18:0/C18:2 PA	1±0.05	1.10±0.09	1.14±0.07	1.08±0.08
C16:0/C16:0 PI	1±0.14	1.03±0.16	1.04±0.11	1.01±0.14
C16:0e/18:1 PIe	1±0.11	1.10±0.22	1.18±0.12	1.07±0.12
C16:0/C18:1 PI	1±0.14	0.99±0.17	1.02±0.12	1.03±0.13
C16:0e/20:4 PIe	1±0.09	1.44±0.25	1.27±0.18	1.56±0.22
C18:0e/C18:1 PIe	1±0.22	0.95±0.44	0.70±0.24	0.60±0.12
C16:0/C20:4 PI	1±0.13	0.99±0.14	1.04±0.11	1.03±0.11
C18:0/C18:1 PI	1±0.13	1.04±0.17	1.01±0.11	1.05±0.13
C18:0e/C20:4 PIe	1±0.16	0.88±0.12	0.99±0.11	1.01±0.12
C18:0/C20:4 PI	1±0.15	0.99±0.14	1.09±0.12	1.07±0.12
C18:0/C18:2 PI	1±0.11	1.24±0.08	1.16±0.07	1.21±0.19
C16:0/C22:6 PI	1±0.07	0.48±0.03[a]	1.16±0.06	0.66±0.12[a]
C18:0/C22:6 PI	1±0.10	0.32±0.02[a]	1.16±0.07	0.44±0.12[a]
C16:0/C22:6 PC	1±0.05	0.45±0.01[a]	0.83±0.09	0.54±0.07[a]
C18:0/C20:5 PC	1±0.05	0.87±0.02[a]	0.92±0.04	0.92±0.07
C18:0/C22:6 PC	1±0.05	0.46±0.01[a]	0.87±0.09	0.57±0.07[a]
C18:0/C18:2 PC	1±0.04	1.20±0.05[a]	0.96±0.05	1.19±0.11
C16:0/C18:2 PC	1±0.06	1.66±0.03[a]	1.19±0.11	1.83±0.22[a]
C16:0/C20:5 PC	1±0.06	1.25±0.05[a]	1.18±0.07	1.32±0.14
C18:0e/C18:1 PCe	1±0.07	1.06±0.11	0.94±0.05	1.00±0.07
C16:0/C20:4 PC	1±0.02	1.34±0.04[a]	0.96±0.06	1.28±0.07[a]
C18:0/C18:1 PC	1±0.05	0.98±0.07	0.92±0.06	0.96±0.06
C18:0p/C20:4 PCp	1±0.04	1.00±0.06	0.90±0.07	1.06±0.04
C18:0e/C20:4 PCe	1±0.04	1.14±0.06	0.94±0.06	1.08±0.06
C16:0e/C18:1 PCe	1±0.06	1.22±0.15	0.97±0.10	1.12±0.08
C16:0/C18:1 PC	1±0.04	1.04±0.08	0.90±0.06	0.97±0.06
C16:0p/C20:4 PCp	1±0.05	0.85±0.05	0.85±0.06	0.90±0.06
C16:0e/C20:4 PCe	1±0.04	1.18±0.06[a]	0.95±0.06	1.21±0.05[a]
C18:0/C20:4 PC	1±0.04	1.26±0.07[a]	0.96±0.08	1.21±0.09
C16:0/C22:6 PG	1±0.06	1.61±0.10[a]	0.98±0.13	1.58±0.28
C18:0/C20:5 PG	1±0.04	1.42±0.10[a]	1.03±0.13	1.36±0.24
C18:0/C22:6 PG	1±0.07	1.45±0.09[a]	1.02±0.12	1.46±0.23
C16:0/C18:2 PG	1±0.06	0.74±0.05[a]	0.84±0.03[b]	0.79±0.08
C18:0/C18:2 PG	1±0.06	0.62±0.03[a]	0.85±0.05	0.70±0.07

C16:0/C20:5 PG	1±0.07	1.62±0.07[a]	1.05±0.12	1.63±0.27
C16:0/C20:4 PG	1±0.11	1.30±0.15	0.99±0.13	1.19±0.08
C18:0/C18:1 PG	1±0.08	0.48±0.06[a]	0.79±0.09	0.56±0.12
C18:0/C20:4 PG	1±0.17	1.26±0.07	0.89±0.11	1.27±0.07[a]
C16:0e/C20:4 PGe	1±0.16	0.95±0.18	0.88±0.21	0.70±0.11
C18:0e/C18:1 PGe	1±0.05	0.50±0.03[a]	0.81±0.10	0.57±0.08
C16:0/C18:1 PG	1±0.11	0.85±0.06	0.77±0.11	0.78±0.12
C16:0/C18:1 PS	1±0.09	1.05±0.07	0.98±0.06	1.10±0.07
C16:0/C18:2 PS	1±0.09	0.84±0.09	0.89±0.09	0.90±0.14
C18:0/C22:6 PS	1±0.06	0.78±0.04[a]	0.86±0.04	0.83±0.09
C18:0/C20:5 PS	1±0.06	0.93±0.05	0.96±0.05	1.01±0.10
C16:0/C22:6 PS	1±0.10	0.81±0.09	0.93±0.06	0.87±0.12
C18:0/C18:2 PS	1±0.06	0.98±0.05	0.92±0.04	1.01±0.13
C18:0e/C20:4 PSe	1±0.07	1.26±0.11	0.92±0.03	1.24±0.09[a]
C16:0/C20:4 PS	1±0.07	1.13±0.07	1.08±0.07	1.20±0.08
C18:0/C18:1 PS	1±0.06	1.06±0.08	0.90±0.07	1.06±0.04
C18:0e/C18:1 PSe	1±0.06	1.09±0.08	1.00±0.05	1.07±0.03
C16:0e/C20:4 PSe	1±0.14	1.62±0.39	1.35±0.18	1.57±0.31
C18:0/C20:4 PS	1±0.07	2.03±0.12[a]	1.01±0.09	1.84±0.21[a]
C16:0/C20:5 PS	1±0.08	1.16±0.08	1.22±0.12	1.27±0.13
C16:0e/C18:1 PSe	1±0.10	1.07±0.09	0.89±0.09	1.03±0.07
C16:0e/C18:1 PEe	1±0.07	1.21±0.07	0.90±0.07	1.17±0.05[a]
C16:0/C18:1 PE	1±0.02	1.24±0.07[a]	0.85±0.07	1.08±0.03[a]
C16:0p/C20:4 PEp	1±0.04	2.09±0.09[a]	1.06±0.18	1.77±0.18[a]
C16:0e/C20:4 PEe	1±0.02	1.37±0.10[a]	0.97±0.07	1.27±0.08[a]
C18:0e/C18:1 PEe	1±0.07	1.05±0.08	0.90±0.08	1.01±0.09
C16:0/C20:4 PE	1±0.05	1.66±0.09[a]	0.95±0.09	1.50±0.12[a]
C18:0/C18:1 PE	1±0.03	1.09±0.11	0.82±0.07	0.96±0.04
C18:0/C20:5 PE	1±0.04	1.02±0.05	0.92±0.05	1.03±0.10
C16:0/C22:6 PE	1±0.04	0.46±0.02[a]	0.84±0.09	0.56±0.08[a]
C18:0/C18:2 PE	1±0.04	0.98±0.05	0.89±0.06	0.94±0.07
C16:0/C20:5 PE	1±0.04	0.92±0.04	0.89±0.06	0.94±0.07
C16:0/C18:2 PE	1±0.06	1.34±0.05[a]	0.97±0.07	1.45±0.16[a]
C18:0/C22:6 PE	1±0.05	0.41±0.02[a]	0.81±0.10	0.49±0.06[a]

C18:0p/C20:4 PEp	1±0.04	1.49±0.07[a]	0.98±0.08	1.29±0.07[a]
C18:0e/C20:4 PEe	1±0.05	1.45±0.10[a]	0.93±0.10	1.22±0.07[a]
C18:0/C20:4 PE	1±0.01	2.04±0.09[a]	1.00±0.17	1.80±0.18[a]
C16:0e MAGe	1±0.10	0.98±0.09	0.95±0.10	0.93±0.07
16:0 MAG	1±0.15	1.12±0.16	1.13±0.07	1.31±0.13
C18:1e MAGe	1±0.09	0.92±0.11	0.95±0.18	0.99±0.06
C18:0e MAGe	1±0.18	0.79±0.23	0.70±0.27	1.06±0.22
C18:2 MAG	1±0.19	1.31±0.22	1.24±0.14	1.47±0.25
C18:1 MAG	1±0.16	0.92±0.16	0.96±0.10	1.01±0.17
C16:0e/C2:0 MAGe	1±0.21	0.87±0.11	1.42±0.22	1.16±0.11
C18:0 MAG	1±0.21	0.98±0.12	1.40±0.23	1.20±0.13
C20:4 MAG	1±0.17	0.89±0.14	0.94±0.10	1.13±0.11
C18:1e/C2:0 MAGe	1±0.11	0.49±0.06[a]	0.78±0.12	0.66±0.13
C18:0e/C2:0 MAGe	1±0.10	0.91±0.12	0.91±0.11	0.95±0.07
C22:6 MAG	1±0.15	0.40±0.07[a]	0.82±0.14	0.54±0.10
C16:0/C18:1 DAG	1±0.05	1.28±0.16	0.80±0.10	1.11±0.05[a]
C16:0/C20:4 DAG	1±0.10	0.93±0.07	0.74±0.08	0.98±0.09
C18:0/C18:1 DAG	1±0.18	0.97±0.15	0.77±0.13	0.94±0.14
C18:0/C20:4 DAG	1±0.07	1.15±0.15	0.92±0.12	1.08±0.10
C16:0/C18:2 DAG	1±0.09	0.47±0.11[a]	0.88±0.11	0.50±0.08[a]
C16:0/C20:5 DAG	1±0.07	1.09±0.08	0.90±0.12	1.17±0.11
C18:0/CC18:2 DAG	1±0.10	0.49±0.04[a]	1.00±0.14	0.67±0.13
C18:0/C22:6 DAG	1±0.10	0.55±0.01[a]	0.83±0.07	0.58±0.08[a]
C16:0/C22:6 DAG	1±0.05	0.30±0.02[a]	0.74±0.11	0.37±0.09[a]
C16:0/C20:5 DAG	1±0.09	1.12±0.08	0.91±0.11	1.17±0.11
C18:0/C18:2 DAG	1±0.08	0.50±0.04[a]	1.01±0.14	0.70±0.13
C16:0/C16:0/C16:0 TAG	1±0.02	2.04±0.36[a]	1.14±0.09	1.60±0.23
C16:0/C18:1/C16:0 TAG	1±0.05	1.71±0.15[a]	1.03±0.08	1.51±0.16[a]
C16:0/C20:4/C16:0 TAG	1±0.06	1.78±0.41	0.91±0.09	1.29±0.14[a]
C18:0/C18:1/C18:0 TAG	1±0.02	1.45±0.08[a]	1.09±0.05	1.41±0.11[a]
C18:0/C18:0/C18:0 TAG	1±0.04	1.38±0.10[a]	1.19±0.05[b]	1.38±0.10
C18:0/C20:4/C18:0 TAG	1±0.06	1.58±0.08[a]	1.14±0.10	1.54±0.13[a]

C16:0/C18:2/C16:0 TAG	1±0.04	2.02±0.28[a]	1.02±0.09	1.56±0.19[a]
C16:0/C20:5/C16:0 TAG	1±0.07	1.69±0.09[a]	1.11±0.06	1.59±0.19[a]
C16:0/C22:6/C16:0 TAG	1±0.07	1.66±0.10[a]	1.09±0.07	1.60±0.18[a]
C18:0/C18:2/C16:0 TAG	1±0.08	1.37±0.07[a]	0.95±0.04	1.25±0.10[a]
C18:0/C20:5/C16:0 TAG	1±0.15	1.52±0.09[a]	1.32±0.04	1.56±0.18
C18:0/C22:6/C16:0 TAG	1±0.07	1.31±0.05[a]	1.12±0.05	1.29±0.07
C16:0 acyl carnitine	1±0.12	1.15±0.15	0.96±0.15	1.43±0.27
C18:0 acyl carnitine	1±0.13	1.08±0.15	0.96±0.15	1.42±0.19
C18:2 acyl carnitine	1±0.08	1.25±0.12	1.49±0.40	2.20±0.66
C20:5 acyl carnitine	1±0.07	0.83±0.05	1.00±0.12	0.82±0.07
C22:6 acyl carnitine	1±0.08	1.35±0.19	1.35±0.6[b]	1.66±0.22
Lanosterol	1±0.08	1.03±0.09	1.05±0.11	1.11±0.15
C16:0 Ceramide	1±0.14	0.96±0.09	0.92±0.07	0.99±0.07
18:0/C16:0 ceramide-1-phosphate*	1±0.15	0.85±0.20	1.44±0.25	1.08±0.19
sphingosine	1±0.10	0.89±0.11	1.00±0.06	1.08±0.06
sphinganine	1±0.12	0.81±0.09	1.07±0.11	0.98±0.13
C16:0 SM	1±0.10	1.07±0.10	0.98±0.05	1.10±0.06
C18:1 SM	1±0.04	1.23±0.08[a]	0.89±0.05	1.21±0.09[a]
C18:0 SM	1±0.11	0.91±0.08	0.93±0.05	1.02±0.04
C20:4 SM	1±0.05	1.54±0.05[a]	1.08±0.10	1.65±0.15[a]
C16:0 NAE	1±0.14	1.13±0.13	1.06±0.11	1.41±0.18
C18:1 NAE	1±0.12	0.95±0.09	0.93±0.08	1.01±0.10
C18:0 NAE	1±0.16	1.08±0.13	1.01±0.13	1.46±0.22
Cholesterol/cholesteryl esters	1±0.11	0.97±0.13	0.97±0.11	1.04±0.09

Supplemental Methods

ACS Assay: Total membrane fraction was prepared from midbrain and cortex. Acyl-CoA synthetase activity was measured in membrane fractions (5ug) incubated at 37°C for 5 minutes with 5mM ATP, 0.5mM CoA, 1mM DTT, 10mM Mgcl2, 50mM Tris, and 0.05mM fatty acid: [1- 14C]Oleate (PerkinElmer), [1- 14C]Palmitate (PerkinElmer), [1- 14C] Arachidonic Acid (American Radiolabeled Chemicals), or [1- 14C] Docosahexaenoic Acid (Moravek) performed as described (100).

Behavioral Assessment: Wire Hang Test: Mice on a cage top were flipped, leaving the mice upside-down, and the latency to fall was recorded and multiplied by body weight to determine the minimal holding impulse (224). One training and four testing sessions were performed, each with three trials. Adhesive Removal Test: Performed as described, (225). Open Field: Mice were monitored in open field apparatus over 20 minutes using the MotorMonitor instrument (Kinder Scientific). Whole-limb Grip Strength: The gripping strength, defined as the peak force (N), was recorded for 4-5 trials, and the average was calculated (226). Pre-Pulse Inhibition: Pre-pulse inhibition was assessed using the Kinder Startle Monitor equipment (Coulbourn Instruments) using the protocol as described (13). Fear Potentiated Startle: Using the Coulbourn Instruments Animal Acoustic Startle System (Allentown, PA) as described (227). Briefly, mice were exposed to light or acoustic stimuli paired with (conditioning) or without (fear) electrical stimuli to the foot pad and the startle response was recorded.

Immunoblots and Histology: Sub-cellular fractionations were collected from mouse brain homogenates through a series of centrifugation and lysis steps according to (228). Mouse tissue lysates or membrane fractions were collected in lysis buffer (50mM Tris-

HCl, 150mM NaCl, 1mM EDTA, and 1% Triton X-100) and sucrose medium (10mM Tris, 1mM EDTA, and 250mM sucrose), respectively. Protein concentration was quantified using Pierce BCA Protein Assay Kit (Thermo Fisher Scientific). 18ug of protein were subjected to SDS PAGE electrophoresis, transferred to nitrocellulose membranes, and blocked for 1 hour with 3% Bovine Serum Albumin-TBST (Tris Buffered saline, 0.1% Tween 20). The membrane were probed for primary antibody (1:1000) ACSL6 (raised against the peptide CNLLKQSEEVEDGGGAR), heat shock protein 60 (Santa Cruz), and beta-tubulin (Sigma), washed with 5% milk-TBST, and incubated with anti-mouse or anti-rabbit IRDye-conjugated secondary antibodies (LiCor). Membranes were exposed to Odyssey (LiCor) instrument and protein was quantified using LiCor software. For immunohistochemistry, brains were surgically removed, post-fixed in 4% PFA for 7 days, and then saturated with 30% sucrose at 4 °C for at least 7 days. Each brain was coronally sectioned on a frozen sliding microtome (Microm HM 450, Thermo Scientific) at a 35 µm thickness and stored in cryoprotectant at −20 °C. Brain sections containing cerebellum were randomly selected, rinsed 6 times with PBS at RT for 10 min at RT with shaking; blocked in 10% normal donkey serum (NDS) in PBS-T (0.3%) for 1hr at RT; incubated with primary antibodies (GFAP, abcam 134014; NeuN abcam 53554; tyrosine hydroxylase, Millipore AB1542; Iba1, Wako WEE4506) for 24-48 h in PBS-T with 1% NDS at 4 °C; rinsed 3 times with PBS at RT for 10 min; incubated with secondary antibodies (Alexa Fluor 488 anti-goat; Alexa Fluor 647 anti-chicken; Cy3 anti-sheep; Alexa Fluor 488 anti-rabbit from ImmunoJackson Laboratories, and sheep anti-Dylight800 from Rockland 613-745-168) in PBS-T with 1% NDS for 2hrs at RT; and rinsed 6 times 3 with PBS at RT for 10 min each time before mounting on slides. Slides were dehydrated in graded alcohol

and histoclear before coverslipped. Images were captured on an inverted Nikon D-Eclipse C1 confocal microscope. All slides were scanned under the same conditions for magnification, exposure time, lamp intensity and camera gain. For GFAP fluorescence quantification, a core of white matter (the arbor vitae) was analyzed. Mean intensity of fluorescence of GFAP+ cells and area fraction occupied by GFAP+ within arbor vitae were obtained by using NIS-Elements Basic Research software (Nikon). Mean intensity value is a statistical mean of intensity values of pixels derived from the intensity histogram. GFAP immunoreactivity was quantified by determining mean intensity of fluorescence of GFAP+ cells and area fraction occupied by GFAP+ in white matter of cerebellum with the NIS-Elements Basic Research software (Nikon). Briefly, white matter of cerebellum was delineated as region of interest and the binary overlay of GFAP+ cells was created by defining the threshold for background correction. For all images, same threshold value was established at the level at which the binary overlay entirely encloses the cell body and projections. Thus, mean intensity of the binary images were used for GFAP immunoreactivity and the area fraction of GFAP immunoreactivity was calculated by dividing the binarized GFAP+ area by the area occupied by the outlined region of interest and expressed as a percentage. For electron microscopy, the cerebellum was processed, stained, and prepared for transmission electron microscope with the Life Sciences Microscope Facility at Purdue. Images were captured on a FEI Tecnai G2 20 Transmission Electron Microscope.

RT-PCR: Total tissue RNA was extracted using TRIzol (Life Technologies), purified (PureLink RNA Mini Kit, Life Technologies), quantified by NanoDrop 2000 spectrophotometer (ThermoFisher Scientific), and use to synthesize cDNA with High

Capacity cDNA Reverse Trancriptase (Applied Biosystems). Real-Time PCR was performed using SYBR Green Master Mix (Bio-Rad) and primers for the target genes and analyzed by using a StepOnePlus Real Time PCR System thermocycler (Applied Biosystems). Gene expression was normalized to the average Ct values of the housekeeping gene Rpl22 and expressed as 2 -△CT.

Lipidomics: Data presented in Figure 3 and supplemental Table 1, performed as previously described (229). Nonpolar lipid metabolites from mouse cerebellum were extracted in chloroform/methanol/PBS (2:1:1, v/v/v, 4ml) with the addition of 10nmol internal standards dodecylglycerol and pentadecanoic acid (Santa Cruz Biotechnology and Sigma-Aldrich, respectively). The organic layer was separated from the aqueous layer by centrifugation at 1000g for 5 min, dried down under flowing nitrogen, and resuspended in 120µl of chloroform. 10ul aliquots were analyzed by liquid chromatography as previously described (229-231). Metabolites separation from mouse hippocampus was obtained using a Luna reverse-phase C5 column (50 × 4.6 mm and 5 µm diameter particles, Phenomenex). Mobile phase A was composed of water/methanol (95:5, v/v) and mobile phase B of isopropanol:methanol:water (60:35:5, v/v/v). Solvent modifiers 0.1% formic acid with 5 mM ammonium formate and 0.1% ammonium hydroxide were used to facilitate ion formation in addition to improving the LC resolution in both positive and negative ionization modes, respectively. Mass spectrometry (MS) analysis was performed on an Agilent 6430 QQQ LC-MS/MS (Agilent Technologies). Metabolites were identified by SRM of the transition from precursor to product ions at associated optimized collision 4 energies and retention times as previously described (230, 231). Metabolites quantification was performed by integrating the area under the curve followed

by normalization to internal standard values. Results are expressed as relative levels compared to controls. Lipid profiling presented in Figure 4 was performed with Purdue's Bindley Metabolite Profiling Facility. Lipids were extracted from tissues using Bligh and Dyer Method (232). The lipid phase was dried, resuspended and injected through a micro-autosampler (G1377A) into a QQQ6410 triple quadrupole mass spectrometer (Agilent Technologies, San Jose, CA) operated in the positive ion mode and equipped with Jet stream ESI ion source (47). Data was analyzed by calculating the percent distribution for each ion (ion peak of m/z intensity/total ion intensity).

CHAPTER IV

AGE-RELATED INFLUENCE OF ACSL6 ACTIVITY IN NEURAL FUNCTION AND BEHAVIOR

The previous manuscript focused on the initial studies of our novel conditional *Acsl6*$^{-/-}$ mice where we showed that the ACSL6-mediated DHA deficiency in 6-month old mice induced microglia activation and astrogliosis in the brain, indicating neurological stress. Clinical, epidemiological data, and mechanistic research suggest that DHA is required for protection against numerous age-related neurological diseases. Thus, we hypothesized that *Acsl6*$^{-/-}$ mice are susceptible to age-induced neuropathology. For Aim 2, we investigated the extent to which ACSL6-mediated DHA deficiency exacerbates normal age-related neurological dysfunction. Our findings revealed that aging increased gliosis and the expression of neuroinflammatory markers in *Acsl6*$^{-/-}$ brains, which were not triggered by changes in the levels of lipid-derived bioactive mediators. Behaviorally, we showed that the loss of ACSL6 induced hyperlocomotion and alterations in memory. Together, these data suggest that the loss of ACSL6 renders the aging brain more susceptible to neuropathology.

Acyl-CoA synthetase 6 is required for brain docosahexaenoic acid retention and neuroprotection during aging

Regina F. Fernandez[1], Andrea S. Pereyra[1], Victoria Diaz[2], Emily S. Wilson[3], Karen A. Litwa[3], Jonatan Martinez-Gardeazabal[4], Shelley N. Jackson[5], J. Thomas Brenna[6], Brian P. Hermann[2], Jeffrey B. Eells[3], Jessica M. Ellis[1]

[1]Brody School of Medicine at East Carolina University, Department of Physiology and East Carolina Diabetes and Obesity Institute, Greenville, NC, 27834

[2]Department of Biology, University of Texas San Antonio, San Antonio, TX, 78249

[3]Department of Anatomy and Cell Biology, East Carolina University, Brody School of Medicine, Greenville, NC, 27834

[4]Department of Pharmacology, University of Basque Country, Leioa, Spain, 48940

[5]National Institute on Drug Abuse, Intramural Research Program, Structural Biology Core, Baltimore, MD, 21224

[6]Departments of Pediatrics, Chemistry, and Nutrition, Dell Pediatric Research Institute, University of Texas at Austin, Austin, Texas, 78723

[1]To whom correspondence should be addressed. Email: ellisje18@ecu.edu

The authors have declared that no conflict of interest exists.

Abstract

The omega-3 fatty acid docosahexaenoic acid (DHA) inversely relates to neurological impairments with aging; however, limited non-dietary models manipulating brain DHA have hindered direct linkage. We discovered that loss of long-chain acyl-CoA synthetase 6 in mice (*Acsl6*$^{-/-}$) depletes brain membrane phospholipid DHA levels, independent of diet. Here, *Acsl6*$^{-/-}$ brains contained lower DHA, compared to controls, across the lifespan. The loss of DHA- and increased arachidonate-enriched phospholipids was visualized by MALDI imaging predominantly in neuronal-rich regions where smFISH localized *Acsl6* to neurons. ACSL6 is also astrocytic; however, we found that astrocyte-specific ACSL6 depletion did not alter membrane DHA because astrocytes express a non-DHA preferring ACSL6 variant. Across the lifespan, *Acsl6*$^{-/-}$ mice exhibited hyperlocomotion, impairments in working spatial memory, and increased cholesterol biosynthesis genes. Aging caused *Acsl6*$^{-/-}$ brains to decreased expression of membrane, bioenergetic, ribosomal, and synaptic genes, and increase expression of immune response genes. With age *Acsl6*$^{-/-}$ cerebellum became inflamed and gliotic. Together, our findings suggest that ACSL6 promotes membrane DHA enrichment in neurons, but not in astrocytes, and is important for neuronal DHA levels across the lifespan. Loss of ACSL6 impacts motor function, memory, and age-related neuroinflammation, reflecting the importance of neuronal ACSL6-mediated lipid metabolism across the lifespan.

Introduction

The brain is heavily enriched with phospholipids making it the second most fatty organ of the body. Phospholipids are the major component of membranes and in general, contain high levels of polyunsaturated fatty acids (PUFAs) thus, the brain is highly enriched with PUFAs, to a level 3-4-fold higher than other tissues (194, 233). Several PUFAs are essential, meaning they cannot be synthesized endogenously, but instead, must be obtained from the diet. Essential fatty acid-derived PUFAs enriched in the brain include the omega-6 arachidonic acid (AA, 20:4n6) and the omega-3 docosahexaenoic acid (DHA, 22:6n3) (194, 234). While omega-6 fatty acids are heavily enriched in westernized diets, the omega-3 DHA is poorly represented (197, 235). Low dietary DHA intake is compounded by aging-related brain DHA decline (5, 236). Both low dietary DHA intake and low brain DHA levels are associated with the development of numerous age-related neurological diseases and disorders characterized by neuroinflammation and cognitive decline (7, 8, 237-239). Reciprocally, DHA intake through diet and/or supplementation confers protection against age-related neurological decline in part due to its ability to serve as precursor to pro-resolving lipid mediators that ameliorate inflammation and DHA's ability to regulate membrane biophysical properties (10, 240). These benefits of DHA serve as a barrier to the brain's susceptibility to neuroinflammation and cognitive decline with age.

While it has been established that the brain contains high levels of DHA and that brain DHA correlated with brain health (45, 241), the direct linkage to health and regulatory mechanisms that enable DHA incorporation into brain membrane lipids remains unclear. Recently, we discovered that long-chain acyl-CoA synthetase 6

(ACSL6) is a major regulator of DHA enrichment in the brain (48, 138). The critical role for ACSL6 in brain DHA enrichment was exemplified in *Acsl6* deficient mice (*Acsl6*$^{-/-}$) by significant reductions (35-72%) in DHA-containing phospholipids (48). Acsl6 is one of the 26-member family of acyl-CoA synthetase enzymes that ligate a Coenzyme A to a fatty acid, generating an acyl-CoA (98). This enzymatic activity both traps free fatty acids within cells and also activates fatty acids for subsequent intracellular metabolism. Each acyl-CoA synthetase enzyme has unique enzymatic preferences, regulatory mechanism, and expression profile across cell types, properties that contribute to cell-type-specific lipid metabolism and composition (1). Here, we investigated how the loss of ACSL6 and the consequential DHA deficiency and AA enrichment within the brain affects aging. We found that ACSL6 deficiency impaired spatial memory, hyperlocomotion, and age-related cerebellar neuroinflammation. Together, these data demonstrate that ACSL6-mediated DHA metabolism is required for age-related neuroprotection.

Results

Acsl6 is critical for retaining DHA during aging

Brain DHA content inversely correlates with the risk of age-related neurological diseases, disorders, and cognitive decline (4, 5, 69). We previously demonstrated that ACSL6 is responsible for enriching the brain and testes with DHA within membrane phospholipids (48, 111). Here, we measured brain lipids in control and *Acsl6*$^{-/-}$ hippocampus, a region important for aging-sensitive functions such as memory and learning. Broad lipidomic profiling of phosphatidylcholine (PC) species demonstrated reductions in predicted DHA-enriched PCs (38:6 and 40:6) and increases in several PCs containing 1-, 2-, or 3- unsaturated bonds (Figure 1A). We next confirmed that the loss of highly unsaturated PCs was due to DHA-deficiency by performing total fatty acid analysis to discover a 32% reduction in DHA (Figure 1B, Table S1). Other 22-carbon long fatty acids were not reduced by the loss of ACSL6, and in fact, adrenic acid (22:4n6) levels were significantly increased (Figure 1C, Table S1). Coincident with the reduction in relative DHA levels in *Acsl6*$^{-/-}$, were reciprocal increases in low abundance fatty acids such as dihomo-γ-linolenic acid (20:3n6), linoleic acid (18:2n6), and a statistically insignificant rise in the high abundance fatty acid arachidonic acid (20:4n6) (Figure 1B,C Table S1). These data suggest that ACSL6 exhibits a substrate specificity to DHA rather than a generalized capacity to metabolize 22-carbon fatty acids and confirms our previous findings that the loss of ACSL6 results in DHA deficit.

A number of results in the literature indicate that astrocytes express ACSL6 (1, 123-125, 242, 243). To directly test the role of astrocytic ACSL6, we generated astrocyte-specific ACSL6 deficient mice using the Glial fibrillary acidic protein (Gfap) promoter Cre

driver (*Acsl6*$^{G-/-}$) (48). Surprisingly, astrocyte-specific ACSL6 knockouts exhibited minimal changes in fatty acid composition in the brain, most notably, unchanged DHA levels (Figure 1B,C). However, total saturated fatty acids were significantly reduced and linoleic acid (LA, 18:2n6) and eicosadienoic acid (20:2n6) were elevated (Figure 1C and Table S1). Partial loss of ACSL6 protein in *Acsl6*$^{G-/-}$ hippocampus was confirmed by western blot and reiterates that a fraction of brain ACSL6 is expressed in astrocytes (Figure 1D). However, the lack of intermediary fatty acid profile phenotype between the complete and astrocytic knockout models suggests differential metabolic roles for ACSL6 found in astrocytes compared to non-astrocytes. Therefore, the expression of ACSL6 variants, with differential fatty acid binding motifs, were assessed in the models(146). Targeted RT-PCR primers demonstrated that while total knockout mice lose expression of both F- and Y-gate domains, the astrocyte-specific loss of ACSL6 retains expression of the F-gate (DHA-preferring) but loses the Y-gate (non-DHA preferring) domain (Figure 1E). These data demonstrate that astrocytes do not express the DHA-preferring ACSL6 variant, thereby explaining the lack of DHA reduction in astrocyte-specific ACSL6 knockout mice.

DHA levels naturally decline in the brain across the lifespan, a phenomenon predicted to increase the risk of age-related neurological impairments. However, the mechanistic underpinnings causing such age-related loss in brain DHA remain elusive. Fatty acid content of aged compared to young mice showed a decrease in DHA by 14% by aging (Figure 1F), consequently reducing total omega-3 fatty acids and increasing the omega-6 to omega-3 ratio (Figure 1G,H and Table S1). In *Acsl6*$^{-/-}$, age did not affect the increased omega-6/omega-3 ratio (Figure 1G and Table S1). Unlike in control mice, *Acsl6*$^{-/-}$ hippocampus resisted aging-related reductions in brain DHA (Figure 1F).

Together, these data suggest that non-astrocytic Acsl6 is critical for enriching the brain with DHA throughout the lifespan.

ACSL6 is expressed in mature neurons and drives neuronal membrane DHA enrichment

To better understand the spatial resolution and the cell type-specific contributions of *Acsl6* to lipid metabolism in the brain, we performed single-molecule RNA *in situ* hybridization (smFISH). *Acsl6* transcripts were evident across the hippocampus but particularly enriched in *Vglut1*-positive pyramidal neurons of the CA3 and dentate gyrus (Figure 2A). We next sought to determine the alignment between *Acsl6* expression and the spatial distribution of phospholipid acyl-chain composition using lipid mapping. Mapping of hippocampal phospholipids in control mice revealed DHA-enriched (40:6 and 38:6) and AA-enriched (36:4 and 38:4) phosphatidylcholine (PC) particularly abundant in the neuronal rich CA1, CA2, CA3, and dentate gyrus regions (Figure 2B,C). Total ACSL6 loss greatly reduced DHA-enriched phospholipids (PC40:6 and PC38:6) across the entire hippocampus (Figure 2B). Consequently, AA-enriched PC36:4 increased in neuronal-rich dentate gyrus, CA1, and CA3 regions (Figure 2C). Astrocytic-specific ACSL6 deletion showed negligible impact on DHA-enriched phospholipids lipid images (Figure 2B). These data suggest that non-astrocytic ACSL6 enriches the hippocampus with membrane DHA, particularly in neuronal-rich regions where ACSL6 is highly abundant.

ACSL6 loss impairs short-term spatial working memory and induces hyperlocomotion

DHA is predicted to improve memory and prevent dementia. Therefore, memory tests were performed to assess behavioral outcomes in DHA-deficient *Acsl6*$^{-/-}$ mice. During Y-maze testing, the *Acsl6*$^{-/-}$ mice had significantly fewer spontaneous alternations indicating impaired short-term spatial working memory (Figure 3A). During Barnes maze test, no genotype effect was observed for learning index or latency to reach the target (Figure 3B,C), but *Acsl6*$^{-/-}$ mice spent less of their time in the target quadrant 1, indicative of a minor defect in spatial learning and memory (Figure 3D). In the novel object test, no genotype effect was observed for novelty preference or discrimination index, suggestive of intact cognition and recognition memory (Figure S1A,B). Together, these data suggest that ACSL6 deficiency impairs spatial working memory.

During the memory tests, *Acsl6*$^{-/-}$ mice also exhibited a significant hyperlocomotion phenotype. Specifically, during the Barnes maze test, both male and female *Acsl6*$^{-/-}$ mice travelled further and froze less (Figure 3E,F and S1C,D). During the Y-maze test, *Acsl6*$^{-/-}$ mice had more arm entries indicating hyperactivity (Figure 3G). Increased activity also manifested as increased maximum speed during an open field test (Figure 3H). Open field did not show indicators of anxiety in *Acsl6*$^{-/-}$ mice who traveled to a similar extent as controls in the center of the open field (Figure 3I). Activity in metabolic cages showed that both male and female *Acsl6*$^{-/-}$ mice had increased ambulatory activity (Figure 3J). During rotarod testing, aged 18-month old *Acsl6*$^{-/-}$ mice developed reduced latency to fall (Figure 3K), suggesting reduced motor coordination, a function under cerebellar control. Together

these data support a hyperlocomotion phenotype in *Acsl6*$^{-/-}$ mice characterized by increased distance, speed, and fewer freezing bouts.

ACSL6 is a major contributor to cerebellar membrane DHA

Motor activity is controlled in part by the cerebellum, a brain region that we previously showed is highly enriched with ACSL6(48). Lipid imaging and phospholipid lipidomics demonstrated that DHA-enriched PCs (38:6 and 40:6) were higher in abundance in the cerebellum relative to the hippocampus (Figure 4A,B). In *Acsl6*$^{-/-}$ cerebellum, MALDI lipid imaging showed largely depleted DHA-enriched PC40:6 (Figure 4C). Spatially, predicted DHA-enriched PCs are most abundant within the Purkinje and granular cell layers of the cerebellar gray matter (Figure 4C). Next, *in situ* hybridization demonstrated that the regional distribution of PC40: 6 was attributed to *Acsl6* expression. Specifically, *Acsl6* transcripts were evident in the granular cell layer and were highly abundant in glutamatergic neurons (*Vglut1*+ cells) and within Purkinje neurons of the Purkinje layer (*Vgat*+ cells) (Figure 4D). The expression of *Acsl6* in Purkinje and granular cells and the loss of DHA-enriched PCs resulting from *Acsl6* deficiency in these cells demonstrates that ACSL6 determines the abundance of membrane DHA in cerebellar neurons.

The effects of age on membrane lipidome in the cerebellum were next assessed by broad untargeted lipidomics. Both young and old *Acsl6*$^{-/-}$ mice exhibited reductions in numerous DHA-enriched phospholipids (Figure 4E). As a consequence of aging, several of these species were reduced in both control and *Acsl6*$^{-/-}$ mice, specifically PE38:6, PE40:6, and PE40:7, with the exception of PC40:6 and PI40:6 which were only reduced in control mice and *Acsl6*$^{-/-}$ mice, respectively by aging (Figure 4E). Both young and old

Acsl6$^{-/-}$ mice exhibited increased AA-enriched phospholipids (Figure 4F). Aging resulted in reduced PC36:4 and PC38:4, and increased PS38:4, in both genotypes (Figure 4F). Phosphatidylinositol was the only phospholipid refractory to increased AA in the *Acsl6*$^{-/-}$ cerebellum (Figure 4F). These data suggest that the cerebellar neurons are highly enriched with ACSL6 and that the cerebellum is highly susceptible to both aging- and *Acsl6*-dependent alterations in membrane lipidome.

Transcriptome profiling reveals multiple roles of ACSL6 in the aging cerebellum

To gain insight into the molecular consequences of *Acsl6* deletion, RNA-seq was performed using cerebellar tissue from young, 2-month old, and aged, 18-month old, *Acsl6*$^{-/-}$ and control mice. Differential genes were identified by comparisons by age within genotype or by genotype within age (Figure 5A). Surprisingly, genes changed ($p \leq 0.01$) by the loss of ACSL6 in young mice were remarkably distinct from the genotype effect in old mice, with only 2% overlap (Figure 5B), suggesting that the molecular consequences caused by the loss of ACSL6, relative to control mice, are highly susceptible to aging. The mere eight genes changed by genotype, independent of aging, included *Acsl6*, and genes related to synaptogenesis (*Sparcl1*), endocytosis (*Synj2*), immunity (*C4b*), and cholesterol biosynthesis (*Dhcr24, Stard4, Srebf2*). Subsequent pathway analysis on a broadened gene set ($p \leq 0.05$) confirmed the upregulation of the SREBP-regulated cholesterol biosynthesis pathway in both young and aged *Acsl6*$^{-/-}$ cerebellum (Figure 5C and S2A). These data agree with the response of SREBP-regulated pathway to changes in membrane DHA content (244-246).

The genes changed by aging in either control mice or *Acsl6*$^{-/-}$ mice overlapped by ~40% (Figure S2). Pathway analysis of the age-affected genes that were similar between

the control and *Acsl6*$^{-/-}$ cohorts, were enriched for increased stress and immune responses and decreased mitochondrial and synaptic genes (Figure S2), consistent with established aging-related phenomenon. However, pathway analysis of genes changed by age only in the *Acsl6*$^{-/-}$ mice, revealed additional reductions in genes related to axonal guidance and mitochondria (Figure S2). Moreover, numerous ribosomal protein genes were reduced in *Acsl6*$^{-/-}$ mice by aging (Figure 5D), a hallmark of natural aging (247, 248). Analysis of genes changed using both Reactome and Gene Ontology (GO) term enrichment analyses, revealed that aged *Acsl6*$^{-/-}$ mice, when compared to aged controls, had increased responses to stress and of the immune system and reduced membrane-related and synaptic proteins (Figure 5E and S2). Synaptic proteins interact with membrane lipids and are therefore susceptible to disruptions in membrane acyl-chain content that alter membrane properties. Reduced gene expression of membrane-related proteins involved in synaptogenesis was confirmed by RT-PCR in 2-month-old *Acsl6*$^{-/-}$ cerebellum for *Snap25*, *Dlg4*/*Psd95*, and *Stxbp1* (Figure 5F). By 18 months of age, these plus additional synaptogenesis-related genes were downregulated, specifically *Sv2b*, *Grin2b*, and *Nlgn1*, all of which have membrane-spanning domains (Figure 5F). While total protein abundance of PSD95 and SNAP25 was not altered in total cerebellar homogenates of aged *Acsl6*$^{-/-}$ cerebellum compared to controls (Figure S4), the alterations in transcript levels of these genes suggest dysregulation of synaptic proteins in *Acsl6*$^{-/-}$ cerebellum and agrees with previously reported findings linking synaptic proteins to membrane DHA abundance (249, 250). These data suggest that ACSL6 loss differentially impacted gene expression in an age-dependent manner, drove the induction

of SREBP, and in response to age reduced genes related to mitochondrial function, synaptic proteins, axonal guidance, and increased immune response genes.

Lipid mediator homeostasis is majorly regulated by age and minorly regulated by membrane acyl-chain composition

Membrane fatty acids are substrates for enzymatic generation of lipid mediators that have multiple downstream regulatory actions including regulation of inflammation. Specifically, lipid mediators derived from enzymatic oxygenation of DHA are generally neuroprotective and pro-resolution, whereas mediators derived from AA and LA are known to modulate inflammation (37-39, 41, 251). Aging, independent of genotype, decreased AA-derived lipid mediators generated from cyclooxygenases, lipoxygenases, and from non-enzymatic oxidation by reactive oxygen species (Figure 6A-D). Conversely, inflammation-promoting LA-derived mediators were increased by age (251), and to a greater degree in *Acsl6*$^{-/-}$ compared to controls, suggesting a possible role for LA-derived mediators in age- and *Acsl6*$^{-/-}$-related neuroinflammation (Figure 6E).

Consistent with increased membrane AA in *Acsl6*$^{-/-}$ mice, higher levels of AA-derived lipid mediators were observed in aged *Acsl6*$^{-/-}$ mice (Figure 6A-D). The omega-3, DHA-derived lipid mediators were far less abundant than those derived from omega-6 fatty acids. Notably, only four of the thirteen DHA-derived lipid mediators assessed were detected (Figure 6 and Supplemental Table S2). Despite this low abundance, lipoxygenase and oxidative-stress derived DHA species were significantly lower in *Acsl6*$^{-/-}$ mice compared with controls at 2 months of age (Figure 6B,D). Specifically, the lipoxygenase product 14(S)-HDHA, the precursor of maresin-like specialized pro-resolving mediators, was significantly reduced in *Acsl6*$^{-/-}$ (Figure 6B). Two non-enzymatic

oxidized DHA-derived lipid mediators, 8-HDoHE and 11-HDoHE, were down more than 2-fold in young *Acsl6*$^{-/-}$ compared with controls (Figure 6D). Because changes in membrane lipids were not as strongly reflected in the lipid mediator content as expected, we next assessed gene expression of the enzymatic machinery that metabolizes lipid mediators. Surprisingly, we did not observe a genotype effect, rather we observed age-induced increases in lipid mediator metabolism genes, including several phospholipases that generate substrate, several enzymes that generate lipid mediators, and those that degrade mediators (Figure 6F). While a majority of the genes increased with age, two phospholipase A2 genes, paraoxonase 2, and glutathione peroxidase 4, which are associated with aging and oxidative stress (252-254), decreased with age (Figure 6F). Together these data indicate that membrane acyl-chain composition does not greatly impact overall lipid mediator homeostasis or expression of related metabolizing enzymes.

Loss of ACSL6 promotes neuroinflammation

DHA consumption is inversely correlated with age-related diseases afflicting the central nervous system. In agreement, the loss of DHA due to ACSL6 deficiency revealed age-dependent increases in transcriptomic profiles related to immune, defense, and stress responses (Figure 5E and S2). To investigate age-related neurology, histological analysis of 1-year old *Acsl6*$^{-/-}$ cerebellum revealed pathological indicators of neuroinflammation. Specifically, aged *Acsl6*$^{-/-}$ cerebellum showed enlarged IBA-1-positive and increased GFAP-positive cells (Figure 7A). The area occupied and signal intensity of GFAP+ cells in the cerebellar white matter were increased by ~2-fold in 1-year old *Acsl6*$^{-/-}$ compared to controls (Figure 7B). For IBA-1+ cells, the soma perimeter and area occupied was ~2-fold greater than controls in *Acsl6*$^{-/-}$ cerebellum (Figure 7C). The

increase in neuroinflammatory pathology did not coincide with apparent neurodegeneration as indicated by no change by genotype in aged brain weight, width or length, and by similar cerebellar protein signal for NeuN, the neuronal cell marker, and Calbindin, the Purkinje cell marker (Figure S4E,F). The effect of age on this neuroinflammatory phenotype was assessed by genes that serve as markers for myeloid cells and inflammation across aging. By 12 and 18 months of age, myeloid cell and inflammatory markers were significantly increased in *Acsl6*$^{-/-}$ relative to age-matched controls (Figure 7D,E). These data demonstrate age-responsive microgliosis and/or astrogliosis, as well as, increases in pro- and anti-inflammatory responses in *Acsl6*$^{-/-}$ cerebellum (Figure 7D,E).

Unlike *Acsl6*$^{-/-}$ mice, and in agreement with minimal impact of astrocytic ACSL6 on cerebellar membrane DHA content, 12-month old *Acsl6*$^{G-/-}$ did not show increased gene expression of myeloid cell nor inflammation markers (Figure S3A,B), suggesting that loss of ACSL6 in astrocytes alone does not initiate an age-related inflammatory response. In summary, these data demonstrate that ACSL6-mediated membrane DHA-deficiency in cerebellar neurons induces characteristics of aging, including reduced expression of genes related to synaptic activity, membrane components, ribosomal machinery, bioenergetics, and immune/stress responses that culminated in age-related pathological and molecular hallmarks of neuroinflammation and gliosis.

Discussion

In this report, we show that ACSL6 deficiency in mice presents with age-related neuropathology akin to early-onset aging. The neuropathology and neuroinflammation were readily detected in the cerebellum, a brain region that contains a high abundance of ACSL6 and membrane DHA, suggesting that regions most highly enriched with membrane DHA are impacted the greatest by ACSL6 deficiency. ACSL6 is downregulated in or has identified single nucleotide polymorphisms associated with age-related neurodegenerative diseases (255-257). Thus, loss of ACSL6 function or availability of its preferred substrate DHA over aging could contribute to age-induced neurological diseases and disorders.

Consistent with an age-related phenomenon, *Acsl6*$^{-/-}$ mice transcriptomes were highly influenced by age and the mice only developed indications of neuroinflammation and pathology with aging. Specifically, the age-dependent increase in reactive glial pathobiology and expression of numerous inflammatory and myeloid markers from 6 to 12 to 18 months of age was evident in *Acsl6*$^{-/-}$ cerebellum. Loss of membrane DHA and increase in membrane AA had a surprisingly limited impact on steady state lipid mediator content. It is possible that these minimal effects are due to lack of pro-inflammatory challenge to the mice, thereby limiting detection of mediators (43, 258). In relation, we found no evidence by our smFISH or from public databases to suggest that ACSL6 is expressed in microglia and we showed herein that astrocytic ACSL6 does not regulate DHA metabolism. Thus, ACSL6 deficiency does not cause DHA deficit in glial cells, arguably the major cell type driving lipid mediator metabolism, thereby potentially limiting the impact of ACSL6 on lipid mediator homeostasis. Because ACSL6 expression is

identified as astrocyte-enriched in numerous databases (24-29), we were surprised that the loss of ACSL6 in astrocytes had minimal impact on brain membrane lipid composition. However, these databases use cells derived from animals early in development, failing to capture transcripts, such as *Acsl6*, that present in late-stage mature neurons. Our smFISH clearly demonstrates abundance of *Acsl6* transcripts in neurons. These data agree with the adult human brain RNAseq dataset from the Allen Brain Atlas showing robust expression of ACSL6 across a large variety of adult neuron subtypes (1, 259). Importantly, we resolved the mechanistic explanation underlying the difference between astrocytic and complete ACSL6-knockout effects on lipid content by demonstrating that astrocytes are enriched with the Y-gate domain but not the DHA-preferring F-gate (146). Thus, we demonstrate that ACSL6 in neurons is DHA-preferring whereas ACSL6 in astrocytes is not. Our observation that ACSL6 loss in astrocytes minimally impacts brain lipid content and phenotype, suggests that astrocytic ACSL6 does not majorly contribute to brain lipid content and is not eliciting the early-onset aging observed in the total body knockout mice.

In relation to cerebellar neurological distress, hyperlocomotion was observed in nearly every test performed on *Acsl6*$^{-/-}$ mice across the lifespan. While the manifestation of hyperlocomotion was not identical (i.e. fewer pauses, faster speed, farther distance traveled) it was consistent, nonetheless. These behavioral abnormalities could be associated with altered neurotransmission due to alterations in membrane properties. Specifically, the kinked nature of DHA contributes to membrane properties such as flexibility, packing defects, and deformation (33, 34). As such, loss of membrane DHA stands to impair processes such as membrane vesicle cycling at neural synapses for

neurotransmission, and membrane-protein interactions which are dependent upon the length and hydrophobicity of the membrane bilayer (22, 32, 35, 36). As such, a strong match was visualized between ACSL6 expression in neurons by smFISH to that of membrane DHA depletion by MALDI in *Acsl6*$^{-/-}$, suggesting that cerebellar neurons are most susceptible to suffer consequences of ACSL6 loss. In agreement, GO term analysis was highly enriched with membrane components, coinciding with reductions in synaptoproteome in the cerebellum. Synaptoproteome deregulation has been previously reported as an effect of DHA deficit during aging and is rescued with DHA replenishment, suggesting a direct role for DHA in maintaining adequate synaptic proteins levels (249, 250, 260). Here, ACSL6-mediated DHA loss reduced gene expression of synaptic proteins as early as 2-months of age suggesting that alteration in synaptic proteins could chronically deregulate synaptic transmission leading to long-term age-related stress and subsequent neuroinflammation in aged *Acsl6*$^{-/-}$ mice.

Motor activity is also largely controlled by dopaminergic control centers, and we previously reported an increase in tyrosine hydroxylase terminal density in the striatum of ACSL6-deficient mice (48). Dopaminergic neuronal projections are particularly abundant in the striatum and dopamine plays a strong role in regulating motor activity suggesting a possible link between ACSL6 and dopamine. Our smFISH demonstrated co-localization of *Acsl6* to dopaminergic, tyrosine hydroxylase-positive neurons and a depletion in membrane PUFAs in this region, visualized by lipid imaging (data not shown). Thus, impaired motor function in *Acsl6*$^{-/-}$ mice could also be contributed by deficits in dopaminergic membrane PUFAs. Indeed, diseases afflicted with imbalances in dopaminergic system, such as Parkinson's disease, schizophrenia, depression, and

attention deficit hyperactivity disorder, have a strong link to DHA. For instance, meta-analysis indicates that DHA supplementation trials have shown relatively consistent and effective benefits for patients with attention deficit hyperactivity disorder (74). Moreover, low levels of DHA and DHA-derived lipid mediators are associated with the pathophysiology of several diseases including Parkinson's, multiple sclerosis, and Alzheimer's (261-263). ACSL6 specific mutations have been linked to schizophrenia and ACSL6 expression is downregulated in Parkinson's disease patients and relevant models (170-172, 218, 255, 256). In agreement with a role for DHA in protection against Alzheimer's disease and dementia, ACSL6 deficient mice had impairments in memory. Since high cholesterol is a strong risk factor for Alzheimer's disease, whereas DHA is a protector (264, 265), it is possible that these two risk factors are linked due to ACSL6-deficiency-induced DHA deficit impact upon SREBP-mediated increases in cholesterol biosynthesis genes, a finding also reported in other models of DHA deficit (244, 266, 267). Thus, low DHA may increase the risk for Alzheimer's directly by a gap in DHA's neuroprotective actions and indirectly due to low DHA's impact on cholesterol biosynthesis. Together, these data suggest that ACSL6 is involved in providing the adequate lipid environment for maintaining motor-controlling mechanisms of the central nervous system.

In summary, we show that ACSL6 is a major contributor to membrane DHA across the brain throughout the lifespan. The loss of ACSL6 results in impaired spatial memory, hyperlocomotion, and early-onset neuroinflammation in the aging cerebellum. Additionally, these data suggest that transcriptional control of synaptic proteins is dysregulated in response to altered membrane acyl-chain composition in a manner that

precedes neurological impairments. Ultimately, this work demonstrates that *Acsl6* is a key regulator of brain DHA metabolism that confers neuroprotection during aging.

Methods

Animals: Mice were maintained on a 12hr light-dark cycle and had *ad libitum* access to chow (Teklad Global 18% protein rodent diet; Envigo) and water. Chow diet essential fatty acids were not of marine sources and was free of DHA. All experiments were approved by the East Carolina University and the Purdue University Animal Care and Use Committees. *Acsl6*$^{flox/flox}$ mice were bred to CMV- or GFAP Cre transgenic mice (Jackson Laboratories stock #006054 and #024098) to generate germ-line global (*Acsl6*$^{-/-}$) or astrocyte-specific (*Acsl6*$^{G-/-}$) knockout mice, respectively and as previously described (48).

Behavioral tests: Locomotor activity of 2-3-month old mice was recorded after two days of acclimation in metabolic chambers using an infrared light beam system integrated to an indirect calorimetry system (CaloSys, V2.1, TSE Systems Inc, Germany) (268) . Open field locomotor activity and exploratory behavior of 18-month old mice were assessed in an open arena (62x62x46 cm) over a 10-minute period. Activity was recorded and analyzed with ANY-MAZE video tracking system (Wood Dale, IL). The Barnes maze (BM) was used to assess hippocampal-dependent spatial learning and memory as previously described (269). The BM consisted of a 1.22m diameter circular platform with 18 holes equally spaced along the outer edges. A dark escape box was placed underneath one of the holes. The BM was conducted over a total of 5 days. Four training days, each with 4 trials separated by 15-20 minutes, and 1 testing day. Prior to the first trial each day, mice were acclimated for 30 minutes in the dark. The mouse was placed in the center of a platform inside a dark plastic cup. After 1 minute the cup was lifted and the mouse was given 3 minutes to find and enter the escape box. If the mouse failed to

find the box after 3 minutes, it was guided to it. On day 5, a probe trial was performed in which the escape box was removed, and the mouse was allowed to explore for 90 seconds to search for the escape box. Performance was recorded and analyzed with ANY-MAZE video tracking system (Wood Dale, IL). The learning index was calculated by subtracting the average latency to reach the escape box on day 4 from day 1 (Learning index > 0 means the mouse learned). Novel object recognition test was used to assess recognition memory. 2-month old mice were placed inside a (25x25 cm) box and allowed to explore two identical objects (familiar) for 10 minutes. Six hours later one object was replaced with a novel object, and mice were placed back into the box to explore for 10 minutes. Discrimination index was calculated as follows: (Time in novel-Time in familiar)/(Time in novel-Time in familiar). The Y-maze spontaneous alternation test was performed to assess spatial working memory. 2-month old mice were placed in a Y-shaped maze composed of 3 equidistant arms and allowed to freely explore for 5-minutes. The alternation percentage was calculated by dividing total alternations by the total number of possible triads [(Total alternations) / (total entries – 2)] * 100.

Molecular: Total tissue RNA isolation was performed using TRIzol (Life Technologies), quantified by NanoDrop 1000 spectrophotometer (Thermo Fisher Scientific), and used to synthesize cDNA with High Capacity cDNA Reverse Transcriptase (Applied Biosystems). Real-Time PCR was performed using SYBR Green Master Mix (Bio-Rad) and primers for the target genes and analyzed using the QuantStudio 3 Real-Time PCR System (Applied Biosystems). Gene expression was normalized to the average Ct values of the housekeeping gene *Rpl22* and expressed as $2^{-\triangle CT}$. For RNAseq, cerebellar RNA was isolated using TRIzol and sent for standard RNA-

seq and initial bioinformatics analysis to Genewiz (South Plainfield, NJ). Libraries were prepared via the Poly(A) selection method and sequenced on one lane of the Illumina HiSeq with 2x150bp configuration. Raw sequences were evaluated for quality and trimmed using Trimmomatic v.0.36. Quality trimmed reads were mapped to the Mus musculus GRCm38 reference genome available on ENSEMBL to create BAM files using the STAR aligner v.2.5.2b. Unique gene hit counts from the reads that fell within exon regions were calculated using the featureCounts function of the Subread package v.1.5.2. Differential gene expression (DEG) analysis was performed using DESeq2. Comparisons by age (2- vs 18-months) and genotype (Control vs *Acsl6*$^{-/-}$) were performed and the Wald test was used to calculate p-values and log2 fold changes. Thresholds were set for p-value<0.05. Enriched pathways of differentially expressed genes were calculated using REACTOME version 72 and the top significant pathways with a minimum of ten genes and belonging to the second, third, and fourth hierarchical levels were plotted (270). If pathways from the same category but different hierarchical levels have gene overlap, then the pathway with the lowest hierarchical level containing >90% of the genes was selected. Analysis for generating the Venn diagram was performed using Venny 2.1 (271). An unbiased analysis of all the samples was performed to obtain normalized counts and generate the heatmaps. Heatmapper (Wishart Research Group, University of Alberta, Edmonton, Canada) was used to cluster genes employing the Pearson distance correlation measurement (272). GO terms were identified using Gene Ontology enRIchment anaLysis and visuaLizAtion tool (GOrilla)(273). For smFISH, HiPlex RNAScope was performed on whole brains from adult mice fixed by immersion in 4% paraformaldehyde at 4ºC, washed in a graded sucrose series (10%, 20%, 30%),

embedded in OCT, frozen, and cryosectioned (5 mm). A series of sections were stained with Nissl to locate the relevant brain slice according to the Allen Mouse Brain Atlas. Twelve-plex smFISH was performed on fixed frozen tissue sections according to manufacturer recommendations using the RNAscope HiPlex8 Reagent kit and RNAscope HiPlex12 Ancillary Kit [Advanced Cell Diagnostics (ACD)] to detect transcripts from the following genes *Acsl6* (#584161), *Meg3* (#527201), *Slc17a7/Vglut1* (#416631), and *Slc32a1/Vgat* (#319191). FISH detection was performed using the RNAscope HiPlex Alternative Display Module (#30040) and DAPI counterstain with an AxioImager M1 microscope equipped with 20x/0.8NA and 63X/1.3NA objectives and an AxioCam MRm (Carl Zeiss Microscopy). Images from multiple rounds were combined using RNAscope HiPlex Registration Software (#300065). Probes targeting a panel of housekeeping gene mRNAs (RNAscope HiPlex12 Positive Control Probe-Mm; #324321) served as positive controls and an irrelevant bacterial gene was the negative control (ACD #324341), which were labeled on adjacent sections.

Lipidomics: Total fatty acid composition was determined on extracted and fatty acid methyl esters (FAME) prepared using a one-step extraction/methylation method as described in detail elsewhere (274). Hippocampal samples were treated with an aqueous solution (CH3OH: 2,2-Dimethoxypropane (DMP): H2SO4= 8.5: 1.1:0.4, v:v:v) and an organic solution (heptane: toluene=6.3:3.7, v:v) at 80°C for 2 h. FAMEs were reconstituted in heptane and stored at 20°C until analysis. FAMEs were positively identified by high-resolution capillary gas chromatography covalent adduct chemical ionization tandem mass spectrometry with GCMS TQ8050 triple quadrupole mass spectrometer equipped with a prototype solvent assisted chemical ionization device

interfaced to a GC QP2010Plus gas chromatograph (Shimadzu Scientific Instruments). FAME were quantified using a separate QP2010 GC with a Flame Ionization Detector (GC-FID). Response factors were measured daily using an external standard and applied to peak areas to yield calibrated weight percents (275). Specialized lipid mediators were profiled by HPLC tandem mass spectrometry (LC-MS/MS) by the University of Colorado, Aurora, Skaggs School of Pharmacy Mass Spectrometry Facility, as described (276). MALDI lipid imaging of flash-frozen whole brains, sliced 10 microns thick was performed by the Structural Biology Core of NIDA IRP, as described (23), using Thermo Scientific MALDI LTQ-XL-Orbitrap (Thermo Fisher Scientific) and Xcalibur software in positive and negative ion mode with a mass resolution of 60,000 in the mass range of 600 - 1000 Da. The raster step size of 40 µm for both the X and Y directions. DHB matrix (at 40 mg/mL concentration in 70% methanol) is sprayed using TM-sprayer (HTX Technologies). Assignment of lipid species identity is based upon accurate mass with mass error ≤2 ppm in positive ion mode and ≤3.5 ppm in negative ion mode. Broad MRM-based lipid profiling was performed with Purdue's Bindley Metabolite Profiling Facility, as described (48). Briefly, lipids were extracted from tissues using Bligh and Dyer Method(232). The lipid phase was dried, resuspended and injected through a micro-autosampler (G1377A) into a QQQ6410 triple quadrupole mass spectrometer (Agilent Technologies) operated in the positive ion mode and equipped with a Jet stream ESI ion source. Data were analyzed by calculating the percent distribution for each ion (ion peak of m/z intensity/total ion intensity) and identified based on LipidMaps database.

Immunoblots and Histology: Mouse brain lysates were collected in lysis buffer (50mM Tris-HCl, 150mM NaCl, 1mM EDTA, and 1% Triton X-100). Proteins were

electrophoresed in 10% gels, transferred to nitrocellulose membranes, and blocked with 5% milk in Tris-buffered saline, containing 0.1% tween 20 (TBS-T) for 1 hour at room temperature (RT). Blots were probed for the primary antibodies ACSL6 (1:1000, Sigma HPA040470), SNAP25 (1:10,000, Abcam ab5666), PSD95 (1:2000, Invitrogen MA1-045), Calbindin (1:1000, Sigma C9848), NeuN (1:1000, Millipore ABN78), and β-tubulin (1:1000, Sigma T0198) in 3% Bovine Serum Albumin (Sigma) in TBS-T overnight at 4°C, washed, and probed for anti-mouse or anti-rabbit IRDye-conjugated secondary antibodies (LiCor) for 1 hour at RT. Membranes were scanned with LiCor Odyssey instrument and protein was quantified using LiCor software. Brains were collected and fixed in 4% PFA for 7 days and then incubated in 30% sucrose for 7 days at 4 °C. Brain coronal sections were cut at 35□m thickness using a frozen sliding microtome (Microm HM 450, Thermo Scientific) and stored in cryoprotectant at −20 °C until use. Cerebellums were selected, washed 6 times for 10 minutes with PBS at RT and blocked in PBS containing 0.3% Triton X-100 (PBS-T) with 10% normal donkey serum (NDS) for 1hr at RT, primaries (GFAP, Abcam 53554; IBA1, Wako WEE4506) for 24-48 h in PBS-T with 1% NDS at 4 °C, washed in PBS, and subsequently incubated with secondary antibodies in PBS-T with 1% NDS for 2hrs at RT (Alexa Fluor 488 anti-goat and Alexa Fluor 647 anti-chicken, Jackson Immunoresearch). After washing with PBS at RT, 6 times for 10 min each, slides were dehydrated through graded alcohol, cleared, and coverslipped. Images were obtained using an inverted Nikon D-Eclipse C1 confocal microscope. GFAP and IBA-1 staining were analyzed using Fiji imaging software. Briefly, for GFAP, the region of interest was delineated, and the threshold background correction was defined using the same automated threshold algorithm for all images to create binary images. Mean

intensity and % area fraction (area occupied by GFAP+ cells/area of white matter*100) above the set threshold were calculated. For Iba-1, % area fraction of IBA-1+ cells and the perimeter of the 10 microglia with the largest body size within the cerebellar white matter were calculated.

Statistics: Data are presented as mean ± SEM for each group, unless otherwise specified. Data were analyzed using Prism 9.0 software (GraphPad). The statistical significance was determined using 2-tailed unpaired Student's t-test for comparison of two groups, one-way ANOVA with Tukey post hoc test for more than 2 groups, and two-way ANOVA with Sidak post hoc test for multivariate analysis and significance level was set at $p<0.05$, unless otherwise specified.

Author Contributions

RFF, ASP, and JME designed and conducted research studies; VD, ESW, KAL, JM, SNJ, JBE, BPH, and JTB acquired data and provided reagents; RFF and JME analyzed data and wrote the manuscript.

Acknowledgements

We thank Dr. Amy Brewster for use of behavioral phenotyping equipment and Sora Q. Kim for assistance with the histology, Purdue University, and Alexis B Knotts for assistance with behavioral phenotyping. This work was supported by the Lina Mae Edwards Young Investigator Award from the Dementia Alliance of North Carolina.

Supplementary Information

This article contains supporting information.

Figure 4.1. Effects of *Acsl6* loss on hippocampal DHA content during aging

(A) Heatmap of PCs clustered by degree of saturation in control and *Acsl6*$^{-/-}$ hippocampus, n=5. Data are presented as % ion intensity distribution, species >0.5% of total are shown. (B,C) % of total hippocampal fatty acid content in 6-month old control, *Acsl6*$^{G-/-}$, and *Acsl6*$^{-/-}$ mice, n=3-6. (D) Hippocampal immunoblot against ACSL6 and (E) cerebellar gate domain-targeted RT-PCR in control, *Acsl6*$^{G-/-}$, and *Acsl6*$^{-/-}$ mice, n=4. (F) % change of DHA from 6-months to 18-months in control and *Acsl6*$^{-/-}$ hippocampus, n=3-6. (G) Omega-6 to omega-3 ratio and (H) % omega-3 and omega-6 total fatty acids in 6- and 18-month old control and *Acsl6*$^{-/-}$ hippocampus, n=3-6. Data represent mean ± SEM; * compared to control, & by age within genotype, # compared to *Acsl6*$^{G-/-}$. p≤0.05 (B, C, E) by one-way ANOVA with Tukey post hoc test, (G, H) by two-way ANOVA with Sidak post hoc test, and (F) by Student's t-test.

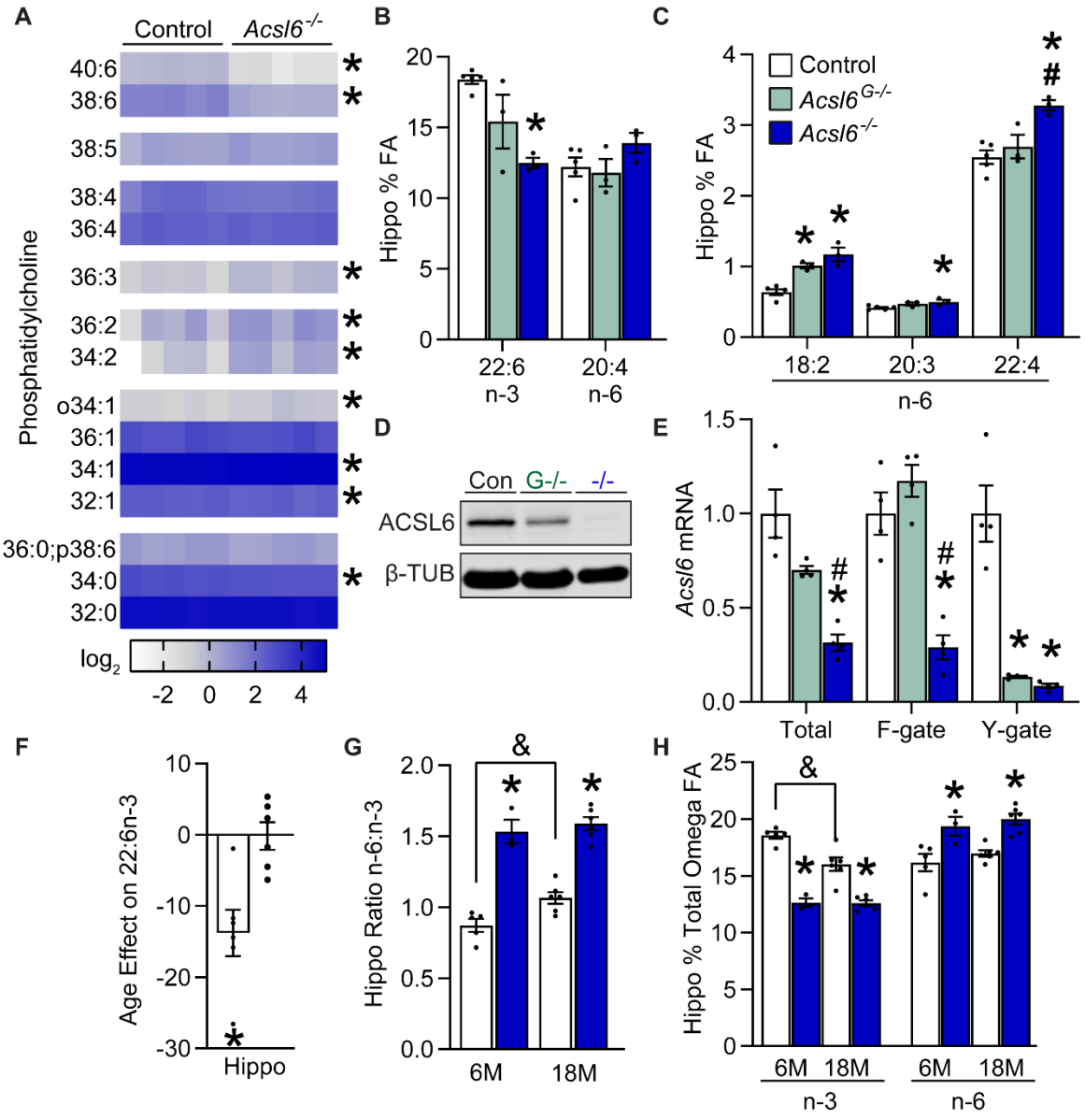

Figure 4.2. *Acsl6* is expressed in neurons and mediates brain DHA enrichment

(A) *Acsl6* detection by smFISH in hippocampus and CA3 and DG regions; Blue: nuclei, green: *Acsl6*, white: *Meg3* (pseudo pan-neuronal nuclear marker), and purple:*Vglut1*. White box indicates area of inset (Scale bars: Hippocampus, 200 μm; CA3 and DG, 50 μm; inset, 5 μm). Lipid imaging by MALDI of predicted (B) DHA-containing PCs (PC 40:6 m/z=872.5566, [M+K]+ and PC 38:6 m/z = 844.5253 $[M+K]^+$) and (C) AA-containing PCs (PC 36:4 m/z = 820.5253 [M+K]+ and PC 38:4 m/z = 848.5566 $[M+K]^+$) in control, *Acsl6*$^{G-/-}$, and *Acsl6*$^{-/-}$ hippocampus (Scale bars: 500 μm).

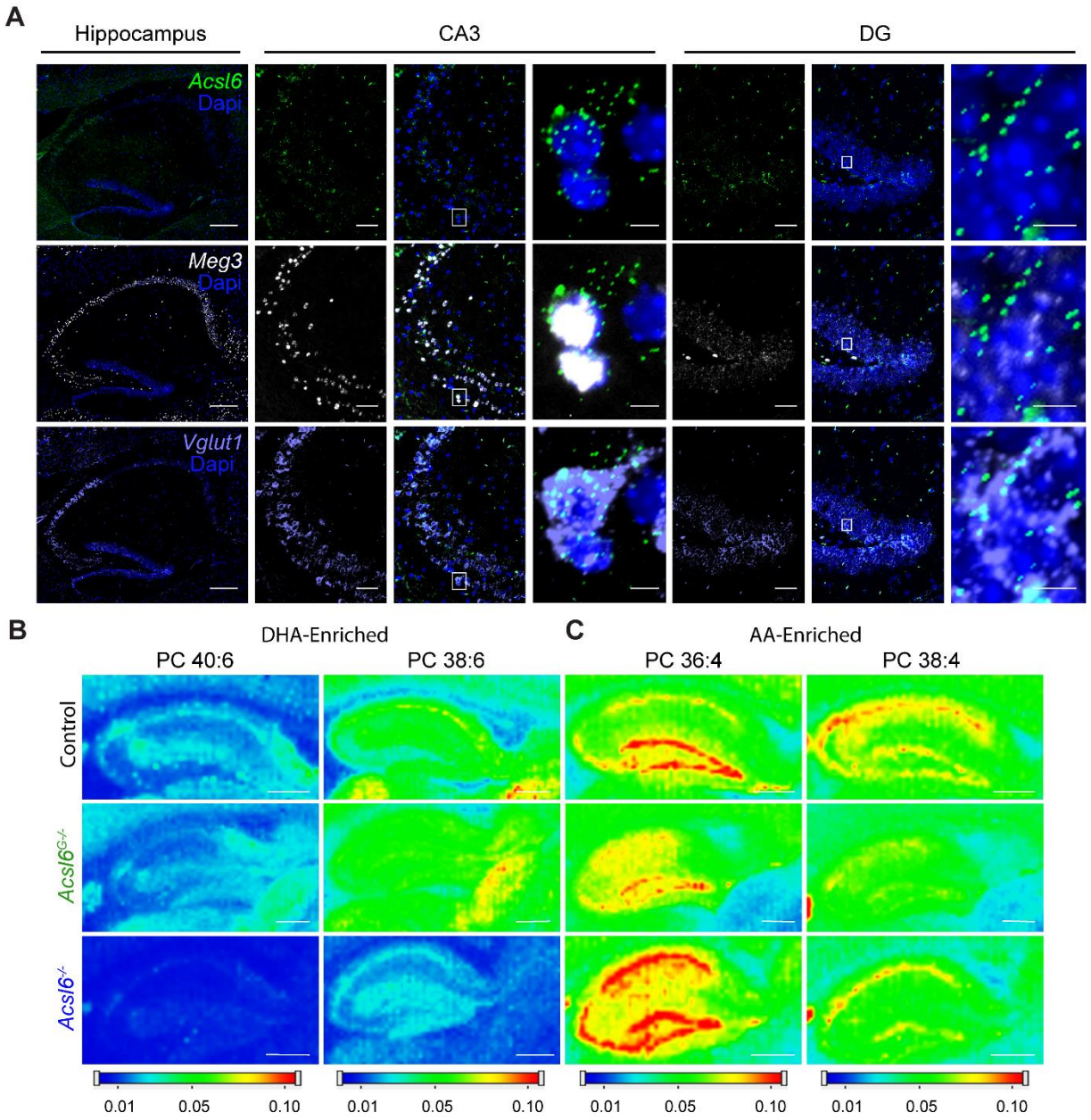

Figure 4.3. *Acsl6* exhibit reduced short term spatial working memory and induces hyperlocomotion

(A) Y-maze % spontaneous alternations of 2-month old female (F) and male (M) control and *Acsl6*$^{-/-}$ mice, n=22-24. Hippocampal-dependent spatial memory and learning was assessed using the Barnes Maze (BM): (B) learning index during training, (C) latency to first enter target zone, (D) % time and (E) distance spent in each quadrant (Q) 1 or Q2-Q4, and (F) freezing bouts during the probe trial for 18-month old control and *Acsl6*$^{-/-}$ males, n=6. (G) Total entries in the Y-maze for 2-month old control and *Acsl6*$^{-/-}$ males and females, n=22-24. (H) Maximum speed and (I) % distance travelled in the center of the open field (OF) achieved over a 10-minute period for 18-month old control and *Acsl6*$^{-/-}$ males (M) and females (F), n=6-10. (J) Total beam breaks in metabolic chambers of 2-month old control and *Acsl6*$^{-/-}$ males (left) and females (right), n=6-13. (K) Latency to fall from the rotarod over 6 trials, 3 per day, n=6. Data represent mean ± SEM; * by genotype, & Q1 versus Q2-Q4, p≤0.05 by Student's t-test.

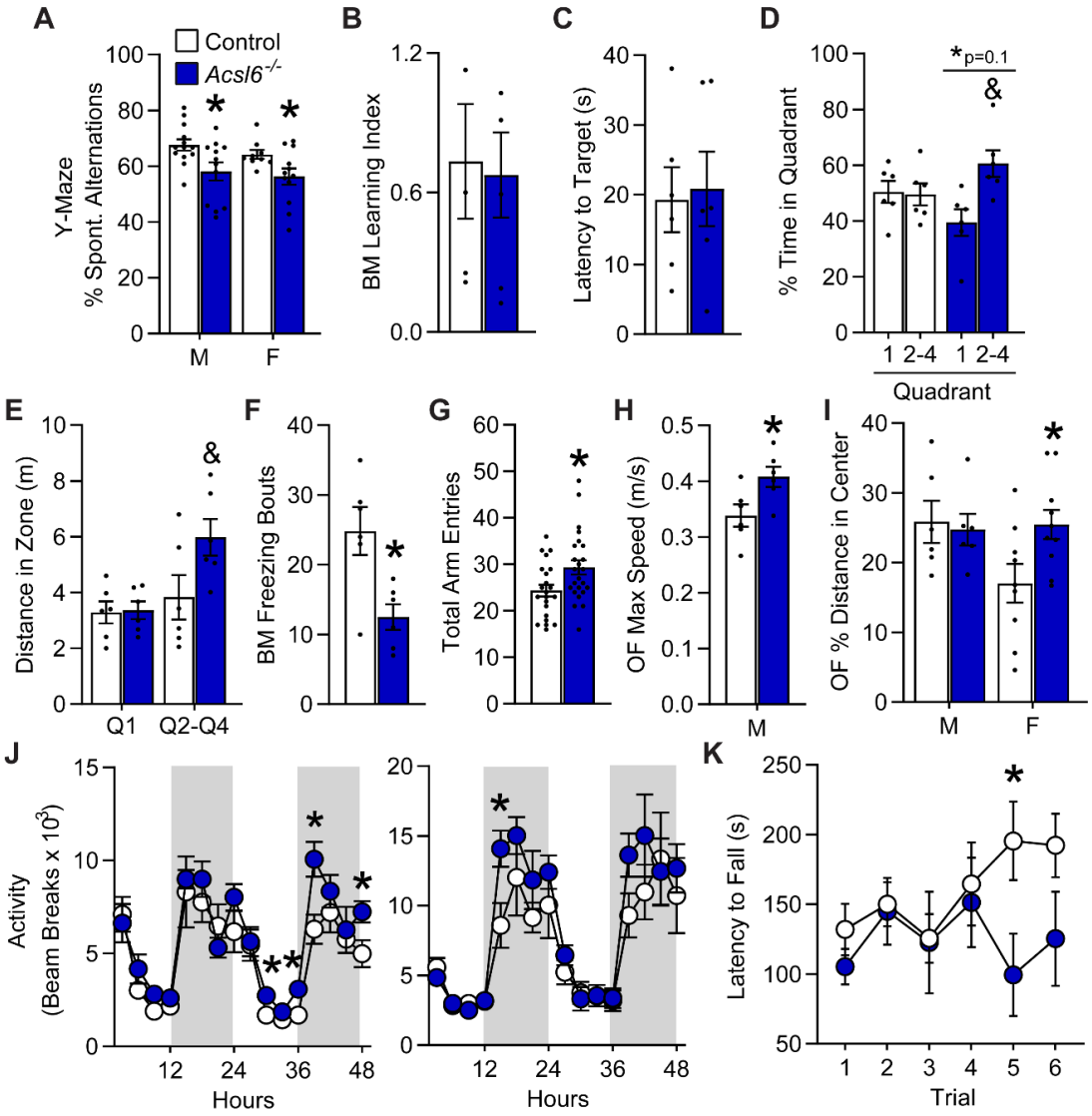

Figure 4.4. *Acsl6* deletion results in DHA deficiency in the cerebellum during aging

(A) Percent of total intensity for DHA-containing PCs (38:6 and 40:6) in hippo and cere, n=6, with MALDI inset of PC40:6 (m/z=872.5566, $[M+K]^+$) in control mice. (B) Percent loss of DHA-containing PCs in *Acsl6*$^{-/-}$ hippocampus (Hip) and cerebellum (Cere) relative to control mice. (C) Lipid imaging by MALDI of the predicted DHA-containing PC 40:6 (m/z=872.5566, $[M+K]^+$) of control and *Acsl6*$^{-/-}$ cerebellum (Scale bars: 500 μm). (D) *Acsl6* detection by smFISH in cerebellum and inset: blue, nuclei; green, *Acsl6;* white, *Meg3;* purple, *Vglut1;* and yellow, *Vgat*. Arrows indicate *Acsl6*+ cells, scale bars: 20 μm; inset, 10μm. (E,F) Distribution of phospholipids in 6 or 18-month-old control and *Acsl6*$^{-/-}$ cerebellum, n=5-6. Data represent mean ± SEM; * by genotype within age, & by age within genotype, and # compared to hippocampus, p≤0.05 (A) by Student's t-test and (E and F) by two-way ANOVA with Sidak post hoc test.

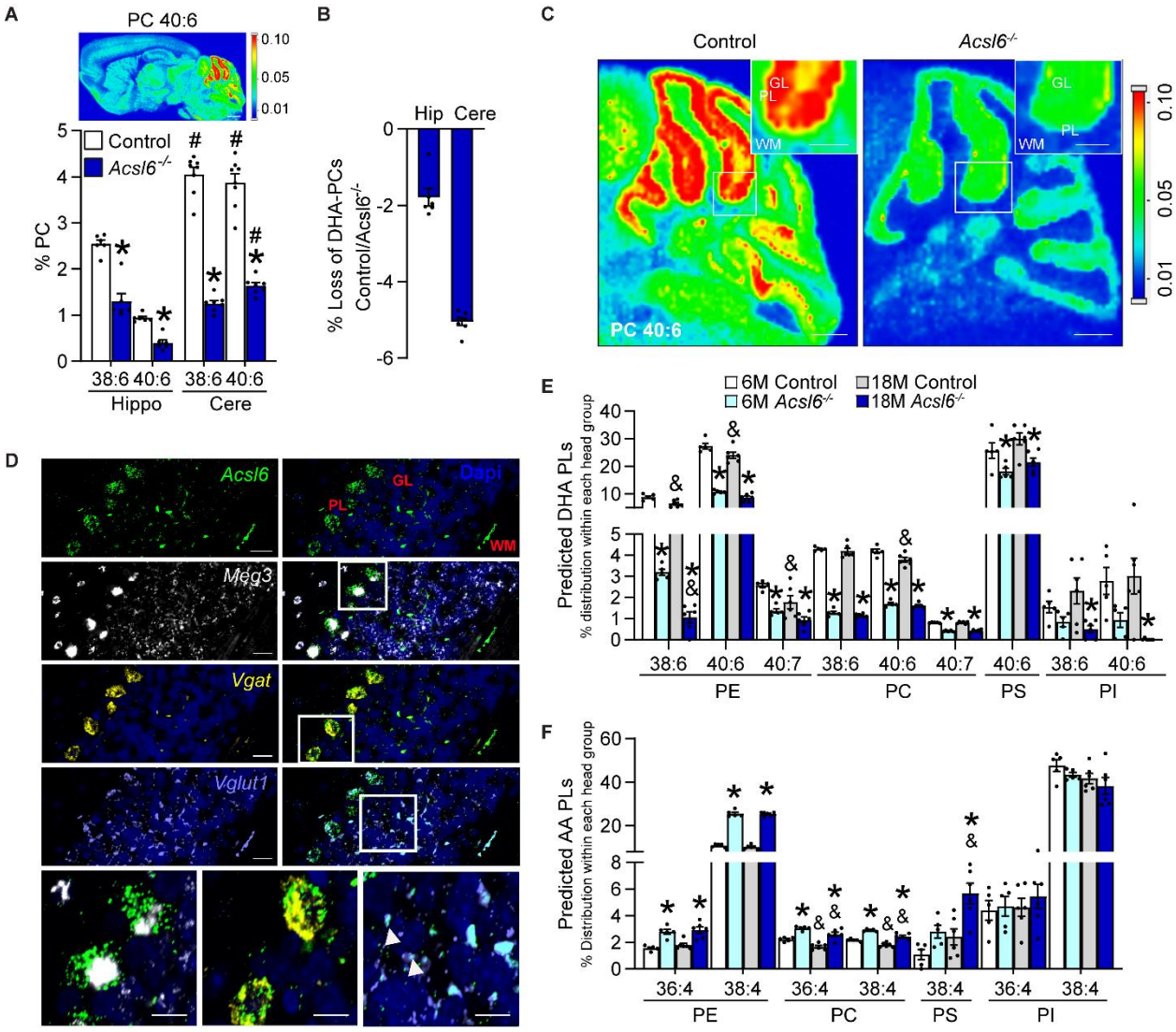

Figure 4.5. Differential expression analysis in young and aged *Acsl6*$^{-/-}$

RNA-seq profiling was performed in young (2-month) and aged (18-month) female control and *Acsl6*$^{-/-}$ cerebellum. (A) Heatmap of all differentially expressed genes (DEGs) by either genotype within age or age within genotype, p≤0.01, graphed according to Pearson's distance and centroid linkage cluster method. (B) Venn diagram of DEGs by padj.≤0.05 for genotype comparison in either young or aged mice. (C) Heatmap of genes associated with the regulation of cholesterol biosynthesis. (D) Volcano plot of aging-effect DEGs of ribosomal protein genes for *Acsl6*$^{-/-}$ compared to controls at either 2- (Young) or 18- (Aged) months of age. (E) GO terms from DEGs p≤0.05 for *Acsl6*$^{-/-}$ compared to controls at 18-months of age (mem, membrane; PM, plasma mem; p, biological process; c, cellular component). (F) mRNA abundance of synaptic proteins of young and aged *Acsl6*$^{-/-}$ cerebellum, expressed relative to age-matched control mice. Data represent mean ± SEM; * by genotype within age, p≤0.05 by Student's t-test.

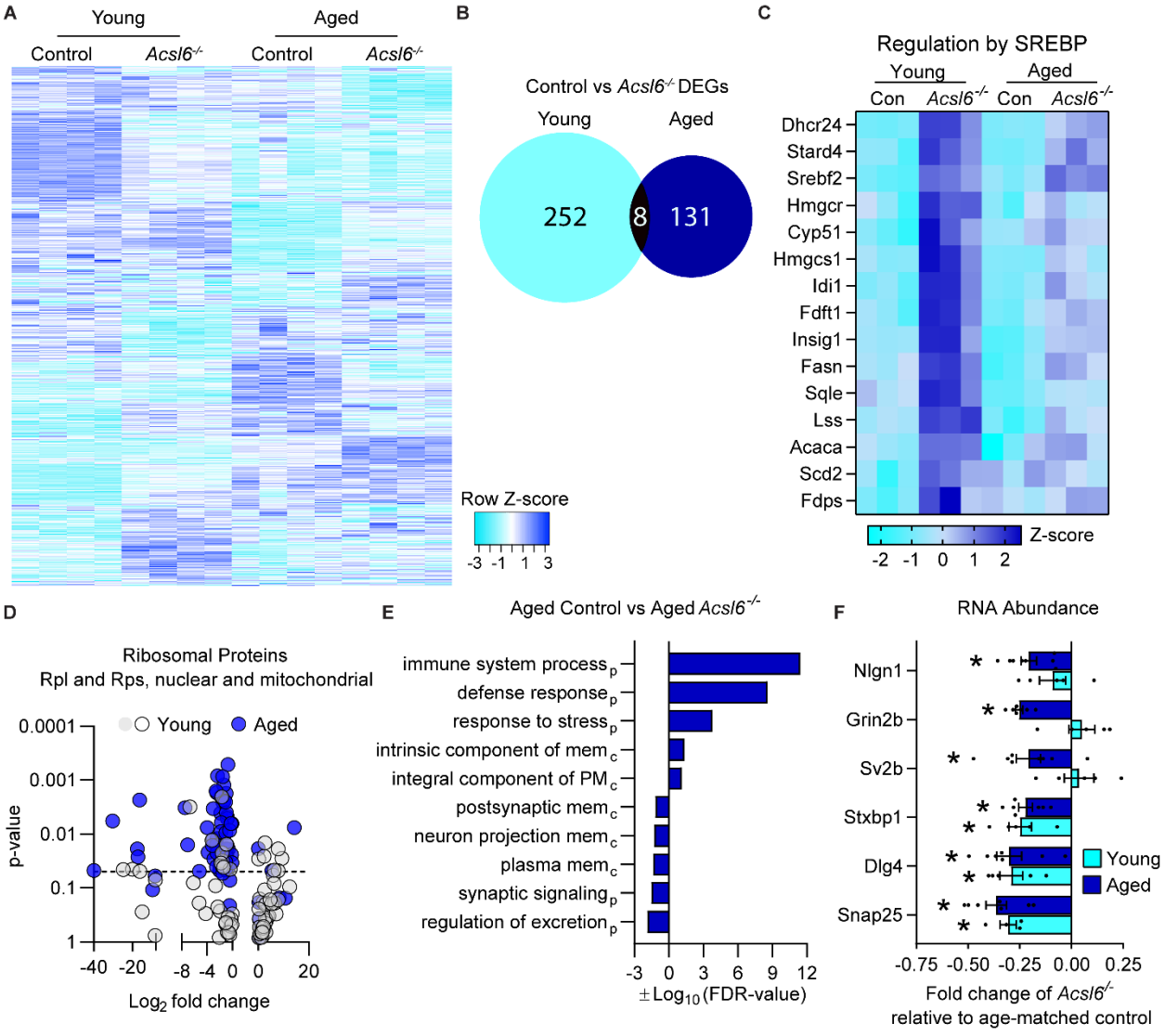

Figure 4.6. *Acsl6* deficiency minimally impacts fatty acid derived lipid mediator profile

Stack bar plot of lipid mediators generated from (A) cyclooxygenase, (B) lipoxygenase, (C) cytochrome oxygenase, (D) reactive oxygen species, and (E) LA-derived lipid mediators in 2- and 18-month old control (C) and *Acsl6*$^{-/-}$ (K) cerebellum, n=5-6. The error bars indicate SEM from each lipid mediator. Statistical significance was calculated from the total amount of lipid mediators in the stacked bar, * by genotype within age, and & by age within genotype, p≤0.05 by Student's t-test. (F) Heatmap of significantly DEGs from RNA-seq (p≤0.05) associated with the biosynthesis of lipid mediators plus the phospholipase A2 enzymes in cerebellum, n=4. DEGs were clustered using the Pearson distance correlation measurement method, *(2M) and *(18M) by genotype, &(control) and #(*Acsl6*$^{-/-}$) by age, p≤0.05 by Student's t-test.

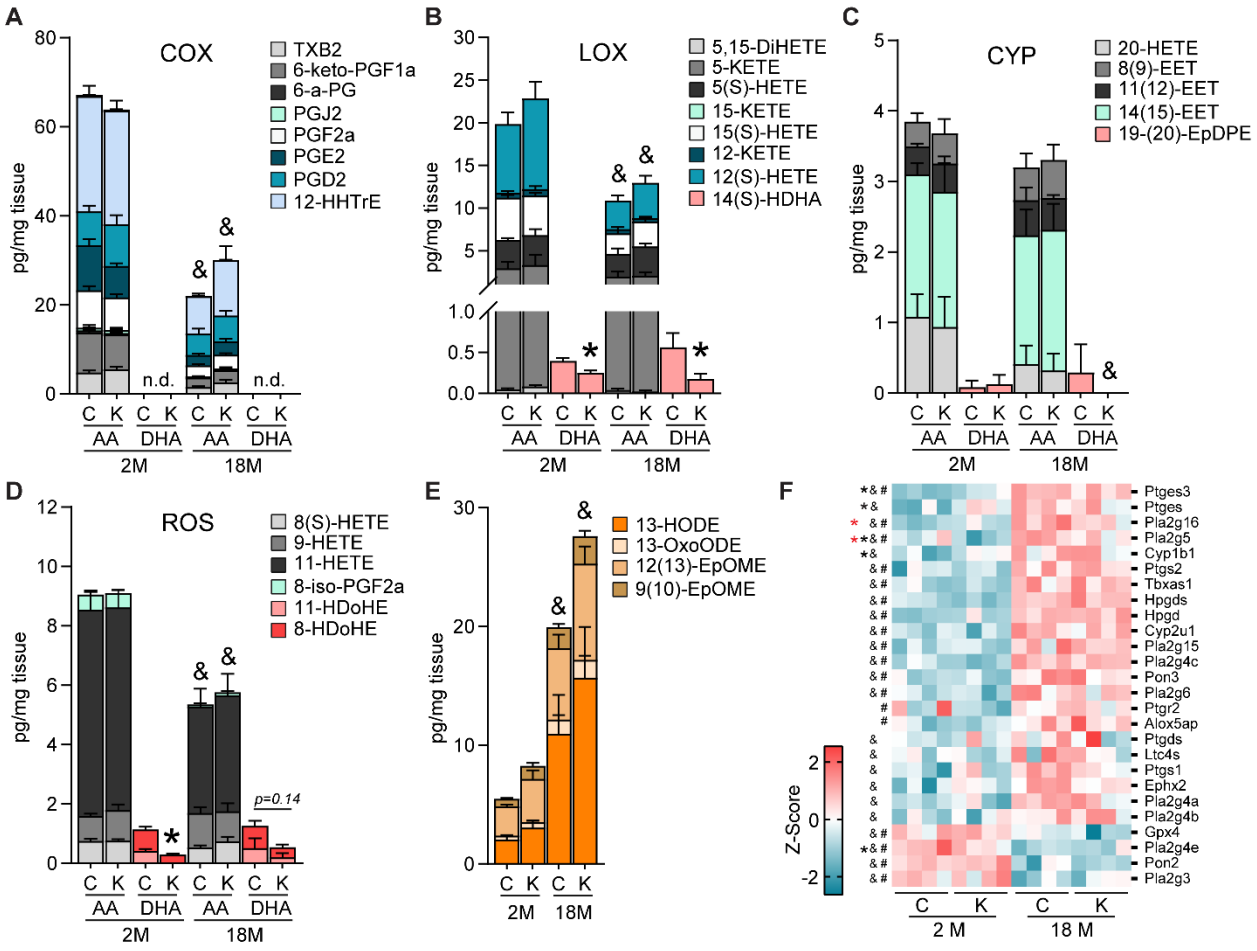

Figure 4.7. *Acsl6* deficiency results in age-related neuroinflammation

(A) Immunostaining representative images of GFAP (green) and IBA-1 (red) in 12-month old male cerebellum (Scale bars: 50 μm and 25 μm). (B) Mean intensity and % area fraction occupied by GFAP+ cells in cerebellar white matter. (C) Soma perimeter of the 10 largest microglia in cerebellar white matter and % area fraction of microglia of 12-month old control and *Acsl6*$^{-/-}$ cerebellum. mRNA abundance of (D) inflammatory and (E) myeloid cell markers of 6-, 12- and 18-month old *Acsl6*$^{-/-}$ male cerebellum normalized to Rpl22 and relative to control, n=6-8. Data represent mean ± SEM; * by genotype, p≤0.05 by Student's t-test.

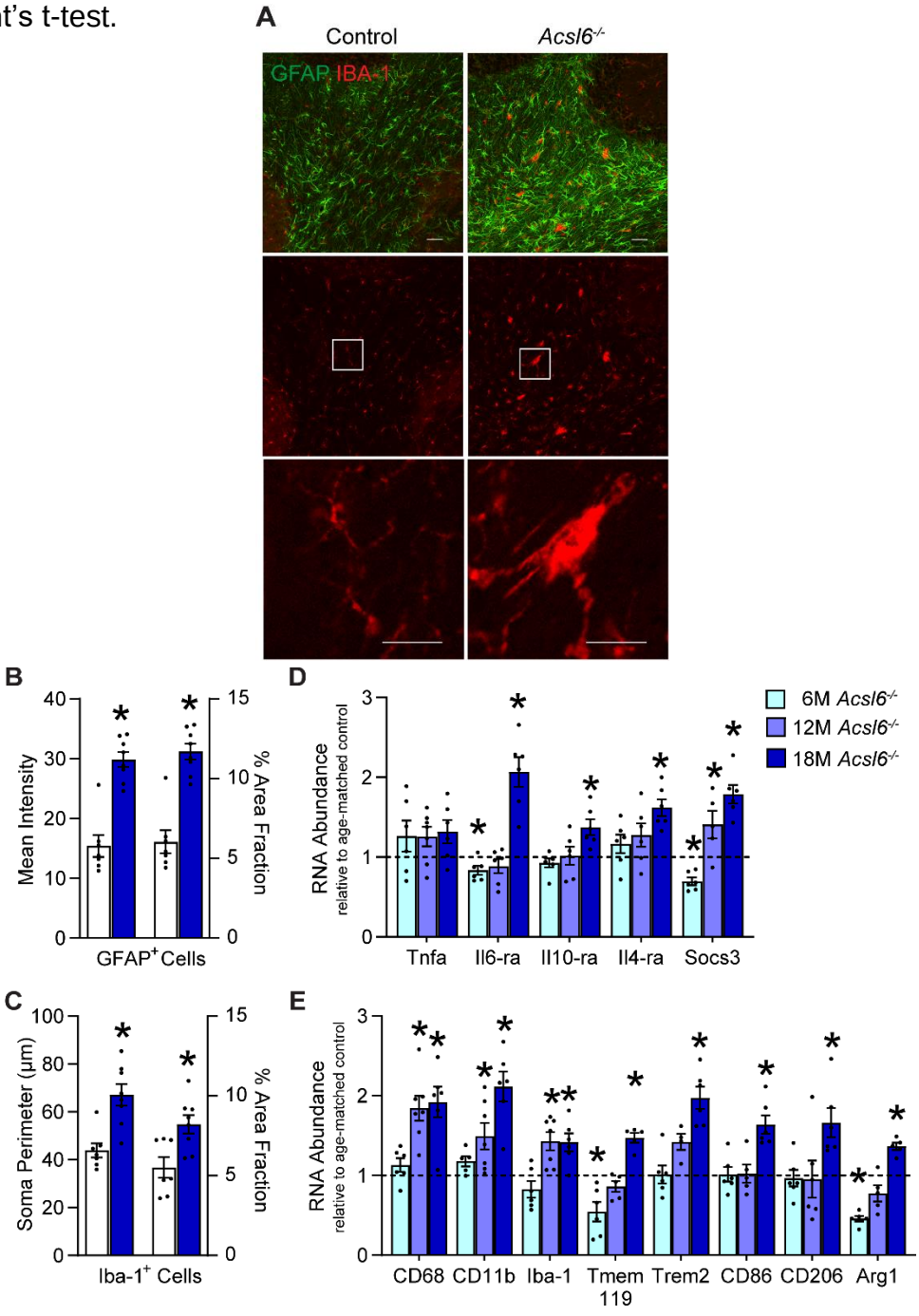

Supplemental Figure 1 (4.8). Behavior Tests

(A) % preference for the familiar (F) and novel (N) objects and (B) discrimination index during the novel object recognition test for 2-month old control and *Acsl6*$^{-/-}$ males, n=9. (C) Distance and (D) freezing bouts spent in each quadrant during the probe trial of the Barnes Maze for 18-month old control and *Acsl6*$^{-/-}$ females, n=9-10. Data represent mean ± SEM;* by genotype, $ within genotype, & within genotype and different from quadrant 1, p≤0.05 by Student's t-test.

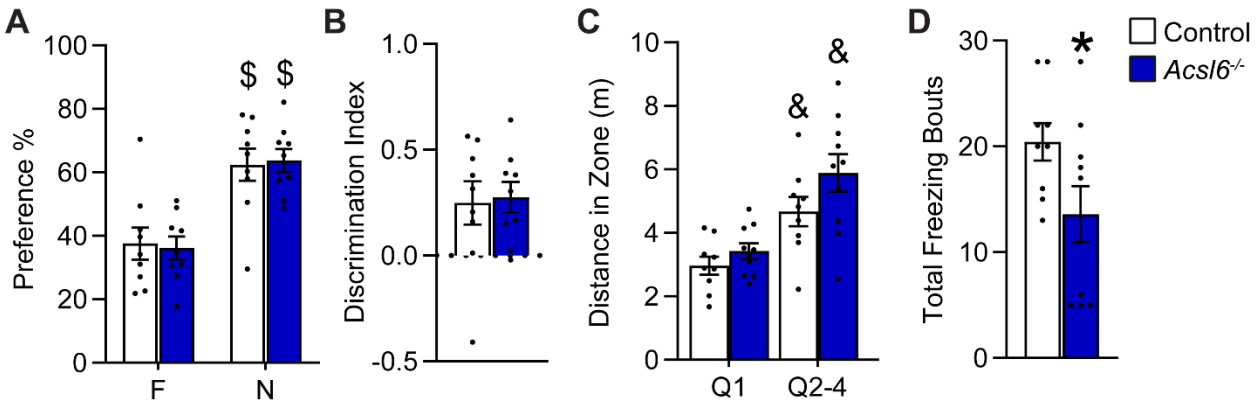

Supplemental Figure 2 (4.9). Differential expression analysis in young and/or aged control and Acsl6$^{-/-}$

RNA-seq profiling was performed in 2- (Young) and 18- (Aged) month old female control and *Acsl6*$^{-/-}$ cerebellum, n=4. (A) Venn diagram and REACTOME pathway analysis of significantly DEGs or pathways comparing control to *Acsl6*$^{-/-}$ at either 2 or 18-months of age. (B) Venn diagram and REACTOME pathway analysis of significantly DEGs or pathways comparing young and aged control or *Acsl6*$^{-/-}$ mice.

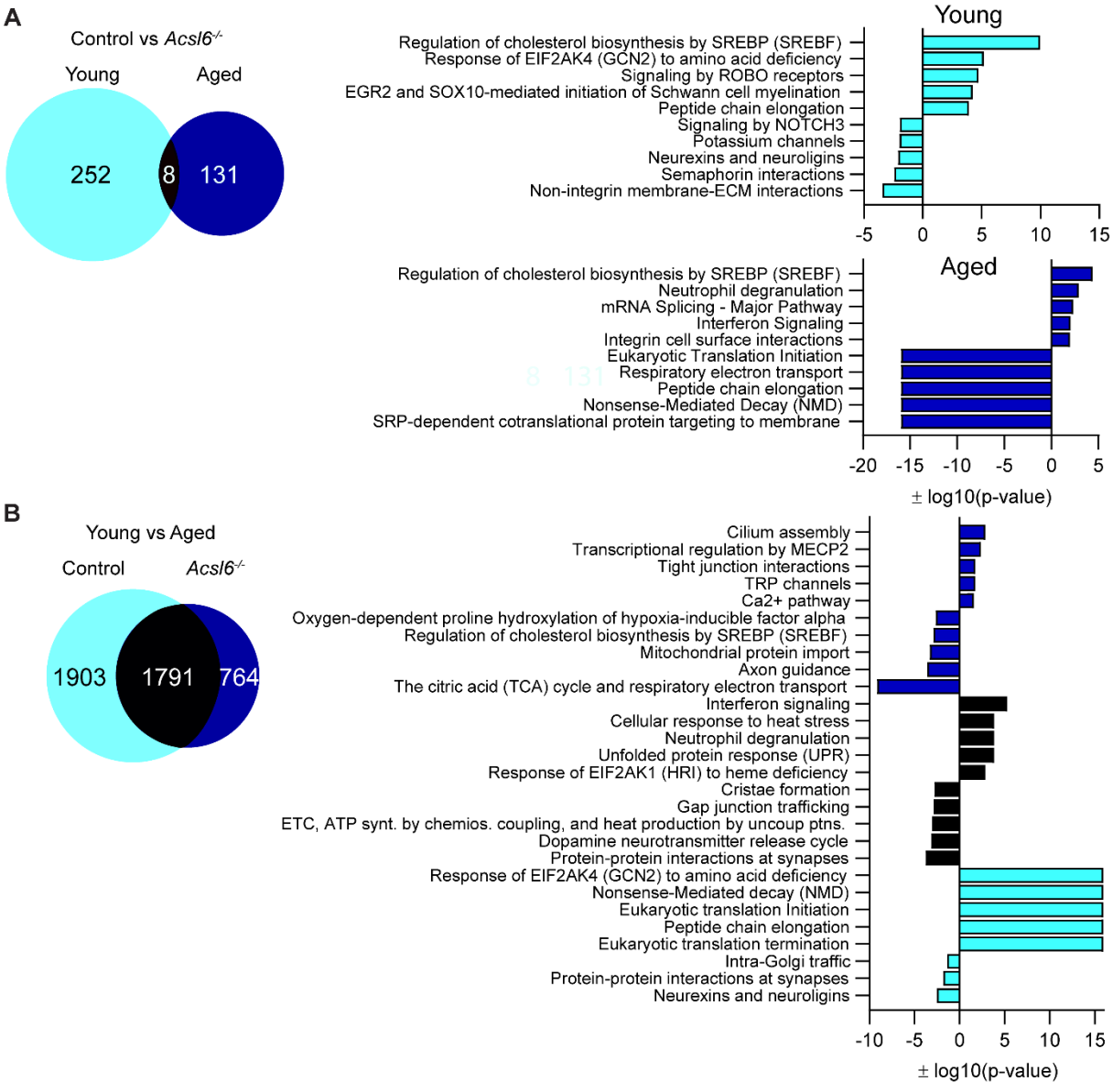

Supplemental Figure 3 (5.0). Effect of astrocytic *Acsl6* loss on lipid content and inflammation

(A) Lipid imaging by MALDI of the predicted DHA-containing PC 40:6 (m/z=872.5566, $[M+K]^+$) of control and *Acsl6*$^{G/-}$ cerebellum (Scale bars: 500μm). (B) mRNA abundance of inflammatory and myeloid cell markers from 12-month old (12M) control and *Acsl6*$^{G/-}$ male cerebellum normalized to housekeeping (average of *Rpl22* and *Tbp*), n=6. Data represent mean ± SEM; * by genotype, p≤0.05 by Student's t-test.

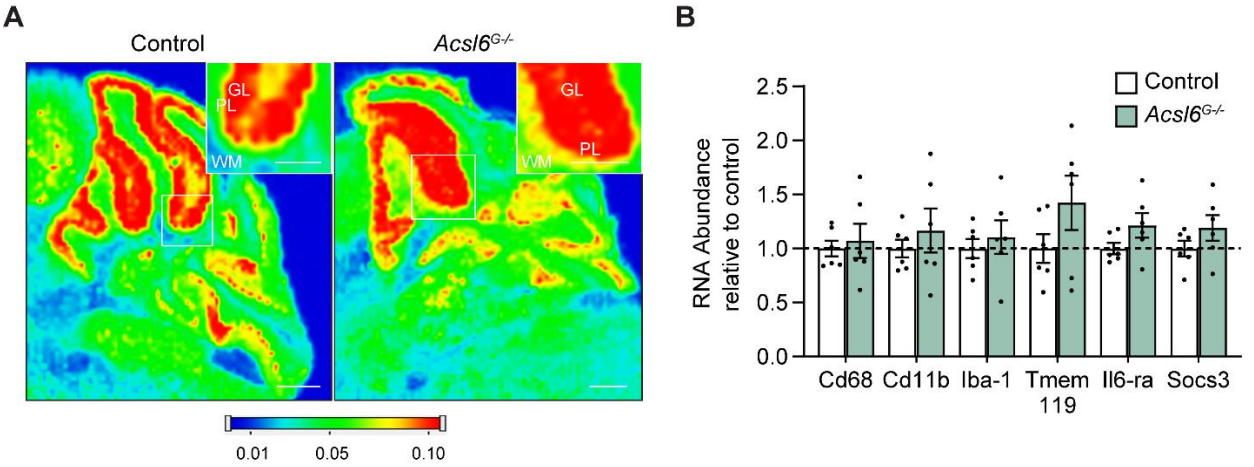

Supplemental Figure 4 (5.1). Indicators of neuronal abundance

(A) Representative immunoblot and (B) quantification of SNAP25 and PSD95 normalized to β-tubulin in 18-month old control and *Acsl6*$^{-/-}$ cerebellum, n=8-9. Brain (C) weight, (D) length, and width from 12-month old control and *Acsl6*$^{-/-}$, n=7-8. (E) Representative immunoblot and (F) quantification of NeuN and Calbindin normalized to β-tubulin in 18-month old control and *Acsl6*$^{-/-}$ cerebellum, n=9.

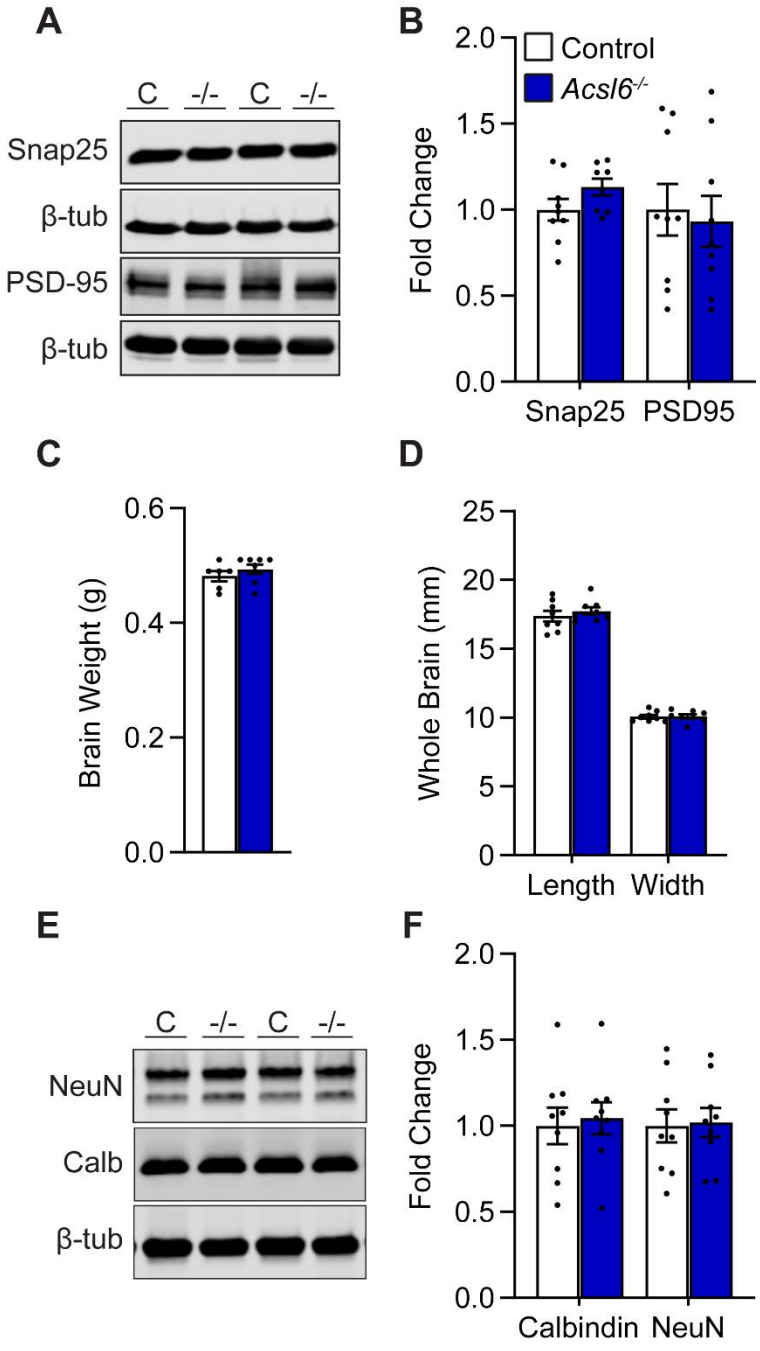

Supplemental Table 1 (4.1). Hippocampal fatty acid profile.

Percent of total fatty acids (%,w/w) in 6-month or 18-month old control, *Acsl6*$^{G-/-}$, and *Acsl6*$^{-/-}$ hippocampus, n=3-6. The omega-3 fatty acid, eicosapentaenoic acid, was below limits of detection. Data represent mean ± SEM;* compare to control, & within genotype, and # compare to 6-month old *Acsl6*$^{-/-}$, p≤0.05 by Student's t-test.

Fatty acid	Common name	6M Control	6M *Acsl6*$^{G-/-}$	6M *Acsl6*$^{-/-}$	18M Control	18M *Acsl6*$^{-/-}$
16:0	PA	22.7 ± 0.23	21.5 ± 1.27	23.1 ± 0.37	21.5 ± 0.59	22.7 ± 0.45
16:1	Palmitoleic acid	0.48 ± 0.02	0.48 ± 0.04	0.57 ± 0.03*	0.55 ± 0.01$^{\&}$	0.56 ± 0.02
18:0	Stearic acid	23.2 ± 0.35	22.3 ± 0.53	22.8 ± 0.15	23.2 ± 0.13	21.7 ± 0.22$^{\&*}$
18:1n9	OA	14.1 ± 0.05	16.8 ± 1.89	15.8 ± 0.64	15.7 ± 0.68	16.5 ± 0.32
18:1n7	Vaccenic acid	3.05 ± 0.14	3.30 ± 0.15	3.32 ± 0.17	3.12 ± 0.10	3.35 ± 0.09
18:2n6	LA	0.64 ± 0.04	1.01 ± 0.04*	1.17 ± 0.09*	0.69 ± 0.04	1.17 ± 0.05*
20:0	Arachidic acid	0.21 ± 0.02	0.34 ± 0.09	0.26 ± 0.02	0.27 ± 0.03	0.26 ± 0.02
20:1	Paullinic acid	0.72 ± 0.15	1.36 ± 0.47	0.87 ± 0.16	1.03 ± 0.20	0.99 ± 0.12
20:2n6	Eicosadienoic acid	0.17 ± 0.01	0.35 ± 0.09*	0.26 ± 0.03*	0.24 ± 0.03	0.25 ± 0.02
20:3n6	DGLA	0.42 ± 0.01	0.47 ± 0.02	0.50 ± 0.03*	0.37 ± 0.02	0.44 ± 0.02*
20:4n6	AA	12.2 ± 0.66	11.8 ± 0.98	13.9 ± 0.70	12.5 ± 0.32	14.0 ± 0.37*
22:0	Behenic acid	0.19 ± 0.03	0.33 ± 0.12	0.24 ± 0.03	0.24 ± 0.03	0.21 ± 0.03
22:1	Erucic acid	0.08 ± 0.01	0.18 ± 0.06	0.12 ± 0.02	0.25 ± 0.06$^{\&}$	0.19 ± 0.02$^{\&}$
22:2n6	Docosadienoic acid	0.18 ± 0.02	0.26 ± 0.06	0.24 ± 0.03	0.25 ± 0.03	0.67 ± 0.49
22:4n6	Adrenic acid	2.55 ± 0.10	2.70 ± 0.17$^{\#}$	3.28 ± 0.07*	2.94 ± 0.12$^{\&}$	3.47 ± 0.10*
24:1	Nervonic acid	0.59 ± 0.11	1.31 ± 0.59	0.98 ± 0.23	1.13 ± 0.21	0.97 ± 0.11
22:5n3	DPA	0.16 ± 0.01	0.16 ± 0.01	0.15 ± 0.01	0.15 ± 0.00	0.14 ± 0.01*
22:6n3	DHA	18.4 ± 0.31	15.4 ± 1.89	12.5 ± 0.36*	15.9 ± 0.60$^{\&}$	12.5 ± 0.24*
SFA		46.2 ± 0.33	44.4 ± 0.55*$^{\#}$	46.4 ± 0.35	45.2 ± 0.63	44.8 ± 0.63
MUFA		19.0 ± 0.85	23.4 ± 3.18	21.6 ± 1.22	21.8 ± 1.20	22.5 ± 0.58
PUFA		34.7 ± 0.79	32.2 ± 2.63	32.0 ± 0.89	33.0 ± 0.70	32.6 ± 0.57
PUFAn-3		18.6 ± 0.31	15.6 ± 1.89	12.6 ± 0.36*	16.0 ± 0.60$^{\&}$	12.6 ± 0.24*
PUFAn-6		16.2 ± 0.77	16.6 ± 0.80	19.4 ± 0.83*	17.0 ± 0.29	20.0 ± 0.48*
n-6:n-3 ratio		0.87 ± 0.05	1.09 ± 0.10$^{\#}$	1.53 ± 0.08*	1.07 ± 0.04$^{\&}$	1.59 ± 0.05*

Supplemental Table 2 (4.2). Cerebellar lipid mediator profile.

Lipid mediator levels (pg/mg tissue) in 2- and 18-month-old control and *Acsl6*$^{-/-}$ cerebellum, n=5-6. Data represent mean ± SEM;* by genotype, $ by age, p≤0.05 by Student's t-test. Lipoxygenases (LOX); Cytochrome oxygenase (CYP); Epoxy hydrolase (EH); Non-enzymatic autooxidation (NA); Cyclooxygenases (COX); Reactive oxygen species (ROS); Glutathione-S-transferase (GST).

Compound	Pathway	Precursor	2M Control	2M *Acsl6*$^{-/-}$	18M Control	18M *Acsl6*$^{-/-}$
13-HODE	15-LOX	LA	2.07 ± 0.28	3.06 ± 0.42	10.95 ± 3.29$^{\$}$	15.69 ± 4.28$^{\$}$
13-OxoODE	15-LOX	LA	0.31 ± 0.07	0.45 ± 0.16	1.22 ± 0.36$^{\$}$	1.51 ± 0.34$^{\$}$
12(13)-EpOME	CYP	LA	2.49 ± 0.13	3.65 ± 0.73	5.98 ± 1.15$^{\$}$	8.10 ± 1.43$^{\$}$
9(10)-EpOME	CYP	LA	0.62 ± 0.07	1.09 ± 0.25	1.78 ± 0.28$^{\$}$	2.32 ± 0.45$^{\$}$
12,13-DiHOME	EH	LA	0.55 ± 0.08	0.69 ± 0.12	0.97 ± 0.22	1.24 ± 0.31
9,10-DiHOME	EH	LA	0.28 ± 0.05	0.38 ± 0.08	0.64 ± 0.15$^{\$}$	0.86 ± 0.23
9-HODE	NA	LA	2.48 ± 0.28	3.67 ± 0.60	14.19 ± 3.98$^{\$}$	19.47 ± 5.13$^{\$}$
9-OxoODE	NA	LA	0.45 ± 0.06	0.62 ± 0.21	2.04 ± 0.45$^{\$}$	2.10 ± 0.44$^{\$}$
EKODE	NA	LA	0.24 ± 0.04	0.41 ± 0.06*	0.58 ± 0.04$^{\$}$	0.61 ± 0.10
13-HOTrE	15-LOX	ALA	0.02 ± 0.00	0.02 ± 0.00	0.03 ± 0.01	0.02 ± 0.01
9-HOTrE	NA	ALA	0.01 ± 0.01	0.00 ± 0.00	0.01 ± 0.01	0.03 ± 0.02
9-KOTrE	NA	ALA	0.00 ± 0.00	0.00 ± 0.00	0.00 ± 0.00	0.00 ± 0.00
15-HETrE	15-LOX	DGLA	0.18 ± 0.02	0.20 ± 0.03	0.13 ± 0.01	0.20 ± 0.05
5-HETrE	5-LOX	DGLA	0.01 ± 0.01	0.02 ± 0.01	0.02 ± 0.01	0.03 ± 0.02
8-HETrE	ROS	DGLA	0.03 ± 0.01	0.08 ± 0.04	0.01 ± 0.01	0.06 ± 0.06
12-KETE	12-LOX	AA	0.55 ± 0.19	0.77 ± 0.36	0.48 ± 0.24	0.39 ± 0.15
12S-HETE	12-LOX	AA	8.06 ± 1.35	10.61 ± 1.98	3.35 ± 0.62$^{\$}$	4.14 ± 0.81$^{\$}$
15-KETE	15-LOX	AA	0.00 ± 0.00	0.00 ± 0.00	0.00 ± 0.00	0.00 ± 0.00
15S-HETE	15-LOX	AA	4.96 ± 0.29	4.62 ± 0.37	2.41 ± 0.37$^{\$}$	2.93 ± 0.47$^{\$}$
15(R)Lipoxin A4	5-LOX	AA	0.01 ± 0.01	0.00 ± 0.00	0.00 ± 0.00	0.00 ± 0.00
20-hydroxy-LTB4	5-LOX	AA	0.00 ± 0.00	0.00 ± 0.00	0.00 ± 0.00	0.00 ± 0.00
5,15-DiHETE	5-LOX	AA	0.05 ± 0.02	0.09 ± 0.02	0.04 ± 0.02	0.02 ± 0.02$^{\$}$
5-KETE	5-LOX	AA	2.89 ± 0.77	3.22 ± 1.22	1.92 ± 0.59	2.05 ± 0.42
5S-HETE	5-LOX	AA	3.34 ± 0.20	3.52 ± 0.70	2.68 ± 0.64	3.44 ± 0.36
6-trans-LTB4	5-LOX	AA	0.00 ± 0.00	0.00 ± 0.00	0.00 ± 0.00	0.00 ± 0.00
8,15-DiHETE	5-LOX	AA	0.04 ± 0.04	0.07 ± 0.07	0.00 ± 0.00	0.00 ± 0.00
Lipoxin A4	5-LOX	AA	0.00 ± 0.00	0.00 ± 0.00	0.00 ± 0.00	0.00 ± 0.00
Lipoxin B4	5-LOX	AA	0.00 ± 0.00	0.00 ± 0.00	0.00 ± 0.00	0.00 ± 0.00
LTB4	5-LOX	AA	0.00 ± 0.00	0.00 ± 0.00	0.00 ± 0.00	0.00 ± 0.00
LTD4_NEG	5-LOX/GST	AA	0.00 ± 0.00	0.00 ± 0.00	0.00 ± 0.00	0.00 ± 0.00
LTE4_NEG	5-LOX/GST	AA	0.00 ± 0.00	0.00 ± 0.00	0.00 ± 0.00	0.00 ± 0.00

Compound	Pathway	Precursor	2M Control	2M *Acsl6*$^{-/-}$	18M Control	18M *Acsl6*$^{-/-}$
11B-PGF2a	COX	AA	0.00 ± 0.00	0.00 ± 0.00	0.00 ± 0.00	0.00 ± 0.00
11-dehydro-tbx3	COX	AA	0.00 ± 0.00	0.00 ± 0.00	0.00 ± 0.00	0.00 ± 0.00
12-HHTrE	COX	AA	25.91 ± 2.31	25.57 ± 2.23	8.42 ± 0.58$^{\$}$	12.42 ± 3.15$^{\$}$
15-deoxy-Delta12,14-PGJ2	COX	AA	0.15 ± 0.02	0.20 ± 0.04	0.03 ± 0.02	0.04 ± 0.02
6-a-Prostaglandin	COX	AA	0.42 ± 0.05	0.35 ± 0.03	0.10 ± 0.01$^{\$}$	0.14 ± 0.02$^{\$}$
6-keto-PGF1a	COX	AA	9.00 ± 1.65	7.77 ± 1.51	2.10 ± 0.18$^{\$}$	2.77 ± 0.65$^{\$}$
Carbocyclic Thromboxane A2	COX	AA	0.06 ± 0.03	0.06 ± 0.02	0.03 ± 0.03	0.00 ± 0.00$^{\$}$
dinor-11b-pgf2a	COX	AA	0.00 ± 0.00	0.00 ± 0.00	0.00 ± 0.00	0.00 ± 0.00
dinor-6-keto-pgf2a	COX	AA	0.00 ± 0.00	0.00 ± 0.00	0.00 ± 0.00	0.00 ± 0.00
dinor-8-iso-pgf2a	COX	AA	0.00 ± 0.00	0.00 ± 0.00	0.00 ± 0.00	0.00 ± 0.00
PGB2	COX	AA	0.00 ± 0.00	0.04 ± 0.02	0.00 ± 0.00	0.00 ± 0.00
PGE2	COX	AA	10.13 ± 1.36	7.08 ± 0.58	2.30 ± 0.38$^{\$}$	3.00 ± 0.57$^{\$}$
PGF2a	COX	AA	8.40 ± 0.96	7.33 ± 0.73	2.45 ± 0.27$^{\$}$	3.04 ± 0.34$^{\$}$
PGJ2	COX	AA	0.61 ± 0.06	0.67 ± 0.10	0.20 ± 0.03$^{\$}$	0.27 ± 0.06$^{\$}$
Prostaglandin D2	COX	AA	7.61 ± 1.27	9.29 ± 2.08	4.84 ± 1.13	5.82 ± 1.06
tetranor-PGEM	COX	AA	0.00 ± 0.00	0.00 ± 0.00	0.00 ± 0.00	0.00 ± 0.00
tetranor-PGFM	COX	AA	0.00 ± 0.00	0.01 ± 0.01	0.00 ± 0.00	0.00 ± 0.00
TXB2	COX	AA	4.86 ± 0.46	5.59 ± 0.57	1.59 ± 0.19$^{\$}$	2.60 ± 0.60$^{\$}$
11(12)-EET	CYP	AA	0.40 ± 0.02	0.40 ± 0.04	0.49 ± 0.08	0.46 ± 0.02
14(15)-EET	CYP	AA	2.02 ± 0.16	1.92 ± 0.41	1.83 ± 0.36	1.99 ± 0.37
20-HETE	CYP	AA	1.08 ± 0.13	0.94 ± 0.19	0.42 ± 0.12$^{\$}$	0.32 ± 0.10$^{\$}$
5(6)-EpETrE	CYP	AA	0.58 ± 0.39	0.00 ± 0.00	0.00 ± 0.00	0.00 ± 0.00
8(9)-EET	CYP	AA	0.35 ± 0.05	0.43 ± 0.09	0.47 ± 0.09	0.53 ± 0.09
11,12-DiHETrE	EH	AA	0.05 ± 0.01	0.05 ± 0.01	0.07 ± 0.02	0.09 ± 0.03
14,15-DiHETrE	EH	AA	0.08 ± 0.01	0.08 ± 0.01	0.10 ± 0.02	0.12 ± 0.02
5,6-DiHETrE	EH	AA	0.00 ± 0.00	0.00 ± 0.00	0.00 ± 0.00	0.00 ± 0.00
8,9-DiHETrE	EH	AA	0.07 ± 0.05	0.09 ± 0.04	0.04 ± 0.04	0.05 ± 0.05
11-HETE	ROS	AA	6.96 ± 0.64	6.84 ± 0.58	3.59 ± 0.61$^{\$}$	3.91 ± 0.72$^{\$}$
8-iso-15R-PGF2a	ROS	AA	0.00 ± 0.00	0.00 ± 0.00	0.00 ± 0.00	0.00 ± 0.00
8-iso-PGF2a	ROS	AA	0.51 ± 0.08	0.48 ± 0.11	0.07 ± 0.04$^{\$}$	0.10 ± 0.05$^{\$}$
8S-HETE	ROS	AA	0.76 ± 0.06	0.76 ± 0.05	0.54 ± 0.07$^{\$}$	0.74 ± 0.16
9-HETE	ROS	AA	0.83 ± 0.08	1.03 ± 0.19	1.15 ± 0.20	1.01 ± 0.27
12-HEPE	12-LOX	EPA	0.00 ± 0.00	0.00 ± 0.00	0.00 ± 0.00	0.00 ± 0.00

Compound	Pathway	Precursor	2M Control	2M *Acsl6*$^{-/-}$	18M Control	18M *Acsl6*$^{-/-}$
15-HEPE	15-LOX	EPA	0.00 ± 0.00	0.00 ± 0.00	0.00 ± 0.00	0.00 ± 0.00
18-HEPE	15-LOX	EPA	0.00 ± 0.00	0.00 ± 0.00	0.00 ± 0.00	0.00 ± 0.00
5-HEPE	5-LOX	EPA	0.00 ± 0.00	0.00 ± 0.00	0.00 ± 0.00	0.00 ± 0.00
LXA5	5-LOX	EPA	0.00 ± 0.00	0.00 ± 0.00	0.00 ± 0.00	0.00 ± 0.00
14(15)-EpETE	CYP	EPA	0.00 ± 0.00	0.00 ± 0.00	0.00 ± 0.00	0.00 ± 0.00
17(18)-EpETE	CYP	EPA	0.01 ± 0.01	0.00 ± 0.00	0.00 ± 0.00	0.00 ± 0.00
Resolvin E1	CYP/5-LOX	EPA	0.00 ± 0.00	0.00 ± 0.00	0.00 ± 0.00	0.00 ± 0.00
14,15-DiHETE	EH	EPA	0.00 ± 0.00	0.00 ± 0.00	0.00 ± 0.00	0.00 ± 0.00
17,18-DiHETE	EH	EPA	0.09 ± 0.03	0.12 ± 0.02	0.04 ± 0.03	0.05 ± 0.03
11-HEPE	ROS	EPA	0.00 ± 0.00	0.00 ± 0.00	0.00 ± 0.00	0.00 ± 0.00
8-HEPE	ROS	EPA	0.01 ± 0.01	0.00 ± 0.00	0.00 ± 0.00	0.00 ± 0.00
9-HEPE	ROS	EPA	0.00 ± 0.00	0.00 ± 0.00	0.00 ± 0.00	0.00 ± 0.00
14(S)-HDHA	12-LOX	DHA	0.40 ± 0.04	0.25 ± 0.03*	0.56 ± 0.18	0.18 ± 0.07*
7R Maresin-1	12-LOX	DHA	0.00 ± 0.00	0.00 ± 0.00	0.00 ± 0.00	0.00 ± 0.00
7S Maresin-1	12-LOX	DHA	0.00 ± 0.00	0.00 ± 0.00	0.00 ± 0.00	0.00 ± 0.00
10(S),17(S)-DiHDoHE	15-LOX	DHA	0.00 ± 0.00	0.00 ± 0.00	0.00 ± 0.00	0.00 ± 0.00
17(R) Resolvin D1	15-LOX	DHA	0.00 ± 0.00	0.00 ± 0.00	0.00 ± 0.00	0.03 ± 0.03
17(S)-HDHA	15-LOX	DHA	0.27 ± 0.17	0.00 ± 0.00	0.00 ± 0.00	0.00 ± 0.00
Resolvin D1	15-LOX	DHA	0.00 ± 0.00	0.00 ± 0.00	0.01 ± 0.01	0.02 ± 0.01
Resolvin D2	15-LOX	DHA	0.00 ± 0.00	0.00 ± 0.00	0.00 ± 0.00	0.00 ± 0.00
Resolvin D3	15-LOX	DHA	0.00 ± 0.00	0.00 ± 0.00	0.00 ± 0.00	0.00 ± 0.00
Resolvin D5	15-LOX	EPA	0.00 ± 0.00	0.00 ± 0.00	0.00 ± 0.00	0.00 ± 0.00
19(20)-EpDPE	CYP	DHA	0.09 ± 0.04	0.13 ± 0.06	0.29 ± 0.18	0.00 ± 0.00*
19,20-DiHDPA	EH	DHA	0.00 ± 0.00	0.00 ± 0.00	0.00 ± 0.00	0.00 ± 0.00
11-HDoHE	ROS	DHA	0.42 ± 0.07	0.00 ± 0.00*	0.51 ± 0.33	0.20 ± 0.15
8-HDoHE	ROS	DHA	0.73 ± 0.09	0.29 ± 0.04*	0.76 ± 0.16	0.35 ± 0.09*

CHAPTER V

SYNTHESIS

Overview of research findings

The purpose of this research was to elucidate the role of ACSL6 in regulating brain fatty acid metabolism *in vivo*. Using a novel conditional *Acsl6* knockout mouse we discovered that ACSL6 in neurons is critical for enriching the brain with the neuroprotective omega-3 DHA (Figure 5.1) and that the loss of ACSL6 results in motor deficits, altered short-term spatial working memory, reduce gene expression of synaptic proteins, and in age-related neuropathology. Studies using our novel conditional ACSL6 deficient mouse are still underway and will add more insight into the role of ACSL6 in the central nervous system and on the impact of ACSL6-mediated DHA deficiency in neurological health.

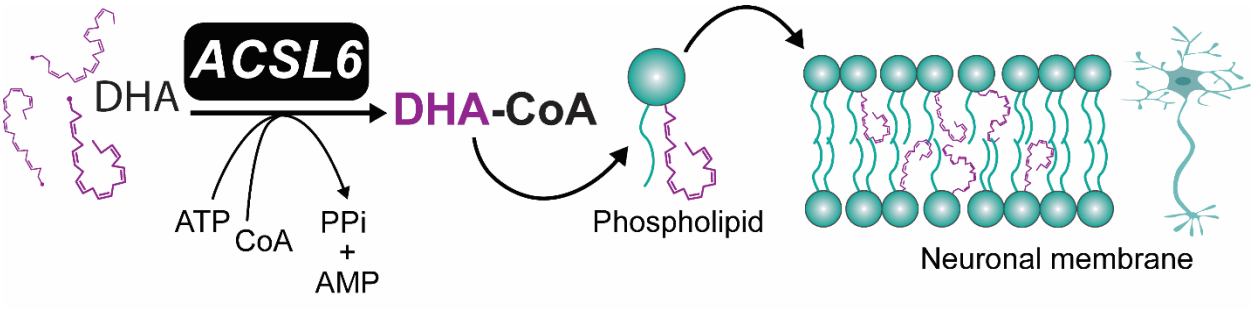

Figure 5.1. Neuronal ACSL6 is required for enriching the brain with the neuroprotective omega-3 DHA.

Outstanding questions on the role of ACSs in the brain (From literature review (1))

What are the true subcellular localizations of ACSs?

A property of ACS enzymes that is predicted to play a large role in how these enzymes dictate fatty acid metabolic fate is their differential localization to distinct organelles. For instance, an ACS at the mitochondria is likely to facilitate fatty acid oxidation or cardiolipin remodeling, whereas an ACS at the endoplasmic reticulum may channel fatty acids into phospholipid or triacylglycerol synthesis. ACSs found at the plasma membrane are likely indirectly localized there due to interactions with plasma membrane proteins and/or due to membrane-membrane contact sites where they likely facilitate fatty acid uptake and/or membrane remodeling. The expression of ACSs at the peroxisome and their possible related roles are reviewed elsewhere (277). However, the precise intracellular spatial distribution of ACSs remains unclear, in part due to the limited availability of immunochemistry-quality antibodies targeting endogenous ACS enzymes. Therefore, a majority of the subcellular location data is generated using models of overexpressed tagged ACSs in cell culture, a method that artifactually results in mislocalization of membrane proteins such as ACSs (117). Another concern of using overexpression of ACSs in cells is the resulting overproduction of toxic acyl-CoAs (80). As a consequence, acyl-CoAs are redirected towards alternative metabolic pathways, such as synthesis of triacylglycerols or phospholipids resulting in excess lipid droplet and membrane accumulation and thereby creating a disease-like state for the cell (80). A secondary method to determine intracellular location is subcellular fractionation, which is often complicated by a high degree of fractional impurity. Thus, the advent of highly

specific and robust antibodies for detection of endogenous ACSs remains a roadblock for understanding ACS subcellular distribution.

How to relate in vitro findings to in vivo brain metabolism?

In relation to connecting ACS function *in vitro* to its function in the brain, concerns are raised regarding the lack of cell culture models to recapitulate mature adult cells, the complex and dynamic interactions between brain cells, and fatty acid metabolism of cells *in vivo*. Cells in culture, either primary or established cell lines, are well known to not fully recapitulate cells *in vivo*. This is particularly true for brain cells types such as neurons that are cultured as precursor/undifferentiated cells and even after differentiation, do not fully depict a mature adult cell. Furthermore, astrocytes are recognized as crucial players in the formation, function, and plasticity of synapses (278, 279). Thus, highlighting the essentiality of neural-astrocyte interactions. The ability to recapitulate these interactions in a dish using mature astrocytes or neurons, or to study neuron-astrocyte metabolic interdependence is challenging. Additionally, cells in culture are grown in high levels of glucose with limited or no fatty acids available, thus the ability to translate *in vitro* findings to *in vivo* is particularly difficult in relation to fatty acid metabolism. Thus, the combination of *in vivo* and *in vitro* research approaches is critical to determine the metabolic role of ACSs in regulating brain metabolism, yet relatively few *in vivo* models of brain ACS manipulation are reported.

How to define comprehensive substrate preferences and kinetics for ACSs?

Comprehensive substrate preferences and kinetics are not established for a vast majority of the ACS enzyme family, in part due to the complex nature of optimizing assay

conditions. Traditional methods to characterize ACS enzyme kinetics require optimization for numerous assay components, such as duration of assay and concentrations of ATP, triton-X, magnesium chloride, and Coenzyme A. Moreover, each fatty acid substrate can yield distinct optimized conditions which may also depend on the fatty acid vehicle (albumin vs. cyclodextrin). Enzyme kinetics are traditionally determined for individual ACSs upon generation of recombinant protein in bacteria, followed by purification using biochemical tags. The assay is performed in test-tube based conditions, often outside of native membrane-associated conditions; is run with individual substrates rather than the mixture of fatty acids that are present within cells from which ACS will normally competitively select; and uses excess amounts of substrate, which does not reflect fatty acid intracellular levels (140, 280). Thus, establishing assay conditions for a single ACS for a single substrate is a complex endeavor performed outside of the enzyme's natural membrane-associated environment. Even within such controlled assays, different labs yield inconsistent enzyme kinetics (94, 98, 119, 165, 168, 189). Moreover, ACS enzymes are predicted to dimerize homo- and heterodynamically (94, 114), therefore assay conditions optimized for a single ACS in isolation may be largely changed upon heterodimerization in the natural environment. Total ACS activity assays within tissues or cell types can provide an indicator of total activity but cannot indicate contribution from individual ACS enzymes. Thus, equating kinetic data pertaining to an ACS in isolation to total ACS activity in tissue-based assays is not feasible.

While several groups have performed enzyme kinetics on recombinant ACSs using up to five fatty acid substrates, the immense pool of possible acyl substrates is highly difficult to assess. Specifically, ACS activity for less abundant fatty acids, such as

oxylipids, neuroprotectins, eicosanoids, and very-long-chain fatty acids is limited (140). The lack of data for these substrates is due to the combined effects of cost, limited availability, and instability of such lipids. With the advent of methodologies relying on mass spectrometry, the limitations in substrates for kinetic analysis can be overcome, but has yet to be widely implemented (281). Additional complications arise because nearly every ACS enzyme has at least one splice variant which are regulated differently by numerous environmental/hormonal factors and in cell-type specific manners. The existence of these variants ultimately increases the diversity of ACS localizations at the subcellular level, binding partners, and enzyme kinetics, thus comprehensive characterizations of each variant across all ACSs is a monumental endeavor (165, 168).

Understanding the role of each ACS enzyme alone on the regulation of cellular and intercellular fatty acid metabolic flux in a substrate dependent manner, and in concert with binding partners, will reveal major regulatory nodes in lipid metabolism. Since ACS enzymes display non-redundant functions and do not compensate for each other's loss, the use of knockout mouse models can be a powerful tool to uncover ACS biochemical characteristics and their biological roles *in vivo*. It is of particular interest to understand how lipid metabolism is controlled across the blood-brain barrier and after subsequent incorporation and recycling within the brain parenchyma. The differential expression of the ACSs across the cells of the brain and within the blood-brain-barrier strongly suggests a degree of regulation conferred by these enzymes but much work remains to further understand this regulation and its importance for neurological health.

Future directions on studying the role of ACSL6 in lipid metabolism

How does ACSL6 regulates fatty acid incorporation into brain lipids?

Loss of ACSL6 results in reduced brain DHA-containing phospholipids. However, it is unclear if ACSL6 activates DHA for new phospholipid synthesis, is involved in DHA uptake into the brain, and/or regulates phospholipid remodeling as part of the Land's cycle. First, ACSL6 subcellular location should be determined. *De novo* phospholipid synthesis occurs in the endoplasmic reticulum (ER). Thus, if ACSL6 targets fatty acids towards phospholipid synthesis, we predict that ACSL6 localizes to the ER. Alternatively, ACSL6 could be associated with the plasma membrane to facilitate fatty acid uptake or DHA recycling via Land's cycle. Besides, we cannot rule out that ACSL6 could be expressed in the microvascular endothelium and facilitate DHA uptake. Future studies should include the generation of an ACSL6-specific antibody suited for immunofluorescence to identify the subcellular localization of ACSL6.

To determine how ACSL6 regulates the rate of fatty acid incorporation into phospholipids, the metabolic flux of radiolabeled fatty acids could be traced in control and *Acsl6*$^{-/-}$ mice *in vivo* after gavage and *ex vivo* using fresh brain slices (Figure 5.2). DHA incorporation into phospholipids can be determined by extracting radiolabeled lipids and running thin layer

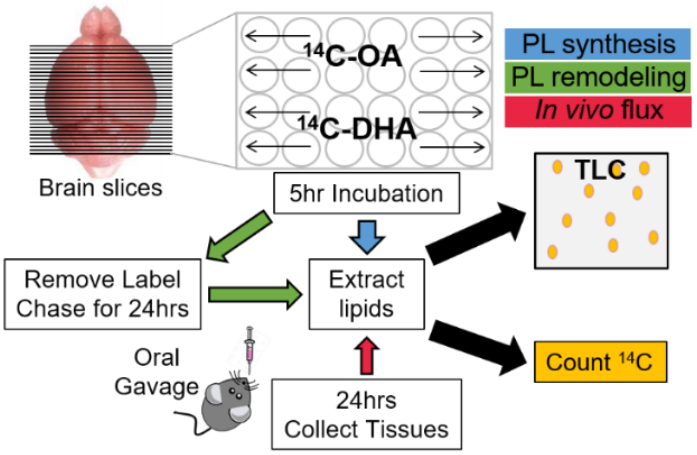

Figure 5.2. Schematic representation of the *ex vivo* and *in vivo* metabolic

chromatography. The proposed experiments will elucidate the molecular mechanisms by which ACSL6 channels DHA into phospholipids.

Kinetic studies can be an informative experiment but a rather complex endeavor that can be performed to address the role of ACSL6 in DHA uptake (137). Infusions of radiolabeled DHA presented in different forms (i.e. free DHA or as LPC-DHA) can inform whether ACSL6 facilitates DHA uptake and its dependence upon the molecular format in which DHA is presented. These data will further improve our scientific knowledge of the mechanisms by which the brain becomes enriched with DHA.

Does ACSL6 loss alters membrane biophysical properties?

Apart from the changes in phospholipid composition, *Acsl6*$^{-/-}$ mice show an upregulation of genes involved in the regulation of cholesterol biosynthesis. Thus, measurements of cholesterol content are required to determine if the levels of this lipid are changed. However, the question remains whether membrane remodeling in *Acsl6*$^{-/-}$ brains affects membrane's biophysical properties. To answer this question, one approach could be to isolate synaptosomes from control and *Acsl6*$^{-/-}$ mice and measure membrane fluidity using the fluorescent probe diphenylhexatriene, whose rotational mobility is influenced by the acyl-chain composition of the lipid bilayer (282, 283). Membrane phase behavior could be assessed using the C-laurdan fluorescent probe, which provides information regarding the degree of lipid packing. The data generated will reveal the requirement of ACSL6 for maintaining membrane homeostasis. Another question remains, if the loss of ACSL6 affects membranes biophysical properties, is it also affecting the rate of synaptic vesicle cycling and consequently neurotransmission?

Electrophysiology studies can be performed to study the kinetics of synaptic vesicle cycling.

What is the role of astrocytic Acsl6?

Data presented in this dissertation shows that fatty acid metabolic handling is distinct between neurons and astrocytes. Astrocytes express the variant containing the non-DHA preferring Y-gate domain. Thus, it is unclear what is the role of ACSL6 in astrocytes. It is known that astrocytes can oxidize fatty acids (19), thus it is possible that ACSL6 in astrocytes directs fatty acids towards oxidation. Fatty acid metabolic flux tracing experiments can be performed in our astrocyte specific ACSL6 knockout mouse to determine the metabolic fate of the fatty acids. Moreover, identifying the subcellular localization of astrocytic ACSL6 can provide a hint to the role of this enzyme. In addition, we cannot rule out that ACSL6 in astrocytes may play a role during pathological conditions such as brain injury where astrocytes undergo changes in morphology and become activated and highly proliferative. Astrocytes may require ACSL6 for supporting membrane formation while proliferating or may transfer lipids to neurons for repair. In this regard, emerging research shows that astrocytes provide various substrates, such as glutamine, lactate, and ketone bodies, to neurons (284, 285). Using our conditional ACSL6 deficient mouse we could generate cell-type specific ACSL6 knockouts combined with molecular and lipid imaging techniques to reveal a novel mechanism by which neurons and astrocytes interact to regulate lipid metabolism.

How does the loss of ACSL6 affects the activity of neuronal sub-types?

From our smFISH data we know that *Acsl6* is express in glutamatergic, GABAergic, and dopaminergic neurons across all brain regions and that *Acsl6*$^{-/-}$ display neurotransmitter imbalances (data not shown). Cell-type specific ACSL6 deficient mice can be used to dissect the specific contribution of each cell-type to the observed phenotype in the ACSL6 whole-body knockout. For example, the increase in hyperlocomotor activity in *Acsl6*$^{-/-}$ could be a result of alterations in the dopaminergic system. To test this hypothesis, *Acsl6* floxed mice can be crossed with mice expressing Cre recombinase under the regulation of the dopamine transporter promoter to ablate *Acsl6* only from dopaminergic neurons. In addition, pharmacological agents, such as amphetamine, can be used to target dopamine neurotransmission. Future studies should also include electrophysiological recordings to interrogate the effect of ACSL6 loss on neural activity.

Does ACSL6-mediated DHA deficiency affect mitochondrial function?

Mitochondrial dysfunction plays a role in the development and progression of age-related neurological diseases (286, 287). In this regard, RNA-seq data obtained from aged *Acsl6*$^{-/-}$ revealed changes in the gene expression of multiple subunits of the respiratory complexes. In addition, ablation of *Acsl6* results in altered levels of energetic metabolites suggesting that ACSL6-mediated DHA deficiency may induce mitochondrial deregulation. In parallel, our findings show that while most phospholipid species presented reductions in DHA, PGs were enriched in *Acsl6*$^{-/-}$ brains. PG is the direct precursor of cardiolipin, a tetra-acylated diphosphatidylglycerol known as the “signature phospholipid” of the mitochondria. Changes in cardiolipin levels and its acyl-chain

composition can result in abnormal mitochondrial structure, defects in electron transport chain super-complex assembly, and impaired oxidative phosphorylation (288-291). Thus, we question whether the loss of ACSL6 affects the acyl-chain composition of cardiolipin. Future studies should include lipidomic analysis on isolated cell-type specific mitochondria from *Acsl6*$^{-/-}$ mice along with a thorough characterization of mitochondrial function. Assessment of synaptic vs non-synaptic mitochondria should be considered. Respirometry flux analysis and measurements of membrane potential and H_2O_2 emission will provide important insights into how ACSL6 influences mitochondrial bioenergetics.

Does dietary DHA supplementation restore brain DHA content and ameliorate the neuropathology observed in Acsl6$^{-/-}$*?*

Because *Acsl6*$^{-/-}$ mice have reduced DHA levels in the brain, an important question is whether increasing substrate availability will overcome this deficiency. This question can be addressed by feeding *Acsl6*$^{-/-}$ mice a diet supplemented with DHA and measuring brain DHA-containing lipids. We hypothesize that increasing DHA availability will not restore brain DHA levels because DHA cannot be activated in the absence of ACSL6. Other ACS could activate DHA, thus this feeding study will inform whether only ACSL6 is required for enriching the brain with DHA independent of substrate availability. In addition, molecular analysis and behavioral tests could be performed to determine the impact of dietary DHA on the neuropathology induced by the loss of ACSL6.

What is the role of Acsl6 in neurological diseases?

Low dietary intake of DHA is associated with an increased risk for numerous neurological diseases, including Alzheimer's disease and Parkinson's disease. To study

the neuroprotective effects of ACSL6-mediated DHA metabolism in specific neurological diseases, studies should include crossing our ACSL6 deficient mouse with mouse models of neurological diseases. Lipidomic, molecular, physiological, and behavioral evaluation of the new ACSL6-deficient transgenic mouse models could help elucidate the mechanism of the specific disease. One such example is the investigation of ACSL6 role in Parkinson's disease.

Synucleinopathies, including Parkinson's disease, are neurodegenerative diseases characterized by α-synuclein aggregation (292). The role of α-synuclein under physiological conditions has not been well established, however, evidence suggests a role in regulating lipid metabolism (293). Previous studies suggest that α-synuclein protects the brain by sequestering oxidized free DHA as well as by binding to membranes to prevent DHA-containing phospholipids from oxidation (293, 294). Conversely, multiple *in vitro* studies suggest that free DHA promotes α-synuclein aggregation (295). Thus, how exactly DHA influences α-synuclein activity and vice versa remains to be elucidated. Our ACSL6 deficient mice can be used as a tool to investigate the effects of DHA on α-synuclein activity *in vivo.*

Ablation of *Snca*, the gene that codes for α-synuclein, results in reduced AA levels in the brain and reduced microsomal total ACS activity in the brain (296). The addition of exogenous α-synuclein restored total ACS activity suggesting that α-synuclein may present the substrate to an ACS or interact directly with the enzyme to regulate fatty acid metabolism (296). Our data show that the loss of ACSL6 in astrocytes results in reduce AA phospholipids. Thus, it is possible that ACSL6 expressing the Y-gate domain interacts with α-synuclein to regulate AA metabolism. The interactions could also occur with the

ACSL6 variant expressing the F-gate domain and thus, affect the metabolism of DHA. Alternatively, α-synuclein could be interacting with another ACS such as ACSL4, which has a preference for AA (297). Immunoprecipitation of ACSL6 to identify binding partners will provide insights into whether ACSL6 and α-synuclein act in concert to regulate fatty acid metabolism. Lastly, the question remains whether mutations in α-synuclein influence ACSL6 activity and DHA metabolism, and thus render the brain more susceptible to develop a synucleinopathy.

What is the role of Acsl6 in other tissues?

While the work in this dissertation focused on the role of ACSL6 in the brain, this enzyme is also expressed in the testis, muscle, red blood cells, spine, and retina (111, 165, 298). We previously reported that ACSL6 in testis is required for enriching germ cells with DHA and male fertility (111). In the muscle, studies in humans and rodent models have shown changes in *Acsl6* mRNA and ACSL6 protein levels in response to high-fat diet and exercise and suggest a role in channeling fatty acids towards phospholipid and triacylglycerol biosynthesis (298). However, mRNA expression, protein levels, and ACS activity of *Acsls* do not always correlate (104). Translational and post-translational modifications may be involved in the regulation of ACSL enzymes (299). Thus, future studies should include the generation of a muscle specific ACSL6 deficient mouse along with dietary and exercise interventions to determine the role of ACSL6 in muscle fatty acid metabolism.

Red blood cells (RBC) lack the machinery for *de novo* phospholipid synthesis, however, their membranes are constantly remodeling (165). Thus, we predict that ACSL6 is involved in the re-acylation of fatty acid through the Land's cycle. Total ACS activity

and lipidomic analysis should be performed to determine the role of ACSL6 in RBC's fatty acid metabolism. Furthermore, RBC's membrane fatty acid composition is highly influenced by circulating plasma fatty acids. Currently, the omega-3 index (EPA and DHA levels in red blood cells) is used in clinical trials to study the associations between omega-3 fatty acid levels and neurological diseases (300, 301). If ACSL6 enriches RBC and brain parenchyma with DHA, then any changes in ACSL6 expression or activity in one of them or in both could impact the interpretation of the results. Thus, understanding the role of ACSL6 in RBC's fatty acid metabolism will provide important information to guide future research.

The spine and retina had a reduction in DHA-containing phospholipids suggesting that the DHA-preferring ACSL6 variant is expressed in these tissues. The mechanisms by which DHA confers neuroprotection to the spine during spinal injury and degeneration could be assessed using our conditional floxed ACSL6 mouse. In the retina, DHA is highly enriched in photoreceptor cells and is required for healthy visual function (91, 245). A retina specific *Acsl6* knockout should be generated to study the effects of ACSL6-mediated DHA deficiency in the retina. Histological and phototransduction analysis along with vision assessment should be performed in the retina specific *Acsl6* knockout. Collaborations with experts in the field of ophthalmology will be crucial to have a better understanding of the role of ACSL6 in visual function in health and disease.

Public Health Significance

The prevalence of neurological diseases will increase as the “baby boom” generation ages highlighting the need for developing prevention and treatment strategies (302). Due to the increased rates of neurological disorders and disease in the aged population, the demands for medical care services and health care costs will rise. While pharmacological therapies for neurodegenerative diseases exist, these therapeutics can be expensive, cause adverse effects, and does not reverse or prevent the progression of neurodegeneration. Therefore, there remains a need to understand the underlying mechanisms that cause neurodegeneration to develop preventive and therapeutic strategies. Evidence suggests an inverse relation between DHA consumption and the risk for developing neurological diseases. However, little was known about the regulatory mechanisms that control the enrichment of the neuroprotective DHA in the brain until now. The work in this dissertation led to the discovery that ACSL6 is a critical enzyme for enriching the brain with DHA and a protector against neural dysfunction. This research has significantly expanded our limited knowledge on brain fatty acid metabolism and lay the foundations for understanding how defects in DHA metabolism influence neurological diseases. Future research will define the potential of ACSL6 to serve as a target for modulating DHA levels in the brain to confer protection.

REFERENCES

1. Fernandez RF, Ellis JM. Acyl-CoA synthetases as regulators of brain phospholipid acyl-chain diversity. Prostaglandins Leukot Essent Fatty Acids. 2020;161:102175. Epub 2020/09/15. doi: 10.1016/j.plefa.2020.102175. PubMed PMID: 33031993.

2. Group GNDC. Global, regional, and national burden of neurological disorders during 1990-2015: a systematic analysis for the Global Burden of Disease Study 2015. Lancet Neurol. 2017;16(11):877-97. Epub 2017/09/17. doi: 10.1016/S1474-4422(17)30299-5. PubMed PMID: 28931491; PubMed Central PMCID: PMCPMC5641502.

3. He W, Goodkind D, Kowal P. An Aging World: 2015. U.S. Census Bureau International Population Reports; 2016. p. P95/16-1.

4. Cardoso C, Afonso C, Bandarra NM. Dietary DHA and health: cognitive function ageing. Nutr Res Rev. 2016;29(2):281-94. Epub 2016/11/21. doi: 10.1017/S0954422416000184. PubMed PMID: 27866493.

5. Lukiw WJ, Bazan NG. Docosahexaenoic acid and the aging brain. J Nutr. 2008;138(12):2510-4. doi: 10.3945/jn.108.096016. PubMed PMID: 19022980; PubMed Central PMCID: PMCPMC2666388.

6. Yashodhara BM, Umakanth S, Pappachan JM, Bhat SK, Kamath R, Choo BH. Omega-3 fatty acids: a comprehensive review of their role in health and disease. Postgrad Med J. 2009;85(1000):84-90. doi: 10.1136/pgmj.2008.073338. PubMed PMID: 19329703.

7. Bazan NG, Molina MF, Gordon WC. Docosahexaenoic acid signalolipidomics in nutrition: significance in aging, neuroinflammation, macular degeneration, Alzheimer's, and other neurodegenerative diseases. Annu Rev Nutr. 2011;31:321-51. doi: 10.1146/annurev.nutr.012809.104635. PubMed PMID: 21756134; PubMed Central PMCID: PMCPMC3406932.

8. McNamara RK, Jandacek R, Rider T, Tso P, Stanford KE, Hahn CG, et al. Deficits in docosahexaenoic acid and associated elevations in the metabolism of arachidonic acid and saturated fatty acids in the postmortem orbitofrontal cortex of patients with bipolar disorder. Psychiatry Res. 2008;160(3):285-99. Epub 2008/08/20. doi: 10.1016/j.psychres.2007.08.021. PubMed PMID: 18715653; PubMed Central PMCID: PMCPMC2620106.

9. McNamara RK. DHA deficiency and prefrontal cortex neuropathology in recurrent affective disorders. J Nutr. 2010;140(4):864-8. Epub 2010/02/10. doi: 10.3945/jn.109.113233. PubMed PMID: 20147466; PubMed Central PMCID: PMCPMC2838627.

10. Bazinet RP, Layé S. Polyunsaturated fatty acids and their metabolites in brain function and disease. Nat Rev Neurosci. 2014;15(12):771-85. doi: 10.1038/nrn3820. PubMed PMID: 25387473.

11. Harayama T, Riezman H. Understanding the diversity of membrane lipid composition. Nat Rev Mol Cell Biol. 2018;19(5):281-96. Epub 2018/02/07. doi: 10.1038/nrm.2017.138. PubMed PMID: 29410529.

12. Bowman CE, Selen Alpergin ES, Ellis JM, Wolfgang MJ. Loss of ACOT7 potentiates seizures and metabolic dysfunction. Am J Physiol Endocrinol Metab. 2019;317(5):E941-E51. Epub 2019/04/30. doi: 10.1152/ajpendo.00537.2018. PubMed PMID: 31039008; PubMed Central PMCID: PMCPMC6879868.

13. Ellis JM, Wong GW, Wolfgang MJ. Acyl coenzyme A thioesterase 7 regulates neuronal fatty acid metabolism to prevent neurotoxicity. Mol Cell Biol. 2013;33(9):1869-82. doi: 10.1128/MCB.01548-12. PubMed PMID: 23459938; PubMed Central PMCID: PMCPMC3624175.

14. Asadollahi R, Oneda B, Joset P, Azzarello-Burri S, Bartholdi D, Steindl K, et al. The clinical significance of small copy number variants in neurodevelopmental disorders. J Med Genet. 2014;51(10):677-88. Epub 2014/08/08. doi: 10.1136/jmedgenet-2014-102588. PubMed PMID: 25106414; PubMed Central PMCID: PMCPMC4173859.

15. Chen CT, Bazinet RP. Beta-oxidation and rapid metabolism, but not uptake regulate brain eicosapentaenoic acid levels. Prostaglandins, Leukotrienes and Essential Fatty Acids. 2015;92:33-40. doi: 10.1016/j.plefa.2014.05.007.

16. Guzmán M, Blázquez C. Ketone body synthesis in the brain: possible neuroprotective effects. Prostaglandins Leukot Essent Fatty Acids. 2004;70(3):287-92. doi: 10.1016/j.plefa.2003.05.001. PubMed PMID: 14769487.

17. Le Foll C, Levin BE. Fatty acid-induced astrocyte ketone production and the control of food intake. Am J Physiol Regul Integr Comp Physiol. 2016;310(11):R1186-92. Epub 2016/04/27. doi: 10.1152/ajpregu.00113.2016. PubMed PMID: 27122369; PubMed Central PMCID: PMCPMC4935491.

18. Thevenet J, De Marchi U, Domingo JS, Christinat N, Bultot L, Lefebvre G, et al. Medium-chain fatty acids inhibit mitochondrial metabolism in astrocytes promoting astrocyte-neuron lactate and ketone body shuttle systems. FASEB J. 2016;30(5):1913-26. Epub 2016/02/02. doi: 10.1096/fj.201500182. PubMed PMID: 26839375.

19. White CJ, Lee J, Choi J, Chu T, Scafidi S, Wolfgang MJ. Determining the bioenergetic capacity for fatty acid oxidation in the mammalian nervous system. Mol Cell Biol. 2020;40(10). Epub 2020/04/28. doi: 10.1128/MCB.00037-20. PubMed PMID: 32123009; PubMed Central PMCID: PMCPMC7189099.

20. Inloes JM, Hsu KL, Dix MM, Viader A, Masuda K, Takei T, et al. The hereditary spastic paraplegia-related enzyme DDHD2 is a principal brain triglyceride lipase. Proc

Natl Acad Sci U S A. 2014;111(41):14924-9. Epub 2014/09/29. doi: 10.1073/pnas.1413706111. PubMed PMID: 25267624; PubMed Central PMCID: PMCPMC4205627.

21. Hamilton JA, Hillard CJ, Spector AA, Watkins PA. Brain uptake and utilization of fatty acids, lipids and lipoproteins: application to neurological disorders. J Mol Neurosci. 2007;33(1):2-11. doi: 10.1007/s12031-007-0060-1. PubMed PMID: 17901539.

22. Lauwers E, Goodchild R, Verstreken P. Membrane lipids in presynaptic function and disease. Neuron. 2016;90(1):11-25. doi: 10.1016/j.neuron.2016.02.033. PubMed PMID: 27054615.

23. Puchkov D, Haucke V. Greasing the synaptic vesicle cycle by membrane lipids. Trends Cell Biol. 2013;23(10):493-503. Epub 2013/06/08. doi: 10.1016/j.tcb.2013.05.002. PubMed PMID: 23756446.

24. Postila PA, Róg T. A perspective: Active role of lipids in neurotransmitter dynamics. Mol Neurobiol. 2020;57(2):910-25. Epub 2019/10/08. doi: 10.1007/s12035-019-01775-7. PubMed PMID: 31595461; PubMed Central PMCID: PMCPMC7031182.

25. Park M, Salgado JM, Ostroff L, Helton TD, Robinson CG, Harris KM, et al. Plasticity-induced growth of dendritic spines by exocytic trafficking from recycling endosomes. Neuron. 2006;52(5):817-30. doi: 10.1016/j.neuron.2006.09.040. PubMed PMID: 17145503; PubMed Central PMCID: PMCPMC1899130.

26. Newpher TM, Ehlers MD. Spine microdomains for postsynaptic signaling and plasticity. Trends Cell Biol. 2009;19(5):218-27. Epub 2009/03/28. doi: 10.1016/j.tcb.2009.02.004. PubMed PMID: 19328694.

27. Padamsey Z, McGuinness L, Bardo SJ, Reinhart M, Tong R, Hedegaard A, et al. Activity-dependent exocytosis of lysosomes regulates the structural plasticity of dendritic spines. Neuron. 2017;93(1):132-46. Epub 2016/12/15. doi: 10.1016/j.neuron.2016.11.013. PubMed PMID: 27989455; PubMed Central PMCID: PMCPMC5222721.

28. Chang KJ, Redmond SA, Chan JR. Remodeling myelination: implications for mechanisms of neural plasticity. Nat Neurosci. 2016;19(2):190-7. doi: 10.1038/nn.4200. PubMed PMID: 26814588; PubMed Central PMCID: PMCPMC4792270.

29. Yang C, Wang X, Wang J, Chen W, Lu N, Siniossoglou S, et al. Rewiring neuronal glycerolipid metabolism determines the extent of axon regeneration. Neuron. 2020;105(2):276-92.e5. Epub 2019/11/27. doi: 10.1016/j.neuron.2019.10.009. PubMed PMID: 31786011; PubMed Central PMCID: PMCPMC6975164.

30. Nikoletopoulou V, Tavernarakis N. Regulation and roles of autophagy at synapses. Trends Cell Biol. 2018;28(8):646-61. Epub 2018/05/03. doi: 10.1016/j.tcb.2018.03.006. PubMed PMID: 29731196.

31. Ziegler AB, Tavosanis G. Glycerophospholipids - Emerging players in neuronal dendrite branching and outgrowth. Dev Biol. 2019;451(1):25-34. Epub 2018/12/18. doi: 10.1016/j.ydbio.2018.12.009. PubMed PMID: 30576627.

32. Kim T, Im W. Revisiting hydrophobic mismatch with free energy simulation studies of transmembrane helix tilt and rotation. Biophys J. 2010;99(1):175-83. doi: 10.1016/j.bpj.2010.04.015. PubMed PMID: 20655845; PubMed Central PMCID: PMCPMC2895360.

33. Scott FE, Gawrisch K, MacKerell ADJ. Polyunsaturated fatty acids in lipid bilayers: Intrinsic and environmental contributions to their unique physical properties. Journal of the American Chemical Society. 2002;124(2). doi: 10.1021/ja0118340.

34. Barelli H, Antonny B. Lipid unsaturation and organelle dynamics. Curr Opin Cell Biol. 2016;41:25-32. Epub 2016/04/07. doi: 10.1016/j.ceb.2016.03.012. PubMed PMID: 27062546.

35. Rohrbough J, Broadie K. Lipid regulation of the synaptic vesicle cycle. Nat Rev Neurosci. 2005;6(2):139-50. doi: 10.1038/nrn1608. PubMed PMID: 15685219.

36. Manni MM, Tiberti ML, Pagnotta S, Barelli H, Gautier R, Antonny B. Acyl chain asymmetry and polyunsaturation of brain phospholipids facilitate membrane vesiculation without leakage. Elife. 2018;7. Epub 2018/03/15. doi: 10.7554/eLife.34394. PubMed PMID: 29543154; PubMed Central PMCID: PMCPMC5903860.

37. Serhan CN. Treating inflammation and infection in the 21st century: new hints from decoding resolution mediators and mechanisms. The FASEB Journal. 2017. doi: 10.1096/fj.201601222R.

38. Inceoglu B, Zolkowska D, Yoo HJ, Wagner KM, Yang J, Hackett E, et al. Epoxy fatty acids and inhibition of the soluble epoxide hydrolase selectively modulate GABA mediated neurotransmission to delay onset of seizures. PLoS One. 2013;8(12):e80922. Epub 2013/12/11. doi: 10.1371/journal.pone.0080922. PubMed PMID: 24349022; PubMed Central PMCID: PMCPMC3862847.

39. Barnig C, Frossard N, Levy BD. Towards targeting resolution pathways of airway inflammation in asthma. Pharmacol Ther. 2018;186:98-113. Epub 2018/01/22. doi: 10.1016/j.pharmthera.2018.01.004. PubMed PMID: 29352860.

40. Serhan CN. Pro-resolving lipid mediators are leads for resolution physiology. Nature. 2014;510(7503):92-101. doi: 10.1038/nature13479. PubMed PMID: 24899309; PubMed Central PMCID: PMCPMC4263681.

41. Chiang N, Serhan CN. Structural elucidation and physiologic functions of specialized pro-resolving mediators and their receptors. Mol Aspects Med. 2017;58:114-29. Epub 2017/03/31. doi: 10.1016/j.mam.2017.03.005. PubMed PMID: 28336292; PubMed Central PMCID: PMCPMC5623601.

42. Basil MC, Levy BD. Specialized pro-resolving mediators: endogenous regulators of infection and inflammation. Nat Rev Immunol. 2016;16(1):51-67. doi: 10.1038/nri.2015.4. PubMed PMID: 26688348.

43. Chiurchiù V, Leuti A, Maccarrone M. Bioactive lipids and chronic inflammation: Managing the fire within. Front Immunol. 2018;9:38. Epub 2018/01/29. doi: 10.3389/fimmu.2018.00038. PubMed PMID: 29434586; PubMed Central PMCID: PMCPMC5797284.

44. Leishman E, Mackie K, Luquet S, Bradshaw HB. Lipidomics profile of a NAPE-PLD KO mouse provides evidence of a broader role of this enzyme in lipid metabolism in the brain. Biochim Biophys Acta. 2016;1861(6):491-500. Epub 2016/03/05. doi: 10.1016/j.bbalip.2016.03.003. PubMed PMID: 26956082; PubMed Central PMCID: PMCPMC4909477.

45. Kim HY, Spector AA. N-Docosahexaenoylethanolamine: A neurotrophic and neuroprotective metabolite of docosahexaenoic acid. Mol Aspects Med. 2018;64:34-44. Epub 2018/03/27. doi: 10.1016/j.mam.2018.03.004. PubMed PMID: 29572109.

46. Park T, Chen H, Kevala K, Lee JW, Kim HY. N-Docosahexaenoylethanolamine ameliorates LPS-induced neuroinflammation via cAMP/PKA-dependent signaling. J Neuroinflammation. 2016;13(1):284. Epub 2016/11/04. doi: 10.1186/s12974-016-0751-z. PubMed PMID: 27809877; PubMed Central PMCID: PMCPMC5096293.

47. Pereyra AS, Hasek LY, Harris KL, Berman AG, Damen FW, Goergen CJ, et al. Loss of cardiac carnitine palmitoyltransferase 2 results in rapamycin-resistant, acetylation-independent hypertrophy. J Biol Chem. 2017;292(45):18443-56. Epub 2017/09/15. doi: 10.1074/jbc.M117.800839. PubMed PMID: 28916721; PubMed Central PMCID: PMCPMC5682957.

48. Fernandez RF, Kim SQ, Zhao Y, Foguth RM, Weera MM, Counihan JL, et al. Acyl-CoA synthetase 6 enriches the neuroprotective omega-3 fatty acid DHA in the brain. Proc Natl Acad Sci U S A. 2018. Epub 2018/11/06. doi: 10.1073/pnas.1807958115. PubMed PMID: 30401738.

49. Destaillats F, Oliveira M, Bastic Schmid V, Masserey-Elmelegy I, Giuffrida F, Thakkar SK, et al. Comparison of the incorporation of DHA in circulatory and neural tissue when provided as triacylglycerol (TAG), monoacylglycerol (MAG) or phospholipids (PL) provides new insight into fatty acid bioavailability. Nutrients. 2018;10(5). Epub 2018/05/15. doi: 10.3390/nu10050620. PubMed PMID: 29762503; PubMed Central PMCID: PMCPMC5986500.

50. Naoe S, Tsugawa H, Takahashi M, Ikeda K, Arita M. Characterization of lipid profiles after dietary intake of polyunsaturated fatty acids using integrated untargeted and targeted lipidomics. Metabolites. 2019;9(10). Epub 2019/10/21. doi: 10.3390/metabo9100241. PubMed PMID: 31640217; PubMed Central PMCID: PMCPMC6836067.

51. Sugasini D, Yalagala PCR, Goggin A, Tai LM, Subbaiah PV. Enrichment of brain docosahexaenoic acid (DHA) is highly dependent upon the molecular carrier of dietary DHA: lysophosphatidylcholine is more efficient than either phosphatidylcholine or triacylglycerol. J Nutr Biochem. 2019;74:108231. Epub 2019/08/31. doi: 10.1016/j.jnutbio.2019.108231. PubMed PMID: 31665653; PubMed Central PMCID: PMCPMC6885117.

52. Tu WC, Mühlhäusler BS, Yelland LN, Gibson RA. Correlations between blood and tissue omega-3 LCPUFA status following dietary ALA intervention in rats. Prostaglandins Leukot Essent Fatty Acids. 2013;88(1):53-60. Epub 2012/04/20. doi: 10.1016/j.plefa.2012.04.005. PubMed PMID: 22521090.

53. Ding N, Xue Y, Tang X, Sun ZM, Yanagita T, Xue CH, et al. Short-term effects of different fish oil formulations on tissue absorption of docosahexaenoic acid in mice fed high- and low-fat diets. J Oleo Sci. 2013;62(11):883-91. doi: 10.5650/jos.62.883. PubMed PMID: 24200935.

54. Adkins Y, Laugero KD, Mackey B, Kelley DS. Accretion of dietary docosahexaenoic acid in mouse tissues did not differ between its purified phospholipid and triacylglycerol forms. Lipids. 2019;54(1):25-37. Epub 2019/01/29. doi: 10.1002/lipd.12115. PubMed PMID: 30697752.

55. Crawford MA, Casperd NM, Sinclair AJ. The long chain metabolites of linoleic avid linolenic acids in liver and brain in herbivores and carnivores. Comp Biochem Physiol B. 1976;54(3):395-401. PubMed PMID: 1277808.

56. McNamara RK, Almeida DM. Omega-3 polyunsaturated fatty acid deficiency and progressive neuropathology in psychiatric disorders: A review of translational evidence and candidate mechanisms. Harv Rev Psychiatry. 2019;27(2):94-107. doi: 10.1097/HRP.0000000000000199. PubMed PMID: 30633010; PubMed Central PMCID: PMCPMC6411441.

57. Lefkowith JB. Essential fatty acid deficiency inhibits the in vivo generation of leukotriene B4 and suppresses levels of resident and elicited leukocytes in acute inflammation. J Immunol. 1988;140(1):228-33. PubMed PMID: 2826589.

58. Vahouny GV, Hodges VA, Treadwell CR. Essential fatty acid deficiency and adrenal cortical function in vitro. J Lipid Res. 1979;20(2):154-61. PubMed PMID: 220357.

59. Holman RT, Johnson SB, Hatch TF. A case of human linolenic acid deficiency involving neurological abnormalities. Am J Clin Nutr. 1982;35(3):617-23. PubMed PMID: 6801965.

60. Fedorova I, Hussein N, Baumann MH, Di Martino C, Salem N. An n-3 fatty acid deficiency impairs rat spatial learning in the Barnes maze. Behav Neurosci. 2009;123(1):196-205. doi: 10.1037/a0013801. PubMed PMID: 19170444.

61. Calder PC. Docosahexaenoic Acid. Ann Nutr Metab. 2016;69 Suppl 1:7-21. Epub 2016/11/15. doi: 10.1159/000448262. PubMed PMID: 27842299.

62. Levant B, Radel JD, Carlson SE. Decreased brain docosahexaenoic acid during development alters dopamine-related behaviors in adult rats that are differentially affected by dietary remediation. Behav Brain Res. 2004;152(1):49-57. doi: 10.1016/j.bbr.2003.09.029. PubMed PMID: 15135968.

63. Lauritzen L, Hansen HS, Jørgensen MH, Michaelsen KF. The essentiality of long chain n-3 fatty acids in relation to development and function of the brain and retina. Prog Lipid Res. 2001;40(1-2):1-94. PubMed PMID: 11137568.

64. Clandinin MT. Brain development and assessing the supply of polyunsaturated fatty acid. Lipids. 1999;34(2):131-7. PubMed PMID: 10102239.

65. Radcliffe JE, Thomas J, Bramley AL, Kouris-Blazos A, Radford BE, Scholey AB, et al. Controversies in omega-3 efficacy and novel concepts for application. 2016;5:11-22.

66. Jiao J, Li Q, Chu J, Zeng W, Yang M, Zhu S. Effect of n-3 PUFA supplementation on cognitive function throughout the life span from infancy to old age: a systematic review and meta-analysis of randomized controlled trials. Am J Clin Nutr. 2014;100(6):1422-36. Epub 2014/10/15. doi: 10.3945/ajcn.114.095315. PubMed PMID: 25411277.

67. Oster T, Pillot T. Docosahexaenoic acid and synaptic protection in Alzheimer's disease mice. Biochim Biophys Acta. 2010;1801(8):791-8. Epub 2010/03/06. doi: 10.1016/j.bbalip.2010.02.011. PubMed PMID: 20211757.

68. Cunnane SC, Plourde M, Pifferi F, Bégin M, Féart C, Barberger-Gateau P. Fish, docosahexaenoic acid and Alzheimer's disease. Prog Lipid Res. 2009;48(5):239-56. Epub 2009/04/10. doi: 10.1016/j.plipres.2009.04.001. PubMed PMID: 19362576.

69. Belkouch M, Hachem M, Elgot A, Lo Van A, Picq M, Guichardant M, et al. The pleiotropic effects of omega-3 docosahexaenoic acid on the hallmarks of Alzheimer's disease. J Nutr Biochem. 2016;38:1-11. Epub 2016/03/24. doi: 10.1016/j.jnutbio.2016.03.002. PubMed PMID: 27825512.

70. Levant B, Ozias MK, Carlson SE. Sex-specific effects of brain LC-PUFA composition on locomotor activity in rats. Physiol Behav. 2006;89(2):196-204. Epub 2006/07/27. doi: 10.1016/j.physbeh.2006.06.007. PubMed PMID: 16875705.

71. Sublette ME, Galfalvy HC, Hibbeln JR, Keilp JG, Malone KM, Oquendo MA, et al. Polyunsaturated fatty acid associations with dopaminergic indices in major depressive disorder. Int J Neuropsychopharmacol. 2014;17(3):383-91. Epub 2013/12/03. doi: 10.1017/S1461145713001399. PubMed PMID: 24300434; PubMed Central PMCID: PMCPMC3956108.

72. Grosso G, Pajak A, Marventano S, Castellano S, Galvano F, Bucolo C, et al. Role of omega-3 fatty acids in the treatment of depressive disorders: a comprehensive meta-analysis of randomized clinical trials. PLoS One. 2014;9(5):e96905. Epub 2014/05/07. doi: 10.1371/journal.pone.0096905. PubMed PMID: 24805797; PubMed Central PMCID: PMCPMC4013121.

73. Joffre C, Nadjar A, Lebbadi M, Calon F, Laye S. n-3 LCPUFA improves cognition: the young, the old and the sick. Prostaglandins Leukot Essent Fatty Acids. 2014;91(1-2):1-20. doi: 10.1016/j.plefa.2014.05.001. PubMed PMID: 24908517.

74. Chang JP, Su KP, Mondelli V, Pariante CM. Omega-3 polyunsaturated fatty acids in youths with attention deficit hyperactivity disorder: a systematic review and meta-analysis of clinical trials and biological studies. Neuropsychopharmacology. 2018;43(3):534-45. Epub 2017/07/25. doi: 10.1038/npp.2017.160. PubMed PMID: 28741625; PubMed Central PMCID: PMCPMC5669464.

75. Yurko-Mauro K, Alexander DD, Van Elswyk ME. Docosahexaenoic acid and adult memory: a systematic review and meta-analysis. PLoS One. 2015;10(3):e0120391. Epub 2015/03/18. doi: 10.1371/journal.pone.0120391. PubMed PMID: 25786262; PubMed Central PMCID: PMCPMC4364972.

76. Chew EY, Clemons TE, Agrón E, Launer LJ, Grodstein F, Bernstein PS, et al. Effect of omega-3 fatty acids, lutein/zeaxanthin, or other nutrient supplementation on cognitive function: The AREDS2 randomized clinical trial. JAMA. 2015;314(8):791-801. doi: 10.1001/jama.2015.9677. PubMed PMID: 26305649; PubMed Central PMCID: PMCPMC5369607.

77. Weylandt KH, Serini S, Chen YQ, Su HM, Lim K, Cittadini A, et al. Omega-3 polyunsaturated fatty acids: The way forward in times of mixed evidence. Biomed Res Int. 2015;2015:143109. Epub 2015/08/02. doi: 10.1155/2015/143109. PubMed PMID: 26301240; PubMed Central PMCID: PMCPMC4537707.

78. Watkins PA, Maiguel D, Jia Z, Pevsner J. Evidence for 26 distinct acyl-coenzyme A synthetase genes in the human genome. J Lipid Res. 2007;48(12):2736-50. doi: 10.1194/jlr.M700378-JLR200. PubMed PMID: 17762044.

79. Coleman RA. How do I fatten thee? Let me count the ways.. Cell Metab. 2007;5(2):87-9. doi: 10.1016/j.cmet.2007.01.004. PubMed PMID: 17276351; PubMed Central PMCID: PMCPMC2819350.

80. Grevengoed TJ, Klett EL, Coleman RA. Acyl-CoA metabolism and partitioning. Annu Rev Nutr. 2014;34:1-30. doi: 10.1146/annurev-nutr-071813-105541. PubMed PMID: 24819326.

81. Shindou H, Hishikawa D, Harayama T, Eto M, Shimizu T. Generation of membrane diversity by lysophospholipid acyltransferases. J Biochem. 2013;154(1):21-8. Epub 2013/05/21. doi: 10.1093/jb/mvt048. PubMed PMID: 23698096.

82. Chen CT, Green JT, Orr SK, Bazinet RP. Regulation of brain polyunsaturated fatty acid uptake and turnover. Prostaglandins Leukot Essent Fatty Acids. 2008;79(3-5):85-91. doi: 10.1016/j.plefa.2008.09.003. PubMed PMID: 18938067.

83. Rapoport SI. In vivo fatty acid incorporation into brain phosholipids in relation to plasma availability, signal transduction and membrane remodeling. J Mol Neurosci. 2001;16:243-61.

84. Cheon Y, Kim HW, Igarashi M, Modi HR, Chang L, Ma K, et al. Disturbed brain phospholipid and docosahexaenoic acid metabolism in calcium-independent phospholipase A(2)-VIA (iPLA(2)β)-knockout mice. Biochim Biophys Acta. 2012;1821(9):1278-86. Epub 2012/02/10. doi: 10.1016/j.bbalip.2012.02.003. PubMed PMID: 22349267; PubMed Central PMCID: PMCPMC3393806.

85. Eto M, Shindou H, Yamamoto S, Tamura-Nakano M, Shimizu T. Lysophosphatidylethanolamine acyltransferase 2 (LPEAT2) incorporates DHA into phospholipids and has possible functions for fatty acid-induced cell death. Biochem Biophys Res Commun. 2020;526(1):246-52. Epub 2020/03/21. doi: 10.1016/j.bbrc.2020.03.074. PubMed PMID: 32204912.

86. Hashidate-Yoshida T, Harayama T, Hishikawa D, Morimoto R, Hamano F, Tokuoka SM, et al. Fatty acid remodeling by LPCAT3 enriches arachidonate in phospholipid membranes and regulates triglyceride transport. Elife. 2015;4. Epub 2015/04/21. doi: 10.7554/eLife.06328. PubMed PMID: 25898003; PubMed Central PMCID: PMCPMC4436788.

87. Wang B, Tontonoz P. Phospholipid remodeling in physiology and disease. Annu Rev Physiol. 2019;81:165-88. Epub 2018/10/31. doi: 10.1146/annurev-physiol-020518-114444. PubMed PMID: 30379616; PubMed Central PMCID: PMCPMC7008953.

88. Harayama T, Shimizu T. Roles of polyunsaturated fatty acids, from mediators to membranes. J Lipid Res. 2020;61(8):1150-60. Epub 2020/06/02. doi: 10.1194/jlr.R120000800. PubMed PMID: 32487545; PubMed Central PMCID: PMCPMC7397749.

89. Iizuka-Hishikawa Y, Hishikawa D, Sasaki J, Takubo K, Goto M, Nagata K, et al. Lysophosphatidic acid acyltransferase 3 tunes the membrane status of germ cells by incorporating docosahexaenoic acid during spermatogenesis. J Biol Chem. 2017;292(29):12065-76. Epub 2017/06/03. doi: 10.1074/jbc.M117.791277. PubMed PMID: 28578315; PubMed Central PMCID: PMCPMC5519358.

90. Koeberle A, Shindou H, Harayama T, Yuki K, Shimizu T. Polyunsaturated fatty acids are incorporated into maturating male mouse germ cells by lysophosphatidic acid acyltransferase 3. FASEB J. 2012;26(1):169-80. Epub 2011/10/03. doi: 10.1096/fj.11-184879. PubMed PMID: 21968070.

91. Shindou H, Koso H, Sasaki J, Nakanishi H, Sagara H, Nakagawa KM, et al. Docosahexaenoic acid preserves visual function by maintaining correct disc morphology

in retinal photoreceptor cells. J Biol Chem. 2017;292(29):12054-64. Epub 2017/06/03. doi: 10.1074/jbc.M117.790568. PubMed PMID: 28578316; PubMed Central PMCID: PMCPMC5519357.

92. Lee HC, Inoue T, Sasaki J, Kubo T, Matsuda S, Nakasaki Y, et al. LPIAT1 regulates arachidonic acid content in phosphatidylinositol and is required for cortical lamination in mice. Mol Biol Cell. 2012;23(24):4689-700. Epub 2012/10/24. doi: 10.1091/mbc.E12-09-0673. PubMed PMID: 23097495; PubMed Central PMCID: PMCPMC3521678.

93. Cooper DE, Young PA, Klett EL, Coleman RA. Physiological consequences of compartmentalized acyl-CoA metabolism. J Biol Chem. 2015;290(33):20023-31. doi: 10.1074/jbc.R115.663260. PubMed PMID: 26124277; PubMed Central PMCID: PMCPMC4536410.

94. Soupene E, Kuypers FA. Mammalian long-chain acyl-CoA synthetases. Exp Biol Med (Maywood). 2008;233(5):507-21. doi: 10.3181/0710-MR-287. PubMed PMID: 18375835; PubMed Central PMCID: PMCPMC3377585.

95. Zhao C, Liu G, Shang S, Wei Q, Zhang L, Xia T, et al. Adaptive evolution of the ACSL gene family in Carnivora. Genetica. 2019;147(2):141-8. Epub 2019/03/13. doi: 10.1007/s10709-019-00057-3. PubMed PMID: 30868352.

96. Lopes-Marques M, Cunha I, Reis-Henriques MA, Santos MM, Castro LF. Diversity and history of the long-chain acyl-CoA synthetase (Acsl) gene family in vertebrates. BMC Evol Biol. 2013;13:271. Epub 2013/12/12. doi: 10.1186/1471-2148-13-271. PubMed PMID: 24330521; PubMed Central PMCID: PMCPMC3890633.

97. Ellis JM, Bowman CE, Wolfgang MJ. Metabolic and tissue-specific regulation of acyl-CoA metabolism. PLoS One. 2015;10(3):e0116587. doi: 10.1371/journal.pone.0116587. PubMed PMID: 25760036; PubMed Central PMCID: PMCPMC4356623.

98. Ellis JM, Frahm JL, Li LO, Coleman RA. Acyl-coenzyme A synthetases in metabolic control. Curr Opin Lipidol. 2010;21(3):212-7. PubMed PMID: 20480548; PubMed Central PMCID: PMCPMC4040134.

99. Coleman R, Van Horn C, Gonzalez-Baró M, Lewin T. In: Lipids: Glycerolipid metabolizing enzymes. Haldar D, Das SK, editors. . Research Signpost; Trivandrum; 2002. p. 1-15.

100. Ellis JM, Li LO, Wu PC, Koves TR, Ilkayeva O, Stevens RD, et al. Adipose acyl-CoA synthetase-1 directs fatty acids toward beta-oxidation and is required for cold thermogenesis. Cell Metab. 2010;12(1):53-64. doi: 10.1016/j.cmet.2010.05.012. PubMed PMID: 20620995; PubMed Central PMCID: PMCPMC2910420.

101. Bowman TA, O'Keeffe KR, D'Aquila T, Yan QW, Griffin JD, Killion EA, et al. Acyl CoA synthetase 5 (ACSL5) ablation in mice increases energy expenditure and insulin

sensitivity and delays fat absorption. Mol Metab. 2016;5(3):210-20. doi: 10.1016/j.molmet.2016.01.001. PubMed PMID: 26977393; PubMed Central PMCID: PMCPMC4770262.

102. Bu SY, Mashek DG. Hepatic long-chain acyl-CoA synthetase 5 mediates fatty acid channeling between anabolic and catabolic pathways. J Lipid Res. 2010;51(11):3270-80. doi: 10.1194/jlr.M009407. PubMed PMID: 20798351; PubMed Central PMCID: PMCPMC2952567.

103. Bu SY, Mashek MT, Mashek DG. Suppression of long chain acyl-CoA synthetase 3 decreases hepatic de novo fatty acid synthesis through decreased transcriptional activity. J Biol Chem. 2009;284(44):30474-83. doi: 10.1074/jbc.M109.036665. PubMed PMID: 19737935; PubMed Central PMCID: PMCPMC2781602.

104. Mashek DG, Li LO, Coleman RA. Rat long-chain acyl-CoA synthetase mRNA, protein, and activity vary in tissue distribution and in response to diet. J Lipid Res. 2006;47(9):2004-10. doi: 10.1194/jlr.M600150-JLR200. PubMed PMID: 16772660.

105. Muoio DM, Lewin TM, Wiedmer P, Coleman RA. Acyl-CoAs are functionally channeled in liver: potential role of acyl-CoA synthetase. Am J Physiol Endocrinol Metab. 2000;279(6):E1366-73. doi: 10.1152/ajpendo.2000.279.6.E1366. PubMed PMID: 11093925.

106. Mashek DG, Coleman RA. Cellular fatty acid uptake: the contribution of metabolism. Curr Opin Lipidol. 2006;17(3):274-8. doi: 10.1097/01.mol.0000226119.20307.2b. PubMed PMID: 16680032.

107. Watkins PA. Fatty acid activation. Prog Lipid Res. 1997;36(1):55-83. doi: 10.1016/s0163-7827(97)00004-0. PubMed PMID: 9373621.

108. Marszalek JR, Kitidis C, Dararutana A, Lodish HF. Acyl-CoA synthetase 2 overexpression enhances fatty acid internalization and neurite outgrowth. J Biol Chem. 2004;279(23):23882-91. doi: 10.1074/jbc.M313460200. PubMed PMID: 15051725.

109. Li LO, Mashek DG, An J, Doughman SD, Newgard CB, Coleman RA. Overexpression of rat long chain acyl-coa synthetase 1 alters fatty acid metabolism in rat primary hepatocytes. J Biol Chem. 2006;281(48):37246-55. Epub 2006/10/06. doi: 10.1074/jbc.M604427200. PubMed PMID: 17028193.

110. Mashek DG, McKenzie MA, Van Horn CG, Coleman RA. Rat long chain acyl-CoA synthetase 5 increases fatty acid uptake and partitioning to cellular triacylglycerol in McArdle-RH7777 cells. J Biol Chem. 2006;281(2):945-50. Epub 2005/11/01. doi: 10.1074/jbc.M507646200. PubMed PMID: 16263710.

111. Hale BJ, Fernandez RF, Kim SQ, Diaz VD, Jackson SN, Liu L, et al. Acyl-CoA synthetase 6 enriches seminiferous tubules with the ω-3 fatty acid docosahexaenoic acid and is required for male fertility in the mouse. J Biol Chem. 2019;294(39):14394-405.

Epub 2019/08/09. doi: 10.1074/jbc.RA119.009972. PubMed PMID: 31399511; PubMed Central PMCID: PMCPMC6768642.

112. Ellis JM, Mentock SM, Depetrillo MA, Koves TR, Sen S, Watkins SM, et al. Mouse cardiac acyl coenzyme a synthetase 1 deficiency impairs fatty Acid oxidation and induces cardiac hypertrophy. Mol Cell Biol. 2011;31(6):1252-62. doi: 10.1128/MCB.01085-10. PubMed PMID: 21245374; PubMed Central PMCID: PMCPMC3067914.

113. Grevengoed TJ, Martin SA, Katunga L, Cooper DE, Anderson EJ, Murphy RC, et al. Acyl-CoA synthetase 1 deficiency alters cardiolipin species and impairs mitochondrial function. J Lipid Res. 2015;56(8):1572-82. Epub 2015/07/01. doi: 10.1194/jlr.M059717. PubMed PMID: 26136511; PubMed Central PMCID: PMCPMC4513998.

114. Coleman RA. It takes a village: channeling fatty acid metabolism and triacylglycerol formation via protein interactomes. J Lipid Res. 2019;60(3):490-7. Epub 2019/01/25. doi: 10.1194/jlr.S091843. PubMed PMID: 30683668; PubMed Central PMCID: PMCPMC6399496.

115. Young PA, Senkal CE, Suchanek AL, Grevengoed TJ, Lin DD, Zhao L, et al. Long-chain acyl-CoA synthetase 1 interacts with key proteins that activate and direct fatty acids into niche hepatic pathways. J Biol Chem. 2018;293(43):16724-40. Epub 2018/09/06. doi: 10.1074/jbc.RA118.004049. PubMed PMID: 30190326; PubMed Central PMCID: PMCPMC6204890.

116. Watkins PA. Very-long-chain acyl-CoA synthetases. J Biol Chem. 2008;283(4):1773-7. doi: 10.1074/jbc.R700037200. PubMed PMID: 18024425.

117. Jia Z, Pei Z, Maiguel D, Toomer CJ, Watkins PA. The fatty acid transport protein (FATP) family: very long chain acyl-CoA synthetases or solute carriers? J Mol Neurosci. 2007;33(1):25-31. doi: 10.1007/s12031-007-0038-z. PubMed PMID: 17901542.

118. Tong F, Black PN, Coleman RA, DiRusso CC. Fatty acid transport by vectorial acylation in mammals: roles played by different isoforms of rat long-chain acyl-CoA synthetases. Arch Biochem Biophys. 2006;447(1):46-52. Epub 2006/01/23. doi: 10.1016/j.abb.2006.01.005. PubMed PMID: 16466685.

119. Jia Z, Moulson CL, Pei Z, Miner JH, Watkins PA. Fatty acid transport protein 4 is the principal very long chain fatty acyl-CoA synthetase in skin fibroblasts. J Biol Chem. 2007;282(28):20573-83. Epub 2007/05/23. doi: 10.1074/jbc.M700568200. PubMed PMID: 17522045.

120. Mashek DG, Bornfeldt KE, Coleman RA, Berger J, Bernlohr DA, Black P, et al. Revised nomenclature for the mammalian long-chain acyl-CoA synthetase gene family. J Lipid Res. 2004;45(10):1958-61. doi: 10.1194/jlr.E400002-JLR200. PubMed PMID: 15292367.

121. Uhlén M, Fagerberg L, Hallström BM, Lindskog C, Oksvold P, Mardinoglu A, et al. Proteomics. Tissue-based map of the human proteome. Science. 2015;347(6220):1260419. doi: 10.1126/science.1260419. PubMed PMID: 25613900.

122. Nicholls, et al. From Neuron to Brain. Fourth Edition ed2000.

123. Cahoy JD, Emery B, Kaushal A, Foo LC, Zamanian JL, Christopherson KS, et al. A transcriptome database for astrocytes, neurons, and oligodendrocytes: a new resource for understanding brain development and function. J Neurosci. 2008;28(1):264-78. doi: 10.1523/JNEUROSCI.4178-07.2008. PubMed PMID: 18171944.

124. Zhang Y, Chen K, Sloan SA, Bennett ML, Scholze AR, O'Keeffe S, et al. An RNA-sequencing transcriptome and splicing database of glia, neurons, and vascular cells of the cerebral cortex. J Neurosci. 2014;34(36):11929-47. doi: 10.1523/JNEUROSCI.1860-14.2014. PubMed PMID: 25186741; PubMed Central PMCID: PMCPMC4152602.

125. Sharma K, Schmitt S, Bergner CG, Tyanova S, Kannaiyan N, Manrique-Hoyos N, et al. Cell type- and brain region-resolved mouse brain proteome. Nat Neurosci. 2015;18(12):1819-31. Epub 2015/11/02. doi: 10.1038/nn.4160. PubMed PMID: 26523646.

126. Pélerin H, Jouin M, Lallemand MS, Alessandri JM, Cunnane SC, Langelier B, et al. Gene expression of fatty acid transport and binding proteins in the blood-brain barrier and the cerebral cortex of the rat: differences across development and with different DHA brain status. Prostaglandins Leukot Essent Fatty Acids. 2014;91(5):213-20. doi: 10.1016/j.plefa.2014.07.004. PubMed PMID: 25123062.

127. Tasic B, Yao Z, Graybuck LT, Smith KA, Nguyen TN, Bertagnolli D, et al. Shared and distinct transcriptomic cell types across neocortical areas. Nature. 2018;563(7729):72-8. Epub 2018/10/31. doi: 10.1038/s41586-018-0654-5. PubMed PMID: 30382198; PubMed Central PMCID: PMCPMC6456269.

128. Hodge RD, Bakken TE, Miller JA, Smith KA, Barkan ER, Graybuck LT, et al. Conserved cell types with divergent features in human versus mouse cortex. Nature. 2019;573(7772):61-8. Epub 2019/08/21. doi: 10.1038/s41586-019-1506-7. PubMed PMID: 31435019; PubMed Central PMCID: PMCPMC6919571.

129. Setou M, Kurabe N. Mass microscopy: high-resolution imaging mass spectrometry. J Electron Microsc (Tokyo). 2011;60(1):47-56. Epub 2010/11/24. doi: 10.1093/jmicro/dfq079. PubMed PMID: 21109523.

130. Sugiura Y, Konishi Y, Zaima N, Kajihara S, Nakanishi H, Taguchi R, et al. Visualization of the cell-selective distribution of PUFA-containing phosphatidylcholines in mouse brain by imaging mass spectrometry. J Lipid Res. 2009;50(9):1776-88. Epub 2009/05/05. doi: 10.1194/jlr.M900047-JLR200. PubMed PMID: 19417221; PubMed Central PMCID: PMCPMC2724791.

131. Berry KA, Hankin JA, Barkley RM, Spraggins JM, Caprioli RM, Murphy RC. MALDI imaging of lipid biochemistry in tissues by mass spectrometry. Chem Rev. 2011;111(10):6491-512. Epub 2011/09/26. doi: 10.1021/cr200280p. PubMed PMID: 21942646; PubMed Central PMCID: PMCPMC3199966.

132. Neumann EK, Comi TJ, Rubakhin SS, Sweedler JV. Lipid heterogeneity between astrocytes and neurons revealed by single-cell MALDI-MS combined with immunocytochemical classification. Angew Chem Int Ed Engl. 2019;58(18):5910-4. Epub 2019/03/29. doi: 10.1002/anie.201812892. PubMed PMID: 30811763; PubMed Central PMCID: PMCPMC6461516.

133. Merrill CB, Basit A, Armirotti A, Jia Y, Gall CM, Lynch G, et al. Patch clamp-assisted single neuron lipidomics. Sci Rep. 2017;7(1):5318. Epub 2017/07/13. doi: 10.1038/s41598-017-05607-3. PubMed PMID: 28706218; PubMed Central PMCID: PMCPMC5509708.

134. Nguyen LN, Ma D, Shui G, Wong P, Cazenave-Gassiot A, Zhang X, et al. Mfsd2a is a transporter for the essential omega-3 fatty acid docosahexaenoic acid. Nature. 2014;509(7501):503-6. Epub 2014/05/14. doi: 10.1038/nature13241. PubMed PMID: 24828044.

135. Andreone BJ, Chow BW, Tata A, Lacoste B, Ben-Zvi A, Bullock K, et al. Blood-Brain Barrier Permeability Is Regulated by Lipid Transport-Dependent Suppression of Caveolae-Mediated Transcytosis. Neuron. 2017;94(3):581-94.e5. Epub 2017/04/13. doi: 10.1016/j.neuron.2017.03.043. PubMed PMID: 28416077; PubMed Central PMCID: PMCPMC5474951.

136. Ben-Zvi A, Lacoste B, Kur E, Andreone BJ, Mayshar Y, Yan H, et al. Mfsd2a is critical for the formation and function of the blood-brain barrier. Nature. 2014;509(7501):507-11. Epub 2014/05/14. doi: 10.1038/nature13324. PubMed PMID: 24828040; PubMed Central PMCID: PMCPMC4134871.

137. Chen CT, Kitson AP, Hopperton KE, Domenichiello AF, Trépanier MO, Lin LE, et al. Plasma non-esterified docosahexaenoic acid is the major pool supplying the brain. Sci Rep. 2015;5:15791. Epub 2015/10/29. doi: 10.1038/srep15791. PubMed PMID: 26511533; PubMed Central PMCID: PMCPMC4625162.

138. Chouinard-Watkins R, Bazinet RP. ACSL6 is critical for maintaining brain DHA levels. Proc Natl Acad Sci U S A. 2018;115(49):12343-5. Epub 2018/11/16. doi: 10.1073/pnas.1817557115. PubMed PMID: 30446610; PubMed Central PMCID: PMCPMC6298068.

139. Li LO, Ellis JM, Paich HA, Wang S, Gong N, Altshuller G, et al. Liver-specific loss of long chain acyl-CoA synthetase-1 decreases triacylglycerol synthesis and beta-oxidation and alters phospholipid fatty acid composition. J Biol Chem. 2009;284(41):27816-26. doi: 10.1074/jbc.M109.022467. PubMed PMID: 19648649; PubMed Central PMCID: PMCPMC2788832.

140. Klett EL, Chen S, Yechoor A, Lih FB, Coleman RA. Long-chain acyl-CoA synthetase isoforms differ in preferences for eicosanoid species and long-chain fatty acids. J Lipid Res. 2017;58(5):884-94. Epub 2017/02/16. doi: 10.1194/jlr.M072512. PubMed PMID: 28209804; PubMed Central PMCID: PMCPMC5408607.

141. Zhao L, Pascual F, Bacudio L, Suchanek AL, Young PA, Li LO, et al. Defective fatty acid oxidation in mice with muscle-specific acyl-CoA synthetase 1 deficiency increases amino acid use and impairs muscle function. J Biol Chem. 2019;294(22):8819-33. Epub 2019/04/11. doi: 10.1074/jbc.RA118.006790. PubMed PMID: 30975900; PubMed Central PMCID: PMCPMC6552438.

142. Grevengoed TJ, Cooper DE, Young PA, Ellis JM, Coleman RA. Loss of long-chain acyl-CoA synthetase isoform 1 impairs cardiac autophagy and mitochondrial structure through mechanistic target of rapamycin complex 1 activation. FASEB J. 2015;29(11):4641-53. Epub 2015/07/28. doi: 10.1096/fj.15-272732. PubMed PMID: 26220174; PubMed Central PMCID: PMCPMC4608904.

143. Paul DS, Grevengoed TJ, Pascual F, Ellis JM, Willis MS, Coleman RA. Deficiency of cardiac Acyl-CoA synthetase-1 induces diastolic dysfunction, but pathologic hypertrophy is reversed by rapamycin. Biochim Biophys Acta. 2014;1841(6):880-7. Epub 2014/03/12. doi: 10.1016/j.bbalip.2014.03.001. PubMed PMID: 24631848; PubMed Central PMCID: PMCPMC4047709.

144. Li LO, Grevengoed TJ, Paul DS, Ilkayeva O, Koves TR, Pascual F, et al. Compartmentalized acyl-CoA metabolism in skeletal muscle regulates systemic glucose homeostasis. Diabetes. 2015;64(1):23-35. Epub 2014/07/28. doi: 10.2337/db13-1070. PubMed PMID: 25071025; PubMed Central PMCID: PMCPMC4274800.

145. Fujino T, Kang MJ, Suzuki H, Iijima H, Yamamoto T. Molecular characterization and expression of rat acyl-CoA synthetase 3. J Biol Chem. 1996;271(28):16748-52. PubMed PMID: 8663269.

146. Van Horn CG, Caviglia JM, Li LO, Wang S, Granger DA, Coleman RA. Characterization of recombinant long-chain rat acyl-CoA synthetase isoforms 3 and 6: identification of a novel variant of isoform 6. Biochemistry. 2005;44(5):1635-42. doi: 10.1021/bi047721l. PubMed PMID: 15683247.

147. Saliakoura M, Reynoso-Moreno I, Pozzato C, Rossi Sebastiano M, Galié M, Gertsch J, et al. The ACSL3-LPIAT1 signaling drives prostaglandin synthesis in non-small cell lung cancer. Oncogene. 2020;39(14):2948-60. Epub 2020/02/07. doi: 10.1038/s41388-020-1196-5. PubMed PMID: 32034305; PubMed Central PMCID: PMCPMC7118021.

148. Magtanong L, Ko PJ, To M, Cao JY, Forcina GC, Tarangelo A, et al. Exogenous monounsaturated fatty acids promote a ferroptosis-resistant cell state. Cell Chem Biol. 2019;26(3):420-32.e9. Epub 2019/01/24. doi: 10.1016/j.chembiol.2018.11.016. PubMed PMID: 30686757; PubMed Central PMCID: PMCPMC6430697.

149. Padanad MS, Konstantinidou G, Venkateswaran N, Melegari M, Rindhe S, Mitsche M, et al. Fatty acid oxidation mediated by acyl-CoA synthetase long chain 3 is required for mutant KRAS lung tumorigenesis. Cell Rep. 2016;16(6):1614-28. Epub 2016/07/28. doi: 10.1016/j.celrep.2016.07.009. PubMed PMID: 27477280; PubMed Central PMCID: PMCPMC4981512.

150. Lewin TM, Van Horn CG, Krisans SK, Coleman RA. Rat liver acyl-CoA synthetase 4 is a peripheral-membrane protein located in two distinct subcellular organelles, peroxisomes, and mitochondrial-associated membrane. Arch Biochem Biophys. 2002;404(2):263-70. PubMed PMID: 12147264.

151. Lewin TM, Kim JH, Granger DA, Vance JE, Coleman RA. Acyl-CoA synthetase isoforms 1, 4, and 5 are present in different subcellular membranes in rat liver and can be inhibited independently. J Biol Chem. 2001;276(27):24674-9. doi: 10.1074/jbc.M102036200. PubMed PMID: 11319232.

152. Kang MJ, Fujino T, Sasano H, Minekura H, Yabuki N, Nagura H, et al. A novel arachidonate-preferring acyl-CoA synthetase is present in steroidogenic cells of the rat adrenal, ovary, and testis. Proc Natl Acad Sci U S A. 1997;94(7):2880-4. PubMed PMID: 9096315; PubMed Central PMCID: PMCPMC20291.

153. Kuwata H, Yoshimura M, Sasaki Y, Yoda E, Nakatani Y, Kudo I, et al. Role of long-chain acyl-coenzyme A synthetases in the regulation of arachidonic acid metabolism in interleukin 1β-stimulated rat fibroblasts. Biochim Biophys Acta. 2014;1841(1):44-53. doi: 10.1016/j.bbalip.2013.09.015. PubMed PMID: 24095834.

154. Killion EA, Reeves AR, El Azzouny MA, Yan QW, Surujon D, Griffin JD, et al. A role for long-chain acyl-CoA synthetase-4 (ACSL4) in diet-induced phospholipid remodeling and obesity-associated adipocyte dysfunction. Mol Metab. 2018;9:43-56. Epub 2018/01/31. doi: 10.1016/j.molmet.2018.01.012. PubMed PMID: 29398618; PubMed Central PMCID: PMCPMC5870107.

155. Chang MC, Contreras MA, Rosenberger TA, Rintala JJ, Bell JM, Rapoport SI. Chronic valproate treatment decreases the in vivo turnover of arachidonic acid in brain phospholipids: a possible common effect of mood stabilizers. J Neurochem. 2001;77(3):796-803. PubMed PMID: 11331408.

156. Shimshoni JA, Basselin M, Li LO, Coleman RA, Rapoport SI, Modi HR. Valproate uncompetitively inhibits arachidonic acid acylation by rat acyl-CoA synthetase 4: relevance to valproate's efficacy against bipolar disorder. Biochim Biophys Acta. 2011;1811(3):163-9. doi: 10.1016/j.bbalip.2010.12.006. PubMed PMID: 21184843; PubMed Central PMCID: PMCPMC3037030.

157. Bell RM, Coleman RA. Enzymes of glycerolipid synthesis in eukaryotes. Annu Rev Biochem. 1980;49:459-87. doi: 10.1146/annurev.bi.49.070180.002331. PubMed PMID: 6250446.

158. Cho YY. A novel role of brain-type ACS4 isotype in neuronal differentiation. Biochem Biophys Res Commun. 2012;419(3):505-10. doi: 10.1016/j.bbrc.2012.02.046. PubMed PMID: 22366036.

159. Meloni I, Parri V, De Filippis R, Ariani F, Artuso R, Bruttini M, et al. The XLMR gene ACSL4 plays a role in dendritic spine architecture. Neuroscience. 2009;159(2):657-69. doi: 10.1016/j.neuroscience.2008.11.056. PubMed PMID: 19166906.

160. Jonsson JJ, Renieri A, Gallagher PG, Kashtan CE, Cherniske EM, Bruttini M, et al. Alport syndrome, mental retardation, midface hypoplasia, and elliptocytosis: a new X linked contiguous gene deletion syndrome? J Med Genet. 1998;35(4):273-8. PubMed PMID: 9598718; PubMed Central PMCID: PMCPMC1051272.

161. Piccini M, Vitelli F, Bruttini M, Pober BR, Jonsson JJ, Villanova M, et al. FACL4, a new gene encoding long-chain acyl-CoA synthetase 4, is deleted in a family with Alport syndrome, elliptocytosis, and mental retardation. Genomics. 1998;47(3):350-8. doi: 10.1006/geno.1997.5104. PubMed PMID: 9480748.

162. Meloni I, Muscettola M, Raynaud M, Longo I, Bruttini M, Moizard MP, et al. FACL4, encoding fatty acid-CoA ligase 4, is mutated in nonspecific X-linked mental retardation. Nat Genet. 2002;30(4):436-40. doi: 10.1038/ng857. PubMed PMID: 11889465.

163. Longo I, Frints SG, Fryns JP, Meloni I, Pescucci C, Ariani F, et al. A third MRX family (MRX68) is the result of mutation in the long chain fatty acid-CoA ligase 4 (FACL4) gene: proposal of a rapid enzymatic assay for screening mentally retarded patients. J Med Genet. 2003;40(1):11-7. PubMed PMID: 12525535; PubMed Central PMCID: PMCPMC1735250.

164. Kim HC, Lee SW, Cho YY, Lim JM, Ryoo ZY, Lee EJ. RNA interference of long-chain acyl-CoA synthetase 6 suppresses the neurite outgrowth of mouse neuroblastoma NB41A3 cells. Mol Med Rep. 2009;2(4):669-74. doi: 10.3892/mmr_00000155. PubMed PMID: 21475884.

165. Soupene E, Kuypers FA. Multiple erythroid isoforms of human long-chain acyl-CoA synthetases are produced by switch of the fatty acid gate domains. BMC Mol Biol. 2006;7:21. doi: 10.1186/1471-2199-7-21. PubMed PMID: 16834775; PubMed Central PMCID: PMCPMC1543647.

166. Lee EJ, Kim HC, Cho YY, Byun SJ, Lim JM, Ryoo ZY. Alternative promotion of the mouse acyl-CoA synthetase 6 (mAcsl6) gene mediates the expression of multiple transcripts with 5'-end heterogeneity: genetic organization of mAcsl6 variants. Biochem Biophys Res Commun. 2005;327(1):84-93. doi: 10.1016/j.bbrc.2004.11.141. PubMed PMID: 15629433.

167. Malhotra KT, Malhotra K, Lubin BH, Kuypers FA. Identification and molecular characterization of acyl-CoA synthetase in human erythrocytes and erythroid precursors. Biochem J. 1999;344 Pt 1:135-43. PubMed PMID: 10548543; PubMed Central PMCID: PMCPMC1220623.

168. Soupene E, Dinh NP, Siliakus M, Kuypers FA. Activity of the acyl-CoA synthetase ACSL6 isoforms: role of the fatty acid Gate-domains. BMC Biochem. 2010;11:18. doi: 10.1186/1471-2091-11-18. PubMed PMID: 20429931; PubMed Central PMCID: PMCPMC2868784.

169. Consortium SWGotPG. Biological insights from 108 schizophrenia-associated genetic loci. Nature. 2014;511(7510):421-7. doi: 10.1038/nature13595. PubMed PMID: 25056061; PubMed Central PMCID: PMCPMC4112379.

170. Luo XJ, Diao HB, Wang JK, Zhang H, Zhao ZM, Su B. Association of haplotypes spanning PDZ-GEF2, LOC728637 and ACSL6 with schizophrenia in Han Chinese. J Med Genet. 2008;45(12):818-26. doi: 10.1136/jmg.2008.060657. PubMed PMID: 18718982.

171. Kurotaki N, Tasaki S, Mishima H, Ono S, Imamura A, Kikuchi T, et al. Identification of novel schizophrenia loci by homozygosity mapping using DNA microarray analysis. PLoS One. 2011;6(5):e20589. doi: 10.1371/journal.pone.0020589. PubMed PMID: 21655227; PubMed Central PMCID: PMCPMC3105082.

172. Chen X, Wang X, Hossain S, O'Neill FA, Walsh D, Pless L, et al. Haplotypes spanning SPEC2, PDZ-GEF2 and ACSL6 genes are associated with schizophrenia. Hum Mol Genet. 2006;15(22):3329-42. doi: 10.1093/hmg/ddl409. PubMed PMID: 17030554.

173. de Leon J, Diaz FJ. A meta-analysis of worldwide studies demonstrates an association between schizophrenia and tobacco smoking behaviors. Schizophr Res. 2005;76(2-3):135-57. doi: 10.1016/j.schres.2005.02.010. PubMed PMID: 15949648.

174. Chen J, Brunzell DH, Jackson K, van der Vaart A, Ma JZ, Payne TJ, et al. ACSL6 is associated with the number of cigarettes smoked and its expression is altered by chronic nicotine exposure. PLoS One. 2011;6(12):e28790. doi: 10.1371/journal.pone.0028790. PubMed PMID: 22205969; PubMed Central PMCID: PMCPMC3243669.

175. Steinberg SJ, Morgenthaler J, Heinzer AK, Smith KD, Watkins PA. Very long-chain acyl-CoA synthetases. Human "bubblegum" represents a new family of proteins capable of activating very long-chain fatty acids. J Biol Chem. 2000;275(45):35162-9. doi: 10.1074/jbc.M006403200. PubMed PMID: 10954726.

176. Pei Z, Oey NA, Zuidervaart MM, Jia Z, Li Y, Steinberg SJ, et al. The acyl-CoA synthetase "bubblegum" (lipidosin): further characterization and role in neuronal fatty acid beta-oxidation. J Biol Chem. 2003;278(47):47070-8. doi: 10.1074/jbc.M310075200. PubMed PMID: 12975357.

177. Melton EM, Cerny RL, Watkins PA, DiRusso CC, Black PN. Human fatty acid transport protein 2a/very long chain acyl-CoA synthetase 1 (FATP2a/Acsvl1) has a preference in mediating the channeling of exogenous n-3 fatty acids into phosphatidylinositol. J Biol Chem. 2011;286(35):30670-9. Epub 2011/07/15. doi: 10.1074/jbc.M111.226316. PubMed PMID: 21768100; PubMed Central PMCID: PMCPMC3162428.

178. Melton EM, Cerny RL, DiRusso CC, Black PN. Overexpression of human fatty acid transport protein 2/very long chain acyl-CoA synthetase 1 (FATP2/Acsvl1) reveals distinct patterns of trafficking of exogenous fatty acids. Biochem Biophys Res Commun. 2013;440(4):743-8. Epub 2013/10/08. doi: 10.1016/j.bbrc.2013.09.137. PubMed PMID: 24113382; PubMed Central PMCID: PMCPMC4665974.

179. Hisanaga Y, Ago H, Nakagawa N, Hamada K, Ida K, Yamamoto M, et al. Structural basis of the substrate-specific two-step catalysis of long chain fatty acyl-CoA synthetase dimer. J Biol Chem. 2004;279(30):31717-26. doi: 10.1074/jbc.M400100200. PubMed PMID: 15145952.

180. Heinzer AK, Watkins PA, Lu JF, Kemp S, Moser AB, Li YY, et al. A very long-chain acyl-CoA synthetase-deficient mouse and its relevance to X-linked adrenoleukodystrophy. Hum Mol Genet. 2003;12(10):1145-54. doi: 10.1093/hmg/ddg126. PubMed PMID: 12719378.

181. Hall AM, Wiczer BM, Herrmann T, Stremmel W, Bernlohr DA. Enzymatic properties of purified murine fatty acid transport protein 4 and analysis of acyl-CoA synthetase activities in tissues from FATP4 null mice. J Biol Chem. 2005;280(12):11948-54. Epub 2005/01/14. doi: 10.1074/jbc.M412629200. PubMed PMID: 15653672.

182. Li S, Lee J, Zhou Y, Gordon WC, Hill JM, Bazan NG, et al. Fatty acid transport protein 4 (FATP4) prevents light-induced degeneration of cone and rod photoreceptors by inhibiting RPE65 isomerase. J Neurosci. 2013;33(7):3178-89. doi: 10.1523/JNEUROSCI.2428-12.2013. PubMed PMID: 23407971; PubMed Central PMCID: PMCPMC3625017.

183. Gimeno RE, Hirsch DJ, Punreddy S, Sun Y, Ortegon AM, Wu H, et al. Targeted deletion of fatty acid transport protein-4 results in early embryonic lethality. J Biol Chem. 2003;278(49):49512-6. Epub 2003/09/24. doi: 10.1074/jbc.M309759200. PubMed PMID: 14512415.

184. Herrmann T, van der Hoeven F, Grone HJ, Stewart AF, Langbein L, Kaiser I, et al. Mice with targeted disruption of the fatty acid transport protein 4 (Fatp 4, Slc27a4) gene show features of lethal restrictive dermopathy. J Cell Biol. 2003;161(6):1105-15. doi: 10.1083/jcb.200207080. PubMed PMID: 12821645; PubMed Central PMCID: PMCPMC2173002.

185. Moulson CL, Martin DR, Lugus JJ, Schaffer JE, Lind AC, Miner JH. Cloning of wrinkle-free, a previously uncharacterized mouse mutation, reveals crucial roles for fatty acid transport protein 4 in skin and hair development. Proc Natl Acad Sci U S A. 2003;100(9):5274-9. Epub 2003/04/15. doi: 10.1073/pnas.0431186100. PubMed PMID: 12697906; PubMed Central PMCID: PMCPMC154335.

186. Moulson CL, Lin MH, White JM, Newberry EP, Davidson NO, Miner JH. Keratinocyte-specific expression of fatty acid transport protein 4 rescues the wrinkle-free phenotype in Slc27a4/Fatp4 mutant mice. J Biol Chem. 2007;282(21):15912-20. Epub 2007/03/31. doi: 10.1074/jbc.M701779200. PubMed PMID: 17401141.

187. Yamamoto H, Hattori M, Chamulitrat W, Ohno Y, Kihara A. Skin permeability barrier formation by the ichthyosis-causative gene. Proc Natl Acad Sci U S A. 2020;117(6):2914-22. Epub 2020/01/23. doi: 10.1073/pnas.1917525117. PubMed PMID: 31974308; PubMed Central PMCID: PMCPMC7022171.

188. Mitchell RW, On NH, Del Bigio MR, Miller DW, Hatch GM. Fatty acid transport protein expression in human brain and potential role in fatty acid transport across human brain microvessel endothelial cells. J Neurochem. 2011;117(4):735-46. Epub 2011/03/31. doi: 10.1111/j.1471-4159.2011.07245.x. PubMed PMID: 21395585.

189. Coe NR, Smith AJ, Frohnert BI, Watkins PA, Bernlohr DA. The fatty acid transport protein (FATP1) is a very long chain acyl-CoA synthetase. J Biol Chem. 1999;274(51):36300-4. doi: 10.1074/jbc.274.51.36300. PubMed PMID: 10593920.

190. Kim JK, Gimeno RE, Higashimori T, Kim HJ, Choi H, Punreddy S, et al. Inactivation of fatty acid transport protein 1 prevents fat-induced insulin resistance in skeletal muscle. J Clin Invest. 2004;113(5):756-63. doi: 10.1172/JCI18917. PubMed PMID: 14991074; PubMed Central PMCID: PMCPMC351314.

191. Wu Q, Kazantzis M, Doege H, Ortegon AM, Tsang B, Falcon A, et al. Fatty acid transport protein 1 is required for nonshivering thermogenesis in brown adipose tissue. Diabetes. 2006;55(12):3229-37. doi: 10.2337/db06-0749. PubMed PMID: 17130465.

192. Wu Q, Ortegon AM, Tsang B, Doege H, Feingold KR, Stahl A. FATP1 is an insulin-sensitive fatty acid transporter involved in diet-induced obesity. Mol Cell Biol. 2006;26(9):3455-67. doi: 10.1128/MCB.26.9.3455-3467.2006. PubMed PMID: 16611988; PubMed Central PMCID: PMCPMC1447434.

193. Chekroud K, Guillou L, Grégoire S, Ducharme G, Brun E, Cazevieille C, et al. Fatp1 deficiency affects retinal light response and dark adaptation, and induces age-related alterations. PLoS One. 2012;7(11):e50231. Epub 2012/11/16. doi: 10.1371/journal.pone.0050231. PubMed PMID: 23166839; PubMed Central PMCID: PMCPMC3500375.

194. Crawford MA, Broadhurst CL, Guest M, Nagar A, Wang Y, Ghebremeskel K, et al. A quantum theory for the irreplaceable role of docosahexaenoic acid in neural cell signalling throughout evolution. Prostaglandins Leukot Essent Fatty Acids. 2013;88(1):5-13. Epub 2012/11/30. doi: 10.1016/j.plefa.2012.08.005. PubMed PMID: 23206328.

195. Diau GY, Hsieh AT, Sarkadi-Nagy EA, Wijendran V, Nathanielsz PW, Brenna JT. The influence of long chain polyunsaturate supplementation on docosahexaenoic acid and arachidonic acid in baboon neonate central nervous system. BMC Med. 2005;3:11. Epub 2005/06/23. doi: 10.1186/1741-7015-3-11. PubMed PMID: 15975147; PubMed Central PMCID: PMCPMC1184078.

196. Joffre C, Grégoire S, De Smedt V, Acar N, Bretillon L, Nadjar A, et al. Modulation of brain PUFA content in different experimental models of mice. Prostaglandins Leukot

Essent Fatty Acids. 2016;114:1-10. Epub 2016/09/30. doi: 10.1016/j.plefa.2016.09.003. PubMed PMID: 27926457.

197. Papanikolaou Y, Brooks J, Reider C, Fulgoni VL. U.S. adults are not meeting recommended levels for fish and omega-3 fatty acid intake: results of an analysis using observational data from NHANES 2003-2008. Nutr J. 2014;13:31. Epub 2014/04/02. doi: 10.1186/1475-2891-13-31. PubMed PMID: 24694001; PubMed Central PMCID: PMCPMC3992162.

198. Dennis EA, Norris PC. Eicosanoid storm in infection and inflammation. Nat Rev Immunol. 2015;15(8):511-23. doi: 10.1038/nri3859. PubMed PMID: 26139350; PubMed Central PMCID: PMCPMC4606863.

199. Hong S, Gronert K, Devchand PR, Moussignac RL, Serhan CN. Novel docosatrienes and 17S-resolvins generated from docosahexaenoic acid in murine brain, human blood, and glial cells. Autacoids in anti-inflammation. J Biol Chem. 2003;278(17):14677-87. Epub 2003/02/17. doi: 10.1074/jbc.M300218200. PubMed PMID: 12590139.

200. Fujino T, Yamamoto T. Cloning and functional expression of a novel long-chain acyl-CoA synthetase expressed in brain. J Biochem. 1992;111(2):197-203. PubMed PMID: 1569043.

201. Berger JH, Charron MJ, Silver DL. Major facilitator superfamily domain-containing protein 2a (MFSD2A) has roles in body growth, motor function, and lipid metabolism. PLoS One. 2012;7(11):e50629. Epub 2012/11/29. doi: 10.1371/journal.pone.0050629. PubMed PMID: 23209793; PubMed Central PMCID: PMCPMC3510178.

202. Pan Y, Scanlon MJ, Owada Y, Yamamoto Y, Porter CJ, Nicolazzo JA. Fatty acid-binding protein 5 facilitates the blood-brain barrier transport of docosahexaenoic acid. Mol Pharm. 2015;12(12):4375-85. Epub 2015/10/30. doi: 10.1021/acs.molpharmaceut.5b00580. PubMed PMID: 26455443.

203. Xiao Y, Huang Y, Chen ZY. Distribution, depletion and recovery of docosahexaenoic acid are region-specific in rat brain. Br J Nutr. 2005;94(4):544-50. doi: 10.1079/bjn20051539. PubMed PMID: 16197579.

204. Wong SW, Kwon MJ, Choi AM, Kim HP, Nakahira K, Hwang DH. Fatty acids modulate Toll-like receptor 4 activation through regulation of receptor dimerization and recruitment into lipid rafts in a reactive oxygen species-dependent manner. J Biol Chem. 2009;284(40):27384-92. Epub 2009/08/01. doi: 10.1074/jbc.M109.044065. PubMed PMID: 19648648; PubMed Central PMCID: PMCPMC2785667.

205. Matt SM, Lawson MA, Johnson RW. Aging and peripheral lipopolysaccharide can modulate epigenetic regulators and decrease IL-1β promoter DNA methylation in microglia. Neurobiol Aging. 2016;47:1-9. Epub 2016/07/15. doi: 10.1016/j.neurobiolaging.2016.07.006. PubMed PMID: 27500965; PubMed Central PMCID: PMCPMC5075520.

206. Shi Z, Ren H, Huang Z, Peng Y, He B, Yao X, et al. Fish oil prevents lipopolysaccharide-induced depressive-like behavior by inhibiting neuroinflammation. Mol Neurobiol. 2017;54(9):7327-34. Epub 2016/11/04. doi: 10.1007/s12035-016-0212-9. PubMed PMID: 27815837.

207. Trépanier MO, Hopperton KE, Giuliano V, Masoodi M, Bazinet RP. Increased brain docosahexaenoic acid has no effect on the resolution of neuroinflammation following intracerebroventricular lipopolysaccharide injection. Neurochem Int. 2018;118:115-26. Epub 2018/05/22. doi: 10.1016/j.neuint.2018.05.010. PubMed PMID: 29792954.

208. Trépanier MO, Hopperton KE, Orr SK, Bazinet RP. N-3 polyunsaturated fatty acids in animal models with neuroinflammation: An update. Eur J Pharmacol. 2016;785:187-206. Epub 2015/05/30. doi: 10.1016/j.ejphar.2015.05.045. PubMed PMID: 26036964.

209. Switzer RC, Butt MT. Histological Markers of Neurotoxicity. Wiley, Hoboken, NJ2011.

210. Stigger F, Lovatel G, Marques M, Bertoldi K, Moysés F, Elsner V, et al. Inflammatory response and oxidative stress in developing rat brain and its consequences on motor behavior following maternal administration of LPS and perinatal anoxia. Int J Dev Neurosci. 2013;31(8):820-7. Epub 2013/10/15. doi: 10.1016/j.ijdevneu.2013.10.003. PubMed PMID: 24140242.

211. Qin L, Liu Y, Hong JS, Crews FT. NADPH oxidase and aging drive microglial activation, oxidative stress, and dopaminergic neurodegeneration following systemic LPS administration. Glia. 2013;61(6):855-68. Epub 2013/03/28. doi: 10.1002/glia.22479. PubMed PMID: 23536230; PubMed Central PMCID: PMCPMC3631289.

212. Takaki J, Fujimori K, Miura M, Suzuki T, Sekino Y, Sato K. L-glutamate released from activated microglia downregulates astrocytic L-glutamate transporter expression in neuroinflammation: the 'collusion' hypothesis for increased extracellular L-glutamate concentration in neuroinflammation. J Neuroinflammation. 2012;9:275. Epub 2012/12/23. doi: 10.1186/1742-2094-9-275. PubMed PMID: 23259598; PubMed Central PMCID: PMCPMC3575281.

213. Miles EA, Calder PC. Influence of marine n-3 polyunsaturated fatty acids on immune function and a systematic review of their effects on clinical outcomes in rheumatoid arthritis. Br J Nutr. 2012;107 Suppl 2:S171-84. doi: 10.1017/S0007114512001560. PubMed PMID: 22591891.

214. Serhan CN. Treating inflammation and infection in the 21st century: new hints from decoding resolution mediators and mechanisms. FASEB J. 2017;31(4):1273-88. Epub 2017/01/13. doi: 10.1096/fj.201601222R. PubMed PMID: 28087575; PubMed Central PMCID: PMCPMC5349794.

215. Layé S, Nadjar A, Joffre C, Bazinet RP. Anti-inflammatory effects of omega-3 fatty acids in the brain: Physiological mechanisms and relevance to pharmacology. Pharmacol Rev. 2018;70(1):12-38. doi: 10.1124/pr.117.014092. PubMed PMID: 29217656.

216. Rey C, Nadjar A, Buaud B, Vaysse C, Aubert A, Pallet V, et al. Resolvin D1 and E1 promote resolution of inflammation in microglial cells in vitro. Brain Behav Immun. 2016;55:249-59. Epub 2015/12/21. doi: 10.1016/j.bbi.2015.12.013. PubMed PMID: 26718448.

217. Choi JY, Jang JS, Son DJ, Im HS, Kim JY, Park JE, et al. Antarctic krill oil diet protects against lipopolysaccharide-induced oxidative stress, neuroinflammation and cognitive impairment. Int J Mol Sci. 2017;18(12). Epub 2017/11/28. doi: 10.3390/ijms18122554. PubMed PMID: 29182579; PubMed Central PMCID: PMCPMC5751157.

218. Chowdari KV, Northup A, Pless L, Wood J, Joo YH, Mirnics K, et al. DNA pooling: a comprehensive, multi-stage association analysis of ACSL6 and SIRT5 polymorphisms in schizophrenia. Genes Brain Behav. 2007;6(3):229-39. doi: 10.1111/j.1601-183X.2006.00251.x. PubMed PMID: 16827919.

219. Das UN. Polyunsaturated fatty acids and their metabolites in the pathobiology of schizophrenia. Prog Neuropsychopharmacol Biol Psychiatry. 2013;42:122-34. Epub 2012/06/23. doi: 10.1016/j.pnpbp.2012.06.010. PubMed PMID: 22735394.

220. Lee HJ, Han J, Jang Y, Kim SJ, Park JH, Seo KS, et al. Docosahexaenoic acid prevents paraquat-induced reactive oxygen species production in dopaminergic neurons via enhancement of glutathione homeostasis. Biochem Biophys Res Commun. 2015;457(1):95-100. Epub 2014/12/27. doi: 10.1016/j.bbrc.2014.12.085. PubMed PMID: 25545062.

221. Jagmag SA, Tripathi N, Shukla SD, Maiti S, Khurana S. Evaluation of models of Parkinson's disease. Front Neurosci. 2015;9:503. Epub 2016/01/19. doi: 10.3389/fnins.2015.00503. PubMed PMID: 26834536; PubMed Central PMCID: PMCPMC4718050.

222. Godbout JP, Chen J, Abraham J, Richwine AF, Berg BM, Kelley KW, et al. Exaggerated neuroinflammation and sickness behavior in aged mice following activation of the peripheral innate immune system. FASEB J. 2005;19(10):1329-31. Epub 2005/05/26. doi: 10.1096/fj.05-3776fje. PubMed PMID: 15919760.

223. Norden DM, Trojanowski PJ, Villanueva E, Navarro E, Godbout JP. Sequential activation of microglia and astrocyte cytokine expression precedes increased Iba-1 or GFAP immunoreactivity following systemic immune challenge. Glia. 2016;64(2):300-16. Epub 2015/10/15. doi: 10.1002/glia.22930. PubMed PMID: 26470014; PubMed Central PMCID: PMCPMC4707977.

224. Bonetto A, Andersson DC, Waning DL. Assessment of muscle mass and strength in mice. Bonekey Rep. 2015;4:732. Epub 2015/08/19. doi: 10.1038/bonekey.2015.101. PubMed PMID: 26331011; PubMed Central PMCID: PMCPMC4549925.

225. Fleming SM, Ekhator OR, Ghisays V. Assessment of sensorimotor function in mouse models of Parkinson's disease. J Vis Exp. 2013(76). Epub 2013/06/17. doi: 10.3791/50303. PubMed PMID: 23851663; PubMed Central PMCID: PMCPMC3727502.

226. Castro B, Kuang S. Evaluation of muscle performance in mice by treadmill exhaustion test and whole-limb grip strength assay. Bio Protoc. 2017;7(8). doi: 10.21769/BioProtoc.2237. PubMed PMID: 28713848; PubMed Central PMCID: PMCPMC5510664.

227. Barrenha GD, Chester JA. Genetic correlation between innate alcohol preference and fear-potentiated startle in selected mouse lines. Alcohol Clin Exp Res. 2007;31(7):1081-8. Epub 2007/04/19. doi: 10.1111/j.1530-0277.2007.00396.x. PubMed PMID: 17451404.

228. Dimauro I, Pearson T, Caporossi D, Jackson MJ. A simple protocol for the subcellular fractionation of skeletal muscle cells and tissue. BMC Res Notes. 2012;5:513. Epub 2012/09/20. doi: 10.1186/1756-0500-5-513. PubMed PMID: 22994964; PubMed Central PMCID: PMCPMC3508861.

229. Counihan JL, Duckering M, Dalvie E, Ku WM, Bateman LA, Fisher KJ, et al. Chemoproteomic profiling of acetanilide herbicides reveals their role in inhibiting fatty acid oxidation. ACS Chem Biol. 2017;12(3):635-42. Epub 2017/01/20. doi: 10.1021/acschembio.6b01001. PubMed PMID: 28094496.

230. Louie SM, Grossman EA, Crawford LA, Ding L, Camarda R, Huffman TR, et al. GSTP1 is a driver of triple-negative breast cancer cell metabolism and pathogenicity. Cell Chem Biol. 2016;23(5):567-78. Epub 2016/05/12. doi: 10.1016/j.chembiol.2016.03.017. PubMed PMID: 27185638; PubMed Central PMCID: PMCPMC4876719.

231. Benjamin DI, Cozzo A, Ji X, Roberts LS, Louie SM, Mulvihill MM, et al. Ether lipid generating enzyme AGPS alters the balance of structural and signaling lipids to fuel cancer pathogenicity. Proc Natl Acad Sci U S A. 2013;110(37):14912-7. Epub 2013/08/26. doi: 10.1073/pnas.1310894110. PubMed PMID: 23980144; PubMed Central PMCID: PMCPMC3773741.

232. BLIGH EG, DYER WJ. A rapid method of total lipid extraction and purification. Can J Biochem Physiol. 1959;37(8):911-7. doi: 10.1139/o59-099. PubMed PMID: 13671378.

233. Crawford MA, Casperd NM, Sinclair AJ. The long chain metabolites of linoleic acid linolenic acids in liver and brain in herbivores and carnivores. Comp Biochem Physiol B. 1976;54(3):395-401. PubMed PMID: 1277808.

234. Crawford MA. Docosahexaenoic acid in neural signaling systems. Nutr Health. 2006;18(3):263-76. doi: 10.1177/026010600601800309. PubMed PMID: 17180872.

235. Research FS, M GB. WWEIA Data Tables.

236. Carver JD, Benford VJ, Han B, Cantor AB. The relationship between age and the fatty acid composition of cerebral cortex and erythrocytes in human subjects. Brain Res Bull. 2001;56(2):79-85. doi: 10.1016/s0361-9230(01)00551-2. PubMed PMID: 11704343.

237. Söderberg M, Edlund C, Kristensson K, Dallner G. Fatty acid composition of brain phospholipids in aging and in Alzheimer's disease. Lipids. 1991;26(6):421-5. PubMed PMID: 1881238.

238. Hopiavuori BR, Agbaga MP, Brush RS, Sullivan MT, Sonntag WE, Anderson RE. Regional changes in CNS and retinal glycerophospholipid profiles with age: a molecular blueprint. J Lipid Res. 2017;58(4):668-80. Epub 2017/02/15. doi: 10.1194/jlr.M070714. PubMed PMID: 28202633; PubMed Central PMCID: PMCPMC5392743.

239. Prasad MR, Lovell MA, Yatin M, Dhillon H, Markesbery WR. Regional membrane phospholipid alterations in Alzheimer's disease. Neurochem Res. 1998;23(1):81-8. PubMed PMID: 9482271.

240. Hishikawa D, Valentine WJ, Iizuka-Hishikawa Y, Shindou H, Shimizu T. Metabolism and functions of docosahexaenoic acid-containing membrane glycerophospholipids. FEBS Lett. 2017;591(18):2730-44. Epub 2017/09/07. doi: 10.1002/1873-3468.12825. PubMed PMID: 28833063; PubMed Central PMCID: PMCPMC5639365.

241. Brenna JT, Carlson SE. Docosahexaenoic acid and human brain development: evidence that a dietary supply is needed for optimal development. J Hum Evol. 2014;77:99-106. Epub 2014/05/02. doi: 10.1016/j.jhevol.2014.02.017. PubMed PMID: 24780861.

242. Science AIfB. Allen Cell Types Database 2015. Available from: http://celltypes.brain-map.org/.

243. Orre M, Kamphuis W, Osborn LM, Melief J, Kooijman L, Huitinga I, et al. Acute isolation and transcriptome characterization of cortical astrocytes and microglia from young and aged mice. Neurobiol Aging. 2014;35(1):1-14. Epub 2013/08/15. doi: 10.1016/j.neurobiolaging.2013.07.008. PubMed PMID: 23954174.

244. Zhu H, Fan C, Xu F, Tian C, Zhang F, Qi K. Dietary fish oil n-3 polyunsaturated fatty acids and alpha-linolenic acid differently affect brain accretion of docosahexaenoic acid and expression of desaturases and sterol regulatory element-binding protein 1 in mice. J Nutr Biochem. 2010;21(10):954-60. Epub 2009/12/01. doi: 10.1016/j.jnutbio.2009.07.011. PubMed PMID: 19954955.

245. Lobanova ES, Schuhmann K, Finkelstein S, Lewis TR, Cady MA, Hao Y, et al. Disrupted blood-retina lysophosphatidylcholine transport impairs photoreceptor health but not visual signal transduction. J Neurosci. 2019;39(49):9689-701. Epub 2019/11/01. doi: 10.1523/JNEUROSCI.1142-19.2019. PubMed PMID: 31676603; PubMed Central PMCID: PMCPMC6891062.

246. Levental KR, Malmberg E, Symons JL, Fan YY, Chapkin RS, Ernst R, et al. Lipidomic and biophysical homeostasis of mammalian membranes counteracts dietary lipid perturbations to maintain cellular fitness. Nat Commun. 2020;11(1):1339. Epub 2020/03/12. doi: 10.1038/s41467-020-15203-1. PubMed PMID: 32165635; PubMed Central PMCID: PMCPMC7067841.

247. Kelmer Sacramento E, Kirkpatrick JM, Mazzetto M, Baumgart M, Bartolome A, Di Sanzo S, et al. Reduced proteasome activity in the aging brain results in ribosome stoichiometry loss and aggregation. Mol Syst Biol. 2020;16(6):e9596. doi: 10.15252/msb.20209596. PubMed PMID: 32558274; PubMed Central PMCID: PMCPMC7301280.

248. Li Y, Yu H, Chen C, Li S, Zhang Z, Xu H, et al. Proteomic profile of mouse brain aging contributions to mitochondrial dysfunction, DNA oxidative damage, loss of neurotrophic factor, and synaptic and ribosomal proteins. Oxid Med Cell Longev. 2020;2020:5408452. Epub 2020/06/09. doi: 10.1155/2020/5408452. PubMed PMID: 32587661; PubMed Central PMCID: PMCPMC7301248.

249. Cao D, Kevala K, Kim J, Moon HS, Jun SB, Lovinger D, et al. Docosahexaenoic acid promotes hippocampal neuronal development and synaptic function. J Neurochem. 2009;111(2):510-21. Epub 2009/08/13. doi: 10.1111/j.1471-4159.2009.06335.x. PubMed PMID: 19682204; PubMed Central PMCID: PMCPMC2773444.

250. Sidhu VK, Huang BX, Kim H-Y. Effects of docosahexaenoic acid on mouse brain synaptic plasma membrane proteome analyzed by mass spectrometry and (16)O/(18)O labeling. J Proteome Res. 2011;10(12):5472-80. Epub 2011/10/26. doi: 10.1021/pr2007285. PubMed PMID: 22003853.

251. Taha AY. Linoleic acid–good or bad for the brain? : npj science of food; 2020.

252. Martínez-García A, Sastre I, Recuero M, Aldudo J, Vilella E, Mateo I, et al. PLA2G3, a gene involved in oxidative stress induced death, is associated with Alzheimer's disease. J Alzheimers Dis. 2010;22(4):1181-7. doi: 10.3233/JAD-2010-101348. PubMed PMID: 20930276.

253. Pérez-González M, Mendioroz M, Badesso S, Sucunza D, Roldan M, Espelosín M, et al. PLA2G4E, a candidate gene for resilience in Alzheimer´s disease and a new target for dementia treatment. Prog Neurobiol. 2020;191:101818. Epub 2020/05/05. doi: 10.1016/j.pneurobio.2020.101818. PubMed PMID: 32380223.

254. Imai H, Matsuoka M, Kumagai T, Sakamoto T, Koumura T. Lipid Peroxidation-Dependent Cell Death Regulated by GPx4 and Ferroptosis. Curr Top Microbiol Immunol. 2017;403:143-70. doi: 10.1007/82_2016_508. PubMed PMID: 28204974.

255. Li MD, Burns TC, Morgan AA, Khatri P. Integrated multi-cohort transcriptional meta-analysis of neurodegenerative diseases. Acta Neuropathol Commun. 2014;2:93. Epub 2014/09/04. doi: 10.1186/s40478-014-0093-y. PubMed PMID: 25187168; PubMed Central PMCID: PMCPMC4167139.

256. Pankratz N, Wilk JB, Latourelle JC, DeStefano AL, Halter C, Pugh EW, et al. Genomewide association study for susceptibility genes contributing to familial Parkinson disease. Hum Genet. 2009;124(6):593-605. Epub 2008/11/06. doi: 10.1007/s00439-008-0582-9. PubMed PMID: 18985386; PubMed Central PMCID: PMCPMC2627511.

257. Jun G, Ibrahim-Verbaas CA, Vronskaya M, Lambert JC, Chung J, Naj AC, et al. A novel Alzheimer disease locus located near the gene encoding tau protein. Mol Psychiatry. 2016;21(1):108-17. Epub 2015/03/17. doi: 10.1038/mp.2015.23. PubMed PMID: 25778476; PubMed Central PMCID: PMCPMC4573764.

258. Serhan CN, Gupta SK, Perretti M, Godson C, Brennan E, Li Y, et al. The Atlas of Inflammation Resolution (AIR). Mol Aspects Med. 2020;74:100894. Epub 2020/09/03. doi: 10.1016/j.mam.2020.100894. PubMed PMID: 32893032; PubMed Central PMCID: PMCPMC7733955.

259. Hawrylycz MJ, Lein ES, Guillozet-Bongaarts AL, Shen EH, Ng L, Miller JA, et al. An anatomically comprehensive atlas of the adult human brain transcriptome. Nature. 2012;489(7416):391-9. doi: 10.1038/nature11405. PubMed PMID: 22996553; PubMed Central PMCID: PMCPMC4243026.

260. Talamonti E, Sasso V, To H, Haslam RP, Napier JA, Ulfhake B, et al. Impairment of DHA synthesis alters the expression of neuronal plasticity markers and the brain inflammatory status in mice. FASEB J. 2020;34(2):2024-40. Epub 2019/12/11. doi: 10.1096/fj.201901890RR. PubMed PMID: 31909582; PubMed Central PMCID: PMCPMC7384056.

261. Krashia P, Cordella A, Nobili A, La Barbera L, Federici M, Leuti A, et al. Blunting neuroinflammation with resolvin D1 prevents early pathology in a rat model of Parkinson's disease. Nat Commun. 2019;10(1):3945. Epub 2019/09/02. doi: 10.1038/s41467-019-11928-w. PubMed PMID: 31477726; PubMed Central PMCID: PMCPMC6718379.

262. Wang X, Zhu M, Hjorth E, Cortés-Toro V, Eyjolfsdottir H, Graff C, et al. Resolution of inflammation is altered in Alzheimer's disease. Alzheimers Dement. 2015;11(1):40-50.e1-2. Epub 2014/02/12. doi: 10.1016/j.jalz.2013.12.024. PubMed PMID: 24530025; PubMed Central PMCID: PMCPMC4275415.

263. Kooij G, Troletti CD, Leuti A, Norris PC, Riley I, Albanese M, et al. Specialized pro-resolving lipid mediators are differentially altered in peripheral blood of patients with multiple sclerosis and attenuate monocyte and blood-brain barrier dysfunction. Haematologica. 2020;105(8):2056-70. Epub 2019/11/28. doi: 10.3324/haematol.2019.219519. PubMed PMID: 31780628; PubMed Central PMCID: PMCPMC7395264.

264. Kariv-Inbal Z, Yacobson S, Berkecz R, Peter M, Janaky T, Lütjohann D, et al. The isoform-specific pathological effects of apoE4 in vivo are prevented by a fish oil (DHA) diet and are modified by cholesterol. J Alzheimers Dis. 2012;28(3):667-83. doi: 10.3233/JAD-2011-111265. PubMed PMID: 22057027.

265. Patrick RP. Role of phosphatidylcholine-DHA in preventing APOE4-associated Alzheimer's disease. FASEB J. 2019;33(2):1554-64. Epub 2018/10/05. doi: 10.1096/fj.201801412R. PubMed PMID: 30289748; PubMed Central PMCID: PMCPMC6338661.

266. Kim HW, Rao JS, Rapoport SI, Igarashi M. Dietary n-6 PUFA deprivation downregulates arachidonate but upregulates docosahexaenoate metabolizing enzymes in rat brain. Biochim Biophys Acta. 2011;1811(2):111-7. Epub 2010/11/09. doi: 10.1016/j.bbalip.2010.10.005. PubMed PMID: 21070866; PubMed Central PMCID: PMCPMC3018563.

267. Chan JP, Wong BH, Chin CF, Galam DLA, Foo JC, Wong LC, et al. The lysolipid transporter Mfsd2a regulates lipogenesis in the developing brain. PLoS Biol. 2018;16(8):e2006443. Epub 2018/08/03. doi: 10.1371/journal.pbio.2006443. PubMed PMID: 30074985; PubMed Central PMCID: PMCPMC6093704.

268. Caron A, Dungan Lemko HM, Castorena CM, Fujikawa T, Lee S, Lord CC, et al. POMC neurons expressing leptin receptors coordinate metabolic responses to fasting via suppression of leptin levels. Elife. 2018;7. Epub 2018/03/12. doi: 10.7554/eLife.33710. PubMed PMID: 29528284; PubMed Central PMCID: PMCPMC5866097.

269. Schartz ND, Sommer AL, Colin SA, Mendez LB, Brewster AL. Early treatment with C1 esterase inhibitor improves weight but not memory deficits in a rat model of status epilepticus. Physiol Behav. 2019;212:112705. Epub 2019/10/16. doi: 10.1016/j.physbeh.2019.112705. PubMed PMID: 31628931; PubMed Central PMCID: PMCPMC6879103.

270. Fabregat A, Jupe S, Matthews L, Sidiropoulos K, Gillespie M, Garapati P, et al. The Reactome Pathway Knowledgebase. Nucleic Acids Res. 2018;46(D1):D649-D55. doi: 10.1093/nar/gkx1132. PubMed PMID: 29145629; PubMed Central PMCID: PMCPMC5753187.

271. *Oliveros JC*. *Venny. An interactive tool for comparing lists with Venn's diagrams 2007-2015*. Available from: https://bioinfogp.cnb.csic.es/tools/venny/index.html.

272. Babicki S, Arndt D, Marcu A, Liang Y, Grant JR, Maciejewski A, et al. Heatmapper: web-enabled heat mapping for all. Nucleic Acids Res. 2016;44(W1):W147-53. Epub 2016/05/17. doi: 10.1093/nar/gkw419. PubMed PMID: 27190236; PubMed Central PMCID: PMCPMC4987948.

273. Eden E, Navon R, Steinfeld I, Lipson D, Yakhini Z. GOrilla: a tool for discovery and visualization of enriched GO terms in ranked gene lists. BMC Bioinformatics. 2009;10:48. Epub 2009/02/03. doi: 10.1186/1471-2105-10-48. PubMed PMID: 19192299; PubMed Central PMCID: PMCPMC2644678.

274. Zhou Y, Nijland M, Miller M, Ford S, Nathanielsz PW, Brenna JT. The influence of maternal early to mid-gestation nutrient restriction on long chain polyunsaturated fatty

acids in fetal sheep. Lipids. 2008;43(6):525-31. Epub 2008/05/15. doi: 10.1007/s11745-008-3186-1. PubMed PMID: 18481131.

275. Brenna JT. Fatty acid analysis by high resolution gas chromatography and mass spectrometry for clinical and experimental applications. Curr Opin Clin Nutr Metab Care. 2013;16(5):548-54. doi: 10.1097/MCO.0b013e328363bc0a. PubMed PMID: 23892505.

276. Kilburg-Basnyat B, Reece SW, Crouch MJ, Luo B, Boone AD, Yaeger M, et al. Specialized Pro-Resolving Lipid Mediators Regulate Ozone-Induced Pulmonary and Systemic Inflammation. Toxicol Sci. 2018;163(2):466-77. doi: 10.1093/toxsci/kfy040. PubMed PMID: 29471542; PubMed Central PMCID: PMCPMC5974791.

277. Watkins PA, Ellis JM. Peroxisomal acyl-CoA synthetases. Biochim Biophys Acta. 2012;1822(9):1411-20. Epub 2012/02/17. doi: 10.1016/j.bbadis.2012.02.010. PubMed PMID: 22366061; PubMed Central PMCID: PMCPMC3382043.

278. Chung WS, Allen NJ, Eroglu C. Astrocytes Control Synapse Formation, Function, and Elimination. Cold Spring Harb Perspect Biol. 2015;7(9):a020370. Epub 2015/02/06. doi: 10.1101/cshperspect.a020370. PubMed PMID: 25663667; PubMed Central PMCID: PMCPMC4527946.

279. Sofroniew MV, Vinters HV. Astrocytes: biology and pathology. Acta Neuropathol. 2010;119(1):7-35. doi: 10.1007/s00401-009-0619-8. PubMed PMID: 20012068; PubMed Central PMCID: PMCPMC2799634.

280. Berk PD, Stump DD. Mechanisms of cellular uptake of long chain free fatty acids. Molecular and cellular biochemistry. 1999;192(1):17-31. doi: 10.1023/A:1006832001033.

281. Kasuya F, Masuyama T, Yamashita T, Nakamoto K, Tokuyama S, Kawakami H. Determination of acyl-CoA esters and acyl-CoA synthetase activity in mouse brain areas by liquid chromatography-electrospray ionization-tandem mass spectrometry. J Chromatogr B Analyt Technol Biomed Life Sci. 2013;929:45-50. doi: 10.1016/j.jchromb.2013.03.030. PubMed PMID: 23644500.

282. Tulodziecka K, Diaz-Rohrer BB, Farley MM, Chan RB, Di Paolo G, Levental KR, et al. Remodeling of the postsynaptic plasma membrane during neural development. Mol Biol Cell. 2016;27(22):3480-9. Epub 2016/08/17. doi: 10.1091/mbc.E16-06-0420. PubMed PMID: 27535429; PubMed Central PMCID: PMCPMC5221582.

283. Stott BM, Vu MP, McLemore CO, Lund MS, Gibbons E, Brueseke TJ, et al. Use of fluorescence to determine the effects of cholesterol on lipid behavior in sphingomyelin liposomes and erythrocyte membranes. J Lipid Res. 2008;49(6):1202-15. Epub 2008/02/25. doi: 10.1194/jlr.M700479-JLR200. PubMed PMID: 18299615; PubMed Central PMCID: PMCPMC2386901.

284. Bélanger M, Allaman I, Magistretti PJ. Brain energy metabolism: focus on astrocyte-neuron metabolic cooperation. Cell Metab. 2011;14(6):724-38. doi: 10.1016/j.cmet.2011.08.016. PubMed PMID: 22152301.

285. Schousboe A, Scafidi S, Bak LK, Waagepetersen HS, McKenna MC. Glutamate metabolism in the brain focusing on astrocytes. Adv Neurobiol. 2014;11:13-30. doi: 10.1007/978-3-319-08894-5_2. PubMed PMID: 25236722; PubMed Central PMCID: PMCPMC4667713.

286. Monzio Compagnoni G, Di Fonzo A, Corti S, Comi GP, Bresolin N, Masliah E. The Role of Mitochondria in Neurodegenerative Diseases: the Lesson from Alzheimer's Disease and Parkinson's Disease. Mol Neurobiol. 2020;57(7):2959-80. Epub 2020/05/22. doi: 10.1007/s12035-020-01926-1. PubMed PMID: 32445085.

287. Aufschnaiter A, Kohler V, Diessl J, Peselj C, Carmona-Gutierrez D, Keller W, et al. Mitochondrial lipids in neurodegeneration. Cell Tissue Res. 2017;367(1):125-40. Epub 2016/07/23. doi: 10.1007/s00441-016-2463-1. PubMed PMID: 27449929; PubMed Central PMCID: PMCPMC5203858.

288. Kiebish MA, Han X, Cheng H, Chuang JH, Seyfried TN. Cardiolipin and electron transport chain abnormalities in mouse brain tumor mitochondria: lipidomic evidence supporting the Warburg theory of cancer. J Lipid Res. 2008;49(12):2545-56. Epub 2008/08/13. doi: 10.1194/jlr.M800319-JLR200. PubMed PMID: 18703489; PubMed Central PMCID: PMCPMC2582368.

289. Oemer G, Koch J, Wohlfarter Y, Alam MT, Lackner K, Sailer S, et al. Phospholipid Acyl Chain Diversity Controls the Tissue-Specific Assembly of Mitochondrial Cardiolipins. Cell Rep. 2020;30(12):4281-91.e4. doi: 10.1016/j.celrep.2020.02.115. PubMed PMID: 32209484.

290. Cole LK, Kim JH, Amoscato AA, Tyurina YY, Bay R H, Karimi B, et al. Aberrant cardiolipin metabolism is associated with cognitive deficiency and hippocampal alteration in tafazzin knockdown mice. Biochim Biophys Acta Mol Basis Dis. 2018;1864(10):3353-67. Epub 2018/07/25. doi: 10.1016/j.bbadis.2018.07.022. PubMed PMID: 30055293; PubMed Central PMCID: PMCPMC6532065.

291. Paradies G, Paradies V, De Benedictis V, Ruggiero FM, Petrosillo G. Functional role of cardiolipin in mitochondrial bioenergetics. Biochim Biophys Acta. 2014;1837(4):408-17. Epub 2013/10/29. doi: 10.1016/j.bbabio.2013.10.006. PubMed PMID: 24183692.

292. McCann H, Stevens CH, Cartwright H, Halliday GM. α-Synucleinopathy phenotypes. Parkinsonism Relat Disord. 2014;20 Suppl 1:S62-7. doi: 10.1016/S1353-8020(13)70017-8. PubMed PMID: 24262191.

293. Ruipérez V, Darios F, Davletov B. Alpha-synuclein, lipids and Parkinson's disease. Prog Lipid Res. 2010;49(4):420-8. Epub 2010/05/23. doi: 10.1016/j.plipres.2010.05.004. PubMed PMID: 20580911.

294. De Franceschi G, Fecchio C, Sharon R, Schapira AHV, Proukakis C, Bellotti V, et al. α-Synuclein structural features inhibit harmful polyunsaturated fatty acid oxidation, suggesting roles in neuroprotection. J Biol Chem. 2017;292(17):6927-37. Epub

2017/02/23. doi: 10.1074/jbc.M116.765149. PubMed PMID: 28232489; PubMed Central PMCID: PMCPMC5409462.

295. De Franceschi G, Frare E, Pivato M, Relini A, Penco A, Greggio E, et al. Structural and morphological characterization of aggregated species of α-synuclein induced by docosahexaenoic acid. J Biol Chem. 2011;286(25):22262-74. Epub 2011/04/28. doi: 10.1074/jbc.M110.202937. PubMed PMID: 21527634; PubMed Central PMCID: PMCPMC3121372.

296. Golovko MY, Rosenberger TA, Faergeman NJ, Feddersen S, Cole NB, Pribill I, et al. Acyl-CoA synthetase activity links wild-type but not mutant alpha-synuclein to brain arachidonate metabolism. Biochemistry. 2006;45(22):6956-66. doi: 10.1021/bi0600289. PubMed PMID: 16734431; PubMed Central PMCID: PMCPMC2532510.

297. Kuwata H, Hara S. Role of acyl-CoA synthetase ACSL4 in arachidonic acid metabolism. Prostaglandins Other Lipid Mediat. 2019;144:106363. Epub 2019/07/12. doi: 10.1016/j.prostaglandins.2019.106363. PubMed PMID: 31306767.

298. Teodoro BG, Sampaio IH, Bomfim LH, Queiroz AL, Silveira LR, Souza AO, et al. Long-chain acyl-CoA synthetase 6 regulates lipid synthesis and mitochondrial oxidative capacity in human and rat skeletal muscle. J Physiol. 2017;595(3):677-93. Epub 2016/11/08. doi: 10.1113/JP272962. PubMed PMID: 27647415; PubMed Central PMCID: PMCPMC5285616.

299. Frahm JL, Li LO, Grevengoed TJ, Coleman RA. Phosphorylation and acetylation of acyl-CoA synthetase- I. J Proteomics Bioinform. 2011;4(7):129-37. doi: 10.4172/jpb.1000180. PubMed PMID: 24039348; PubMed Central PMCID: PMCPMC3772793.

300. Pottala JV, Yaffe K, Robinson JG, Espeland MA, Wallace R, Harris WS. Higher RBC EPA + DHA corresponds with larger total brain and hippocampal volumes: WHIMS-MRI study. Neurology. 2014;82(5):435-42. Epub 2014/01/22. doi: 10.1212/WNL.0000000000000080. PubMed PMID: 24453077; PubMed Central PMCID: PMCPMC3917688.

301. Tan ZS, Harris WS, Beiser AS, Au R, Himali JJ, Debette S, et al. Red blood cell ω-3 fatty acid levels and markers of accelerated brain aging. Neurology. 2012;78(9):658-64. doi: 10.1212/WNL.0b013e318249f6a9. PubMed PMID: 22371413; PubMed Central PMCID: PMCPMC3286229.

302. Nations U, Affairs DoEaS, Division P. World Population Ageing

2019: Highlights. 2019.

APPENDIX A

IACUC APPROVAL LETTERS

East Carolina University
Tomorrow starts here.

Animal Care and
Use Committee
212 Ed Warren Life
Sciences Building
East Carolina University
Greenville, NC 27834-4354

252-744-2436 office
252-744-2355 fax

September 7, 2018

Jessica Ellis, Ph.D.
Department of Physiology
Brody 6N-98
East Carolina University

Dear Dr. Ellis:

Your Animal Use Protocol entitled, "Breeding for Fatty Acid Metabolism in Brain and Muscle in Physiology and Disease" (AUP #Q353) was reviewed by this institution's Animal Care and Use Committee on September 7, 2018. The following action was taken by the Committee:

"Approved as submitted"

Please contact Aaron Hinkle at 744-2997 prior to hazard use

A copy is enclosed for your laboratory files. Please be reminded that all animal procedures must be conducted as described in the approved Animal Use Protocol. Modifications of these procedures cannot be performed without prior approval of the ACUC. The Animal Welfare Act and Public Health Service Guidelines require the ACUC to suspend activities not in accordance with approved procedures and report such activities to the responsible University Official (Vice Chancellor for Health Sciences or Vice Chancellor for Academic Affairs) and appropriate federal Agencies. **Please ensure that all personnel associated with this protocol have access to this approved copy of the AUP and are familiar with its contents.**

Sincerely yours,

Susan McRae, Ph.D.
Chair, Animal Care and Use Committee

SM/jd

Enclosure

ECU
Animal Care and Use Committee
212 Ed Warren Life Sciences Building | East Carolina University | Greenville, NC 27834-4354
252-744-2436 office | 252-744-2355 fax

September 4, 2019

Jessica Ellis, Ph.D.
Department of Physiology/ECDOI
ECHI 4th floor
East Carolina University

Dear Dr. Ellis:

The Amendment of your Animal Use Protocol entitled, "Fatty Acid Metabolism in the Central Nervous and Skeletal Systems" (AUP # Q354) was reviewed by this institution's Animal Care and Use Committee on September 4, 2019. The following action was taken by the Committee:

"Approved as submitted"

Please contact Aaron Hinkle at 744-2997 prior to hazard use

A copy is enclosed for your laboratory files. Please be reminded that all animal procedures must be conducted as described in the approved Animal Use Protocol. Modifications of these procedures cannot be performed without prior approval of the ACUC. The Animal Welfare Act and Public Health Service Guidelines require the ACUC to suspend activities not in accordance with approved procedures and report such activities to the responsible University Official (Vice Chancellor for Health Sciences or Vice Chancellor for Academic Affairs) and appropriate federal Agencies. **Please ensure that all personnel associated with this protocol have access to this approved copy of the AUP and are familiar with its contents.**

Sincerely yours,

SB McRae

Susan McRae, Ph.D.
Chair, Animal Care and Use Committee

SM/jd

Enclosure

APPENDIX B

PERMISSION FOR FIGURE 2.6

From: PNAS Permissions <PNASPermissions@nas.edu>
Sent: Monday, January 25, 2021 4:43 PM
To: Fernandez Fernandez, Regina <fernandezfernande18@students.ecu.edu>
Subject: RE: Fernandez - Permission for figure

Thank you for your message. Permission is granted for your use of the material as described in your request. Please include a complete citation for the original PNAS article when reusing its material. Because this material published after 2008, a copyright note is not needed. There is no charge for this material, either. Let us know if you have any questions.

Sincerely,

Kay McLaughlin for
Diane Sullenberger
PNAS Executive Editor

From: Fernandez Fernandez, Regina <fernandezfernande18@students.ecu.edu>
Sent: Saturday, January 23, 2021 2:16 PM
To: PNAS Permissions <PNASPermissions@nas.edu>
Subject: Fernandez - Permission for figure

To whom it may concern,

My name is Regina Fernandez Fernandez and I am a graduate student at East Carolina University working in the lab of Dr. Jessica M. Ellis. In 2018 we published an article in PNAS (Acyl-CoA synthetase 6 enriches the neuroprotective omega-3 fatty acid DHA in the brain) and a commentary was written.

I would like to request permission to use a figure from the commentary in my dissertation.

1. Address: 115 Heart Drive, Greenville, NC - 27834
2. Permission for PNAS commentary figure:
    a. Title: ACSL6 is critical for maintaining brain DHA levels
    b. Authors: Raphaël Chouinard-Watkins and Richard P. Bazinet
    c. Figure 1: Schematic representation of the mechanisms regulating brain DHA uptake

Please let me know if you need additional information.

Thank you and I look forward to hearing from you.

Regina F. Fernandez